## School of Computer Science & Informatics

---

### Doctor of Philosophy Thesis

# Models for Information Propagation in Opportunistic Networks

---

*Author:*
**Richard Paul Coombs**

*Supervisors:*
**Dr. Dafydd Evans**
**Prof. David Walker**

December 2014

# Declarations

This work has not been submitted in substance for any other degree or award at this or any other university or place of learning, nor is being submitted concurrently in candidature for any degree or other award.

Signed _____ (candidate)          Date _____

## Statement 1

This thesis is being submitted in partial fulfillment of the requirements for the degree of Ph.D.

Signed _____ (candidate)          Date _____

## Statement 2

This thesis is the result of my own independent work/investigation, except where otherwise stated. Other sources are acknowledged by explicit references. The views expressed are my own.

Signed _____ (candidate)          Date _____

## Statement 3

I hereby give consent for my thesis, if accepted, to be available for photocopying and for inter-library loan, and for the title and summary to be made available to outside organisations.

Signed _____ (candidate)          Date _____

# Abstract

The topic of this thesis is Opportunistic Networks (OPNETs), a type of mobile ad hoc network in which data are propagated by the movement of the network devices and by short-range wireless transmissions. This allows data to spread to many devices across large distances without the use of any infrastructure or powerful hardware.

OPNET technology is in its fairly early stages of development and has a lot of potential for research. There are many applications that could benefit from OPNETs, such as sensor networks or social networks. However, before the technology can be used with confidence, research must be undertaken to better understand its behaviour and how it can be improved.

In this thesis, the way in which information propagates in an OPNET is studied. Methodical parameter studies are performed to measure the rate at which information reaches new recipients, the speed at which information travels across space, and the persistence of information in the network. The key parameters being studied are device density, device speed, wireless signal radius and message transmission time. Furthermore, device interaction schemes based on epidemiological models are studied to find how they affect network performance.

Another contribution of this thesis is the development of theoretical models for message spread in regions of one-dimensional (1D) and two-dimensional (2D) space. These models are based on preliminary theoretical models of network device interaction; specifically, the rate at which devices move within range of each other and the length of time that they remain within range.

A key contribution of this thesis is in acknowledging that data transmis-

sions between devices do not occur instantaneously. Due to latency in wireless communications, the time taken to transmit data is proportional to the amount of data being transferred. Non-instantaneous transmissions may fail before completion. Investigation is made into the effect this has on the rate of information propagation in OPNETs.

# Acknowledgements

*Thanks to...*

Dr. Dafydd Evans and Prof. David Walker for their time and wisdom.

Cardiff University for their guidance and funding.

My family for their encouragement and support.

My partner Lucy for her love and understanding.

My COMSC friends Speed, Matt, Will, Chris, Greg, Marc, Jon, Martin, Rob, etc. for listening and keeping me sane.

# Contents

# List of Figures

# Introduction

This chapter provides an overview of Opportunistic Networks (OPNETs) and discusses why they are an important research area. The current limitations of OPNETs are discussed, and how these limitations can be overcome. Following this, the research approach is described and the chapter is concluded with an overview of the thesis structure.

## 1.1  Opportunistic Networks

An OPNET is a type of digital communications network that comprises of several wireless, mobile devices. Each device can communicate with any other device in the network that is within range. Movement of the devices enables communication to span many devices over large distances. No single device in the network is necessarily more important than others—successful communication relies on the cooperation of several devices in the network.

### 1.1.1  Types of Wireless Communication Networks

Since Alexander Graham Bell invented the telephone in 1876, technology has progressed to allow communication between remote devices. Any group of devices that can communicate with one another is known as a *communications network*. This chapter starts by considering key developments in wireless communications technology that have led to the possibility of OPNETs.

**Cellular Networks**

As previously mentioned, telephones formed some of the earliest networks. Historically, wires were used as the communication channel; however, telephone communication has directly benefited from advances in network technology. Indeed, the advent of cellular networks allows for the wireless communication of mobile telephones.

Cellular networks consist of several fixed-location wireless transceivers, known as *base stations* (Vodafone Group 2014). Each base station serves mobile telephones within a particular region, known as a *cell*. This type of network is not completely wireless as base stations are connected with cables. When somebody makes a call, the signal is transmitted wirelessly from the handset to the nearest base station. The signal is then transmitted across cables to the base station that is closest to the receiver of the call. From this base station, the signal is transmitted wirelessly to the handset of the call receiver.

**Wireless Mesh Networks**

Wireless mesh networks consist of a number of static, wireless devices (Akyildiz and Wang 2005). If all devices are within communication range of every other device, the network is said to be *fully-connected*. While this is not usually the case, there should always be a communications path between any two devices (possibly via intermediates). Devices in a mesh network are expected to route data for others, as well as send/receive their own data. There is no infrastructure (such as routers or base stations) to manage the routing, and for this reason, a wireless mesh network can be thought of as an ad hoc network.

**Mobile Ad Hoc Networks**

A mobile ad-hoc network (MANET) is a wireless mesh network in which the communicating devices are free to move independently. This type of network is self-configuring as devices continually make and break wireless connections with other devices as they move around. MANETs assume that all devices are willing to participate in synchronous routing (Heinemann 2007), but this is not always achievable. However, OPNETs are able to cope with this situation.

**Opportunistic Network**

An OPNET is simply a highly disconnected MANET, meaning that there is not always a path between two devices. This is due to low device density, and/or the short-range wireless signals of the devices. Increasing the range of these wireless signals may cause the mobile devices to exhaust their battery power supplies too quickly. However, even with short-range signals, it is possible for data to propagate over long distances in physical space by the collaboration of devices.

The way in which OPNET devices collaborate to spread data is known as a *store–carry–forward* approach (Warthman 2003). This is described as follows:

- Devices *store* messages in a local buffer.
- Stored messages are *carried* to new locations by physical movement.
- Messages are *forwarded* to other devices that come within range.

This process can lead to data being spread over a large area and to many devices. Figure 1.1 illustrates how the *store–carry–forward* mechanism disseminates data to many isolated devices across a wide area. It is clear that data can only be forwarded when the opportunity arises, hence the name *opportunistic network*.
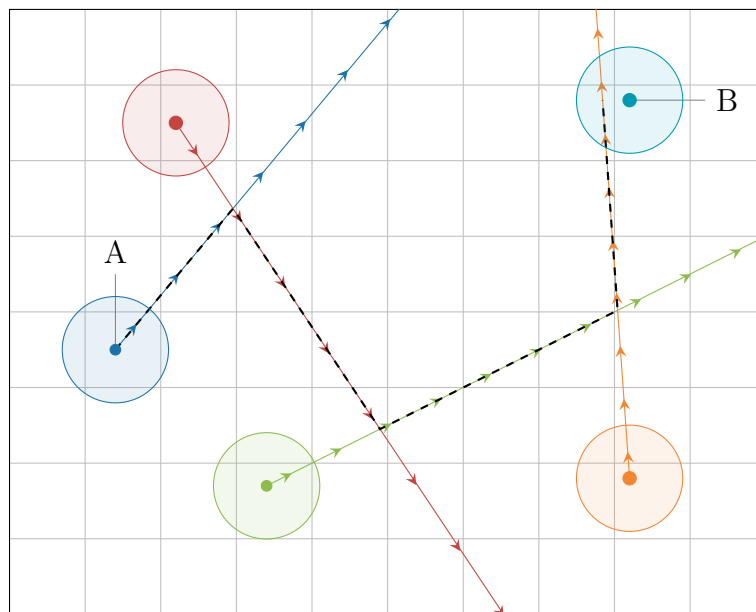


Figure 1.1: Example path of data in an OPNET. Network devices are displayed as dots with their wireless range displayed as circles. The coloured lines show the path each device travels. The dashed line shows the path the data travel to get from device *A* to device *B*.

### 1.1.2   Advantages of OPNETs

**(a) Inexpensive and Convenient**

OPNETs are inexpensive to engineer, with the only hardware cost being the network devices. In their simplest form, devices are made from mass-produced components that are freely available, such as:

- a short-range wireless transceiver,
- memory to store messages,
- a central processing unit (CPU) to manage the components,
- power source (*e.g.* battery).

The chosen components need not be powerful, and can be purchased at low cost. The assembled devices can be small and lightweight—therefore, easily carried by vehicle, animal or person. In fact, many people already carry mobile phones that are suitable for use in OPNETs.

A further cost besides hardware may be the licence required to use certain radio frequencies for communication. However, several frequency bands are available that are free and unlicensed, such as Wi-Fi Direct (Wi-Fi Alliance 2012) or Bluetooth which operates in the 2.4 GHz band (Golmie and Mouveaux 2001).

**(b) Easy Deployment**

OPNETs do not rely on any central infrastructure, such as a server or network backbone. They may be self-configuring and self-organising, meaning only the network devices manage network topology and communications (Misra *et al.* 2009). Because of this, little maintenance is required and human intervention is largely unnecessary besides replacing faulty hardware or recharging batteries. This makes OPNETs an attractive alternative to communication that requires infrastructure, such as cellular networks.

**(c) Robust**

Well configured OPNETs are robust against topology changes and the failure of network devices. If some network devices fail or connections are broken, data can be sent along alternative paths through the network. Furthermore, OPNETs can

accommodate an *abundance* of devices, where many devices attempt to communicate within a small area. This could occur in a football stadium or concert hall, for example. A high device density makes for plenty of communication paths which benefits the network. This is unlike cellular networks, where an abundance of devices may cause the network infrastructure to become overloaded.

**(d) Spatiotemporal Relevance**

Information in an OPNET propagates in the local surrounding area. It usually does not abruptly emerge at disjoint locations, as it might on the Internet or in a cellular network. Equally, OPNET information usually propagates for just a limited amount of time before it disappears from the network (due to the limited data capacity of the network devices). These two factors of spatial and temporal relevance mean that information in an OPNET is usually current. An OPNET user can, therefore, expect that any received information is relevant to their current circumstances.

## 1.1.3   Disadvantages of OPNETs

Due to the network being highly disconnected, delivery of data to a particular recipient in an OPNET cannot be guaranteed. This is especially true in regions of low device density. For the same reason, it is difficult for a sender (and other participating devices) to check if data were successfully received. As well as causing problems with resource consumption, this means OPNETs are not suited to critical communications in which message delivery to a particular recipient is crucial.

Another disadvantage of OPNETs is that the delivery of information may take a long time. This is because there is usually not a direct communication path between a sender and receiver. The delivery of a message relies on new paths being created by the movement of devices, which takes time. Delays in communication may not be a problem for text messages or emails, but it would be unacceptable for voice calls.

Due to their disadvantages, OPNETs may not be suitable for *unicast* transmissions, *i.e.* when a message is sent to one particular device. In unicast transmissions, there could be a single point of failure whereby the sent data do not get received at all. A more suitable transmission type is a *broadcast*, in which messages are spread to as

many devices as possible. Another suitable option is a *multicast* transmission, in which messages are spread to a particular group of devices.

## 1.2 Potential Applications

### 1.2.1 Sensor Networks

A sensor network consists of many wireless devices that use sensors to monitor their surroundings and send their measurements to a central data repository. Sensors can record, among other things, sound, movement or temperature. Recorded data are cooperatively sent to a main location, usually via a wireless network which could be an OPNET. OPNETs could accommodate the fact that some devices may be unreachable for manual maintenance due to the position of the sensors. Most sensor networks can tolerate the disadvantages of OPNETs (see Section 1.1.3), as some delay and data loss is usually acceptable.

One benefit a sensor network would gain from using an OPNET is the ability to accommodate breaks in the network. Such breaks may occur due to broken devices or too much distance between devices for wireless communication to operate. An OPNET is able to cope with this due to the mobility of network devices. For example, static sensor devices could be spread across a mountain by an aeroplane. Some devices may be out of wireless range from any other device and will have no way to communicate. However, if another network device is attached to a mobile agent such as a mountain goat or an unmanned aerial vehicle, it can gather data from isolated devices as the agent moves around the mountain. Figure 1.2 shows an example of such a scenario.
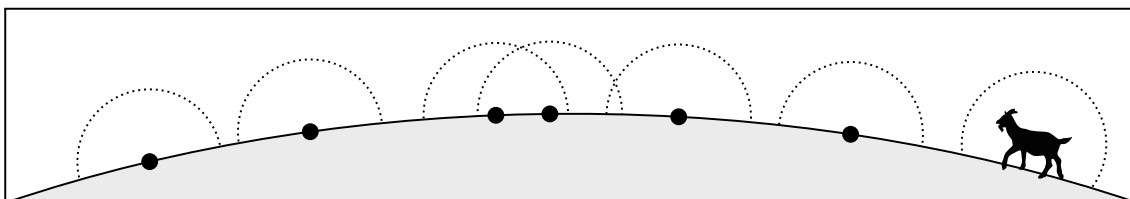


Figure 1.2: Example of coping with a disconnected network. Each black dot represents a static network device (with wireless signal regions shown as dotted circles). The goat carries a mobile device which enables communication between the static devices.

**Deep Ocean Monitoring:** Vahdat and Becker (2000) discuss an example of a sensor network that uses an OPNET for data communication. The network is used to measure temperatures in deep oceans. Sensor devices are attached to seals to gather readings, which are transmitted to a database using an OPNET. The network benefits from the low power consumption of the OPNET devices to enable a lengthy study. This application example shows that OPNETs are useful in situations that are too dangerous or expensive for humans to access.

**Wildlife Monitoring:** Pelusi *et al.* (2006) discuss the use of OPNETs for wildlife monitoring sensor networks. Wildlife monitoring consists of tracking wild species to learn about the behaviour of the animals and how they interact with one another in their natural environment. It is important to ensure that the behaviour of the animals is not affected by the tracking devices; therefore, the devices must be non-intrusive and not require human intervention. OPNET devices can be small, lightweight and require no manual maintenance by humans.

### 1.2.2 Infrastructure Replacement

OPNETs can be used as an alternative to expensive communications infrastructures. Two examples of this are provided below.

**Asynchronous Internet Connection:** It can be difficult to provide a reliable Internet connection to some rural locations. It is disruptive and inconvenient when a wired Internet connection is lost, and it can take weeks before the problem is fixed. In such a situation, OPNETs could be used to provide an intermittent connection to the Internet, satisfying data requests several times a day (Pelusi *et al.* 2006). This is achieved by fitting OPNET devices onto vehicles such as buses, motorcycles or bicycles which regularly travel between rural locations and the city centre. As the devices travel to and from an Internet connection, requests and fulfilments can be exchanged.

**Disaster Recovery:** In the event of a disaster, such as an earthquake or bomb explosion, existing communications infrastructure (such as cellular networks) could be destroyed. In such disasters, effective communication is essential for recovery teams

to work efficiently. An OPNET can be set-up quickly by scattering static devices in the area of the disaster and having recovery workers carry mobile devices.

Attempts are currently in progress to create OPNET communication facilities in disaster situations. The Several Project (Gardner-Stephen and Challans 2012) is developing applications for smartphones to enable opportunistic communications using Wi-Fi technology.

### 1.2.3 Social Networking

Social networks are used by people to socialise with their friends or to meet new friends. Social networks would benefit from OPNETs in densely populated areas. Currently, cellular networks tend to be used for social communication, even if the conversing parties are geographically close. In densely populated areas, such as football stadiums or concert arenas, cellular networks can become overloaded due to the demand. Conversely, an OPNET would actually perform more effectively in the same situation (as discussed in Section 1.1.2).

**Companion Discovery:**   An example of an existing service which would be well-suited to OPNET technology is Grindr (LLC 2012). Grindr is a *smartphone application* that allows people to locate and communicate with compatible people who are geographically nearby. Grindr currently uses the Internet for data transmissions; however, such close-range interactions between mobile devices could be performed by an OPNET.

**Information Service:**   An information service often provides information that is relevant only at a particular time and a particular place. For example, a railway station information service provides information about train times. An OPNET could be used to disseminate train time information from the railway station to the local surrounding area. This would be useful for people who are walking to the station as it would allow them to check the train times before they reach the station.

**Shared Interests:**   OPNETs could be used to target certain types of people and provide them with information which may be of interest to them. For example, people at

an Italian restaurant may wish to share information with each other about similar restaurants nearby.

## 1.3    Area of Research

The aim of this thesis is to better understand the behaviour of OPNETs, specifically how behaviour is affected by certain parameters. The four parameters that have the most significant influence on OPNET behaviour are considered. These parameters will be known as the *fundamental parameters*, and are described in Table 1.1. The fundamental parameters may be grouped into two categories, as described in Table 1.2.

| Parameter | Symbol | Description |
|---|---|---|
| Device density | $\rho$ | The average number of devices per unit area. |
| Device speed | $s$ | The speed at which devices move. |
| Signal radius | $r$ | The radius of the wireless signal range of each device. |
| Transmission time | $\tau$ | The amount of time required to transmit a particular message. This may be directly related to the size of the message. |

Table 1.1: Fundamental parameters.

| Category | Parameters | Description |
|---|---|---|
| Environmental | $\rho$ and $s$ | These parameters exist with or without the presence of an OPNET. |
| Operational | $r$ and $\tau$ | These parameters are only relevant if an OPNET exists. They can be controlled either by the OPNET protocol or by a user of the OPNET. |

Table 1.2: Fundamental parameter categories.

The effects of the fundamental parameters on OPNET behaviour is studied by collecting a series of metrics that would be useful for an engineer who is designing an OPNET. This will allow an engineer to optimise the behaviour of the OPNET according to his/her desires.

Ultimately, the aim is to model the rate at which a message spreads to devices and throughout space and time in terms of the fundamental parameters. This problem can be solved by considering how communication between the network devices is affected by the parameters. For example, a higher device density and device speed

leads to more communication opportunities between devices, which in turn leads to faster dissemination. Similarly, a large signal radius along with a small transmission time helps to ensure a successful message transmission while the devices remain within range of one another.

Rather than modelling message spread directly in terms of the fundamental parameters, device interaction models are used, which are based on the fundamental parameters. Specifically, the rate at which a device comes within communication range of other devices and the length of time devices remain within range is considered.

As well as the spread of a message, the practicality of OPNET technology is of interest. System resources must be used efficiently if OPNETs are to be useful. For this reason, several *interaction schemes* are experimented with, which define the way in which devices manage messages in the network.

Certain interaction schemes allow devices to remove a message from its buffer after a certain amount of time. This is an important aspect of an OPNET as it can prevent the buffer of a device becoming full. It also prevents old messages that may be outdated from remaining in the network. There is a fine balance in how quickly to remove messages, however, as removing a message too quickly will inhibit its dissemination. This behaviour is studied according to a *deletion rate*, $\delta$, which defines the probability per second that a device removes a message from its buffer.

### 1.3.1 Key Contributions

A key original contribution of this thesis is that the applications and experiments are embedded in the acknowledgement that data transmissions are non-instantaneous. The majority of state-of-the-art research on OPNETs makes the simplifying assumption that wireless data transmission occur instantaneously. This thesis instead aims to discover how transmission time affects the behaviour of OPNETs. Transmission time is an important aspect to consider as file sizes are getting ever larger, with the increasing quality of music, video and photographs. It is true that wireless communication is also getting faster, however, data still takes a significant amount of time to transmit. This has an impact on OPNETs as data are only sent during a window of opportunity, so lengthy transmissions may not complete in time. Equally, efficient use of resources

is an important aspect of OPNETs; therefore, transmission speed may be limited in order to save battery power. In this thesis, particular attention is paid to the transmission time parameter, $\tau$, and its effects on data dissemination.

### 1.3.2 Research Hypothesis

The rate and extent of information dissemination in OPNETs can be modelled in terms of four fundamental parameters: the device density ($\rho$), the wireless transmission range ($r$), the speed of the devices ($s$) and the message transmission time ($\tau$). The performance of an OPNET can be optimised by choosing appropriate values of these parameters.

## 1.4 Motivation

As discussed in Section 1.2, there is great potential for widespread OPNET use; however, this has yet to happen. One reason for this may be that there is currently no way of estimating the success of message propagation. For example, the following questions cannot yet be answered accurately:

- If a message is released in an OPNET (with known values of the fundamental parameters) at position $x$ and time $t$, what is the probability that it arrives at position $x'$ before time $t'$?
- If a message is released in a closed environment, what percentage of devices are expected to receive it after a certain time interval has elapsed?
- When and where should a message be introduced to ensure maximum dissemination in the shortest possible time?

To be able to answer questions like these, a thorough understanding of message propagation is required. Some benefits related to data propagation modelling will now be discussed.

### (a) Appeal

OPNETs will become more appealing to potential users if propagation behaviour can be modelled accurately. For example, an organisation is more likely to deploy an

OPNET if it knows that 65–75% of its target audience will receive the information, rather than a completely unknown percentage.

### (b) Optimisation

OPNET models can be used to optimise certain operational parameters. For example, they could be used to find the best time and place to introduce a message in a particular situation. Models can also be used in the development of communication protocols, *i.e.* the set of rules each device follows to make decisions regarding communication. For example, it may be discovered that the following rules make for more efficient message dissemination:

- Do not attempt to transmit a message if less than 50% of devices are within range for less than the required transmission time.
- Only accept 20% of message offers if the rate of offers exceeds five per minute.
- Do not accept a copy of a message less than 1 hour after deleting a previously held copy of the message.

### (c) Cost Reduction

Savings on cost and resources can be achieved with the use of OPNET models. For example, an OPNET engineer would be able to decide on the cheapest hardware available that would still provide the required service quality. Battery life can be preserved with well designed communication protocols that decide whether the next transmission attempt will be worth the power required.

## 1.5  Approach

The area of research is approached by creating a series of OPNET models of increasing complexity. The developed models will represent a complete OPNET, incorporating device communication and the underlying movement of devices. A mixture of theoretical and empirical models will be used; as explained in the following section.

### 1.5.1 Theoretical vs. Empirical Models

OPNETs can be modelled empirically or theoretically. Empirical models can be gathered from real-world experiments or from simulation. Simulations provide an idealistic environment for experimentation, unlike real-world experiments in which the behaviour of a network is affected by many additional factors, such as radio interference. In the context of this thesis, real-world experiments are impractical due to complexity and expense; therefore, simulations are used for all empirical models.

The theoretical models developed in this thesis are comprised of mathematical analytic expressions. The models are based on the general principles of interacting particle systems, and for this reason, devices will be referred to as *particles* throughout this thesis (unless discussed in context of a network). Firstly, well-known compartmental models of epidemic modelling are used. Then, ideas from the kinetic theory of gases are adapted to incorporate a spacial component. The developed models are verified with simulations. Simulations are also used to more thoroughly investigate aspects of the system which are difficult to solve analytically.

A major difference between simulations and analytic expressions is the computational complexity. Simulations are generally far more expensive to compute than equations. This is especially true for Monte Carlo experiments, in which non-deterministic simulations are performed many times and the accuracy of the drawn conclusions depends on the number of simulated trials. It is possible for device protocols to make use of models when making certain decisions (such as those listed in Section 1.4). In this case, it would be impractical for a device to run a batch of simulations every time it needs to make a decision. An analytic expression would be preferable in this situation.

### 1.5.2 Mobility Models

Ideally, the used mobility models will accurately represent the movement of real-world objects. A range of mobility models of increasing complexity are used. Throughout the progression onto more complex models, it becomes clear how the characteristics of the models scale. This allows observations about how an OPNET may react to highly complex movement in real-world scenarios.

The used mobility models will include those where particle movement is confined

to a graph. Movement in discrete space and continuous space is also modelled. Furthermore, models will be provided for 1D and 2D space.

## 1.6   Thesis Outline

**Chapter 2. Background:** Relevant information is provided to allow the reader to understand the research in this thesis. A large part of this information relates to particle movement; however, spatial and temporal considerations, along with communication protocols are also discussed. Following this, a comparison is made between the area of research and those of similar systems. Finally, state-of-the-art research on related topics is presented and reviewed.

**Chapter 3. Non-Spatial Models:** In this chapter, particle movement is constrained to graphs, and communication can only take place between pairs of particles that are at the same graph vertex. In this chapter, analytic and simulated models are created for particle interaction and subsequently, message spread between particles.

**Chapter 4. Discrete Spatial Models:** Similarly to the previous chapter, models are created for particle interaction and message spread. However, in this chapter, particles move on a discrete lattice in 1D and 2D space.

**Chapter 5. Continuous Spatial Models:** This chapter is similar to the previous chapter, except particles move in continuous space. In this chapter, an extension is developed for the work of Klein *et al.* (2010), which uses a reaction-diffusion equation to model message spread in space and time, as explained in Section 2.8.3.

**Chapter 6. Conclusions:** The thesis is summarised, evaluated and concluded in this final chapter. Potential topics for future work are proposed and discussed.

# CHAPTER 2

# Background

This chapter provides the context against which the research is presented. Information such as similar systems, particle movement and empirical/theoretical models are discussed in detail. Following this, a review of current literature relating to the subject of this thesis is presented.

## 2.1 Epidemic Models

Drawing on the research of related systems can be useful, especially for a young research topic like OPNETs. A related system with vast amounts of research can be found in the field of epidemiology (Zhang *et al.* 2007). Epidemiology is the study of epidemics—a widespread biological disease in a population. Specifically, the point at which a disease becomes an epidemic is not well-defined. It could be judged by the number of individuals affected, or by the length of time for which the disease persists (or a combination of the two).

### 2.1.1 Chromatic States

In epidemic models, or *SIR models*, individuals in the population are categorised into a number of *states* (Nelson and Williams 2007):

**Susceptible (S):** Individuals who are capable of contracting the disease but are yet to do so.

15

**Infectious (I):** Individuals who have contracted the disease, are carrying the disease and are capable of infecting others with the disease.

**Recovered (R):** Individuals who have recovered from the disease and are now immune to further infections.

States S, I and R are referred to as the *chromatic states*. This term is used to relate the states to colours, in a similar way to how each states in a forest fire model is assigned a colour. A forest fire model is a cellular automaton in which each cell is either a green tree that is susceptible to fire, a red tree which is on fire or a blue tree which has been extinguished. The fire spreads at random to nearby trees, which are eventually extinguished after some time. This system is comparable to the way in which a disease spreads in a population or a message spreads in an OPNET. Specifically, green, red and blue trees are similar to S, I and R individuals, respectively. For this reason, the following colours are assigned to the chromatic states:

- S: green
- I: red
- R: blue

These colours will be used throughout the thesis in diagrams and plots.

## 2.1.2 Epidemic Models Applied to OPNETs

| Epidemic term | OPNET term |
|---|---|
| Individual | Device (referred to as *particles* in this thesis). |
| Disease | Message. |
| Susceptible | A device that is yet to receive a particular message. |
| Infectious | A device that has received and is spreading the message. |
| Recovered | A device that has erased a message and will not accept it again. |

Table 2.1: Terms from epidemiology used to describe elements of an OPNET.

The discussed terms from epidemiology are related to OPNETs as follows: a message in an OPNET can be seen as similar to a disease spreading in a population. For this reason, a device that is carrying and spreading a message is referred to as *infectious*. Similarly, a device that has not got the message but would accept it is referred to as

*susceptible*. Finally, a device that has not got the message and would not accept it is referred to as *recovered*. This naming scheme is summarised in Table 2.1.

A key difference between epidemiology and OPNETs is that in epidemics, it is generally desirable to inhibit propagation. The opposite is true for OPNETs.

### 2.1.3  Chromatic State Cycle
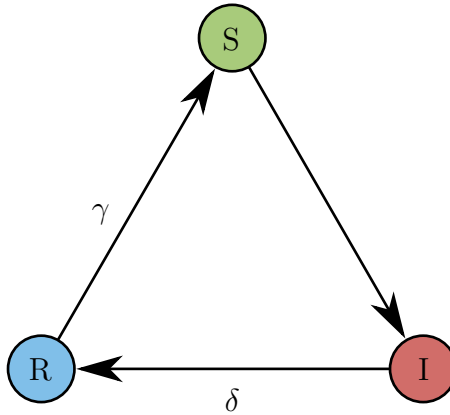


Figure 2.1: Diagram to show the ordering and probability per second of the chromatic state transitions. Note that $\beta$ is not displayed as the S $\rightarrow$ I state transition is also dependent on whether an infectious devices is present.

Figure 2.1 shows the chromatic state transition cycle that individuals/devices follow. Each of these state transitions are discussed as follows.

**I $\rightarrow$ R:**  In epidemic models, an infectious individual (I) may recover (R) from the disease at a certain rate. In an OPNET, this would be equivalent to a device deleting a message from its buffer and refusing to accept the same message again. As discussed in Section 1.3, the probability per second of state transition I $\rightarrow$ R is denoted as $\delta$, the deletion rate.

**R $\rightarrow$ S:**  After some time, a recovered individual (R) may become susceptible (S) to the disease once again. In an OPNET, this would be the equivalent of a device no longer refusing to accept a certain message. The term $\gamma$ is used to denote the probability per second of state transition R $\rightarrow$ S.

**S $\rightarrow$ I:**  A susceptible (S) individual may contract the disease and become infectious (I). This is equivalent to an OPNET device receiving a message. The occurrence of

this state transition (S → I) is more complex to model than the other two state transitions as it relies on the participation of another individual, namely an infectious individual. The term $\beta$ is used to denote the probability per second that a susceptible device receives a particular message, given that it is within communication range of another device that has the message. The aim is to learn more about this state transition throughout this thesis.

### 2.1.4 SIR Models

A variety of epidemic models can be specified by setting the values of $\delta$ and $\gamma$ appropriately. The three most significant variations are described in Table 2.2. Note that the SIR model and all variations will be referred to as *interaction schemes* when used in the context of OPNETs.

| Cycle | $\delta$ | $\gamma$ | Description |
|-------|----------|----------|-------------|
| SI | $\delta = 0$ | N/A | Once infected, an individual cannot recover from the disease. They remain infectious indefinitely. |
| SIS | $0 < \delta < 1$ | $\gamma = 1$ | A disease can be contracted multiple times. Once recovered, an individual becomes susceptible again, rather than immune. |
| SIRS | $0 < \delta < 1$ | $0 < \gamma < 1$ | Immunity is temporary. Once recovered, an individual becomes immune to the disease for a period of time before returning to the susceptible state. |

Table 2.2: Table of various types of epidemic models.

### 2.1.5 Epidemic Threshold

The epidemic threshold is the point at which the system parameters are only just suitable enough for an epidemic to occur. An epidemic is likely to occur if the parameters are any higher than the threshold, and unlikely to occur if the parameters are lower. For example, a population density of 0.01 individuals per square metre could be an epidemic threshold.

### 2.1.6 Existing Research

In this section, literature in the field of epidemiology which may be beneficial in the study of OPNETs is reviewed.

## Epidemics

Various mathematical models for epidemics are provided by Kermack and McKendrick (1927). A key focus of their paper is on epidemic thresholds, which are studied with regard to population density and rate of infection. Further mathematical models can be found in Brauer *et al.* (2008), which aims to provide an introduction to mathematical epidemiology. In this paper, studies are performed on the epidemic size, the introduction and removal of individuals, the isolation of infectious individuals, and endemic equilibria (meaning the disease steadily persists in the population). Neither Kermack and McKendrick (1927) nor Brauer *et al.* (2008) attempt to relate models to computer networks; therefore, leaving potential to extend this work.

Stehlé *et al.* (2011) introduce the *exposed* (E) state to the SIR model, forming an SEIR epidemic model. The exposed state represents an incubation period that occurs when an individual has contracted the disease but is not yet infectious. This creates a delay in the spread of the disease which is similar to non-instantaneous transmissions in OPNETs (see Section 1.3.1), except that an exposed individual becomes infectious regardless of whether it remains in contact with other infectious individuals.

## Social Diffusion

Research from the field of epidemiology can also be used to study the diffusion of information, such as beliefs or marketing. In Arndt (1967), diffusion of information via word-of-mouth comments is studied. The study aims to find how product sales are affected by word-of-mouth comments. A 16 day field test was performed in which participants received a money-off coupon for a particular food product in a local shop. 42% of participants purchased the product within the 16 days. The buyers were then interviewed to find whether their choice was influenced by word-of-mouth comments. The study reveals that positive comments benefit product sales while negative comments hinder sales.

A similar topic is addressed in Bass (1969). In this paper, a theoretical model is derived for the forecast of product sales, based on the previous number of buyers. The mathematics used in the theoretical model is based on the diffusion of information and stems from the field of epidemiology. The theoretical model is verified with empirical data gathered for eleven different products.

In Khelil *et al.* (2002), a simple SI model is applied to a simulated MANET. A study is performed on how particle density affects data propagation. Using the least squares method, a curve is fitted to the simulation results to produce an analytic expression for data propagation. This analytic expression is derived for use with the Random Waypoint (RWP) mobility model with specific parameter values (see Section 2.3.3.4). A limitation of this is that it may not extend to other mobility models.

Similar research can be found in Scellato *et al.* (2007), in which SIR and SIS interaction schemes are used with a simulated MANET. Again, the RWP model is used in the studies. Additionally, movement traces from CRAWDAD—a website that archives wireless network data (Kotz *et al.* 2004)—are used in the simulations. This research shows that both the SIR and SIS models spread messages at the same rate, however, the SIR model yields fewer message duplications. Therefore, the SIR model can reach the same number of devices with fewer transmissions. This is a useful finding in the interest of energy conservation. The SIR model will be studied in more detail in Section 2.2.4.

## 2.2   Study on Epidemic Models

This section studies the epidemic models discussed in Section 2.1. The equilibria of these systems is investigated and their behaviour in the context of OPNETs is discussed. This work is presented as a reflection on the literature discussed in Section 2.1, framed specifically in the context of OPNETs. Note that epidemic models are not perfectly suited for use with OPNETs; however, they are used to illustrate the approach.

Recall the epidemic models described in Section 2.1, where at any time a particle may be susceptible (S) or infectious (I) depending on whether they are carrying the message. Additionally, if the model allows, particles may be in a recovered (R) state in which they have received the message but are no longer spreading it. Therefore, the state of each particle is an element of the set $\{S, I, R\}$ and the state of the system consisting of $N$ particles can be represented by a vector of length $N$, over this set. The set $\{S, I, R\}^N$ is the state space of the system.

The states S, I and R are referred to collectively as the *chromatic states*. The terms $S(t)$, $I(t)$ and $R(t)$ will be defined as the respective proportions of S, I and R particles at time $t$. Therefore, at time $t$, there are $NS(t)$ susceptible particles in the system and likewise for $I(t)$ and $R(t)$. Only closed systems are considered, in which particles cannot enter or leave. The following expresses the *conservation of particles*:

$$S(t) + I(t) + R(t) = 1 \text{ for all } t \geq 0. \tag{2.1}$$

For continuous time models (see Section 2.5), $\dot{S}(t) = \frac{\mathrm{d}S}{\mathrm{d}t}$ will be used to denote the rate of change in the proportion of susceptible particles (with respect to time) at time $t$. In a similar fashion, $\dot{I}(t) = \frac{\mathrm{d}I}{\mathrm{d}t}$ and $\dot{R}(t) = \frac{\mathrm{d}R}{\mathrm{d}t}$. A steady state occurs when $\left(\dot{S}(t), \dot{I}(t), \dot{R}(t)\right) = (0, 0, 0)$, *i.e.* the proportion of each chromatic state does not change with time.

## 2.2.1  Equilibria

Throughout this thesis, the distinction between *stable* and *unstable* equilibria is made. When the system is in a stable equilibrium, it will tend to revert to this state after a small perturbation. Conversely, any perturbation to the system state when in an unstable equilibrium will cause the system to move away from the steady state. See Fig. 2.2 for an illustration comparing these types of equilibria.
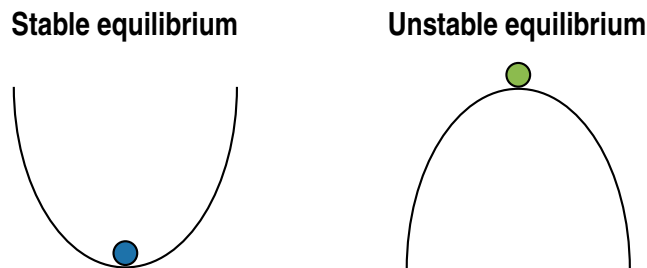


Figure 2.2: Diagram to show the difference between stable and unstable equilibria.

Throughout the thesis, experiments of a stochastic nature are considered. This allows the unstable equilibrium to be reached, unlike in a deterministic model. The unstable equilibrium is reached when the source particle recovers before infecting other particles. In other cases, it is reached after a few particles become infected initially but recover in the early stages, leaving no copies of the message in the system. Different parameter values lead to a different probability of reaching the unstable equilibrium.

### 2.2.2 Urn Models

The following four subsections explore different models of interaction between particles. These models are based on the well-known *Urn models* of probability theory. Particles will be called *balls* for the purpose of this discussion.

Consider a system consisting of $n$ urns, and suppose that $N$ balls are distributed uniformly and independently among urns. At every time-step, each ball independently moves to a randomly chosen urn with probability $\theta$. This is a closed system, meaning no balls can enter or exit the system.

The spread of a single message within this system is studied. Initially, all balls are in the susceptible state, except for a single infectious ball known as the *source ball*. At each time-step, $N$ pairs of balls are chosen at random (from the entire system, not individual urns). Therefore, some balls may be chosen several times, and others not at all. If any of the pairs of balls happen to be in the same urn, they are considered *within range*. If one of these balls is infectious and the other is susceptible, an attempt is made to infect the susceptible ball, succeeding with probability $\tau^{-1}$.

Depending on the interaction scheme, infectious balls may change to the recovered state with probability $\delta$ per second. Similarly, the interaction scheme may allow recovered balls to become susceptible. In this case, each recovered ball becomes susceptible with probability $\gamma$ per second.

A steady state occurs when the net change in the number of infectious, susceptible and recovered balls is zero. The aim is to theoretically find the steady state of the system for the following types of interaction schemes: SI, SIR, SIS, SIRS. The developed theoretical models will be verified by simulation. Table 2.3 lists the default parameter values used for all simulations. These values were decided by trial and error using preliminary simulations. Depending on the interaction scheme, the values of $\delta$ and $\gamma$ may differ or may be irrelevant. All deviations from the default values will be made explicit in the relevant subsections.

### 2.2.3 SI Model

In the SI model, infectious particles cannot recover or revert to the susceptible state. In this case $\delta = 0$, therefore $R = 0$ and $\gamma$ becomes irrelevant. The following system

| Parameter | Default Value |
| --- | --- |
| $N$ | 100 |
| $n$ | 100 |
| $\theta$ | 0.1 |
| $\tau$ | 30 |
| $\delta$ | 0.002 |
| $\gamma$ | 0.005 |

Table 2.3: Default parameter values used for the Urn models.

of ordinary differential equations (ODEs) describes the dynamics of the system state (S, I, R) for continuous time:

$$\dot{S}(t) = -\beta S(t)I(t),$$
$$\dot{I}(t) = \beta S(t)I(t),$$
$$\dot{R}(t) = 0,$$

where $\beta$ is some combination of the contact rate and contact duration distribution (as discussed in Section 2.1.3) and, therefore, indicates the probability per second of becoming infectious.

The solution of this system of ODEs yields an expression for $I(t)$ which is a logistic equation, meaning growth is exponential in the initial stages but slows and only reaches 1 as $t \to \infty$. The steady states are found by solving $\dot{S} = \dot{I} = 0$, which gives:

$$\beta S(t)I(t) = 0. \tag{2.2}$$

Therefore, either $S(t) = 0$ or $I(t) = 0$. From Eq. (2.1) (conservation of particles), the corresponding values of $S(t)$ and $I(t)$ can be found, leading to the following solutions for the steady state:

$$\big(S(t), I(t)\big) = \begin{cases} (1,0) & \text{(unstable equilibrium)} \\ (0,1) & \text{(stable equilibrium)} \end{cases}$$

The unstable equilibrium can only occur if the message has not yet been introduced into the system, because under the SI model, a single infectious particle will remain infectious, making it impossible to return to a state where all particles are in the

susceptible state. This equilibrium is unstable as a single infectious particle will cause the system to move away from this state. When the system is in the stable equilibrium, all particles are infectious and the system will return to this state if more susceptible particles are introduced.

Figure 2.3 presents the results of 30 and 200 simulations using the SI model. From these results, it is clear that the message eventually reaches all particles, which then remain infectious indefinitely.



(a) 30 separate results.      (b) Average of 200 results.
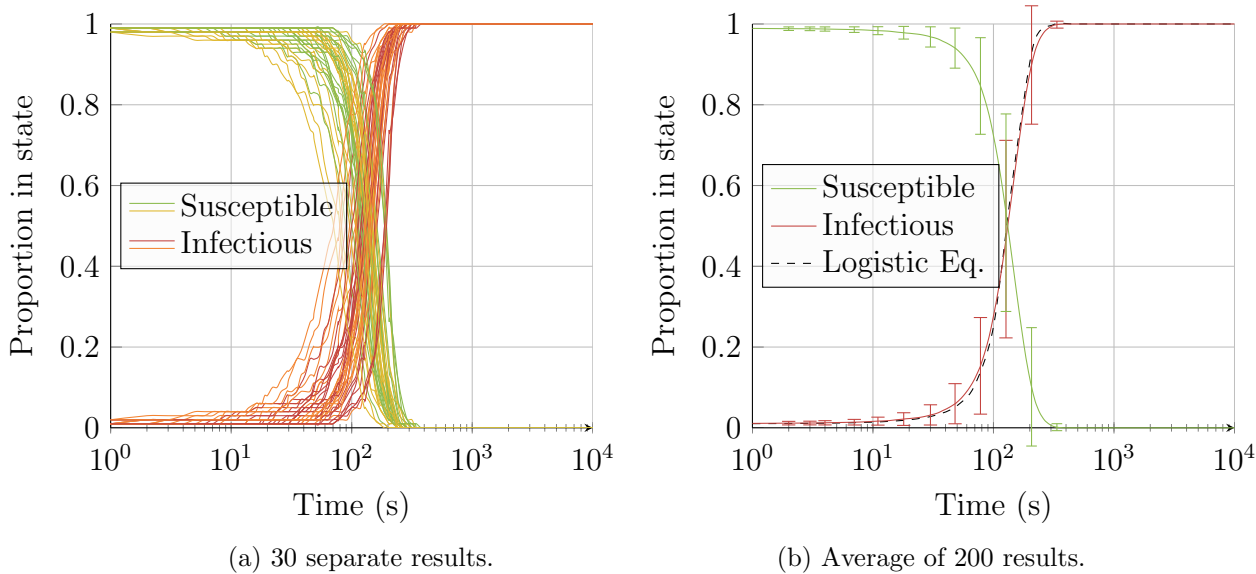
Figure 2.3: Graphs to show results of several simulations using the SI model. 30 separate results are shown in sub-figure (a), while sub-figure (b) shows the average of 200 results with standard deviation error bars. A logistic equation has been fitted to sub-figure (b), with $\beta$ manually approximated at 0.035, as explained in Section 2.2.3.1. All simulations use an Urn model with the parameter values listed in Table 2.3 and $\delta = 0$.

### 2.2.3.1  Fitting a Logistic Equation

The term $\beta$ can be approximated by fitting a logistic equation to sub-figure (b) in Fig. 2.3. Recall that:

$$\frac{\mathrm{d}I(t)}{\mathrm{d}t} = \beta I(t)\big(1 - I(t)\big).$$

24

Rearrange to get:

$$\frac{1}{I(t)\big(1 - I(t)\big)} \frac{\mathrm{d}I(t)}{\mathrm{d}t} = \beta.$$

Both sides are integrated with respect to $t$, as follows:

$$\int_{I(0)}^{I(t)} \frac{1}{I(t)\big(1 - I(t)\big)} \,\mathrm{d}I(t) = \int_0^t \beta \,\mathrm{d}t.$$

Evaluating this integral (by partial fractions for the left-hand side) leads to:

$$ln\left(\frac{I(t)}{I(0)} \cdot \frac{1 - I(0)}{1 - I(t)}\right) = \beta t$$

$$\frac{I(t)}{I(0)} \cdot \frac{1 - I(0)}{1 - I(t)} = e^{\beta t}.$$

Rearrange to isolate $I(t)$ as follows (see Austin *et al.* (1998) for a full derivation):

$$I(t) = \frac{I(0)}{\big(1 - I(0)\big)e^{-\beta t} + I(0)}.$$

This equation is plotted in Fig. 2.3 with the name *Logistic Eq.* The value of $\beta$ is manually approximated by eye as 0.035.

> The behaviour of the SI model is not desirable for OPNETS. If all devices eventually receive the message then carry it indefinitely, less of the limited buffer space is available for other messages. Furthermore, it is not useful to carry the same message forever as it will invariably become irrelevant over time.

### 2.2.4  SIR Model

In the standard SIR model, infectious particles can recover (with probability $\delta$ per second) but, as with the SI model, particles cannot return to the susceptible state ($\gamma = 0$). The following system of equations shows the evolution of the system state:

$$\dot{S}(t) = -\beta S(t)I(t),$$
$$\dot{I}(t) = \beta S(t)I(t) - \delta I(t),$$
$$\dot{R}(t) = \delta I(t).$$
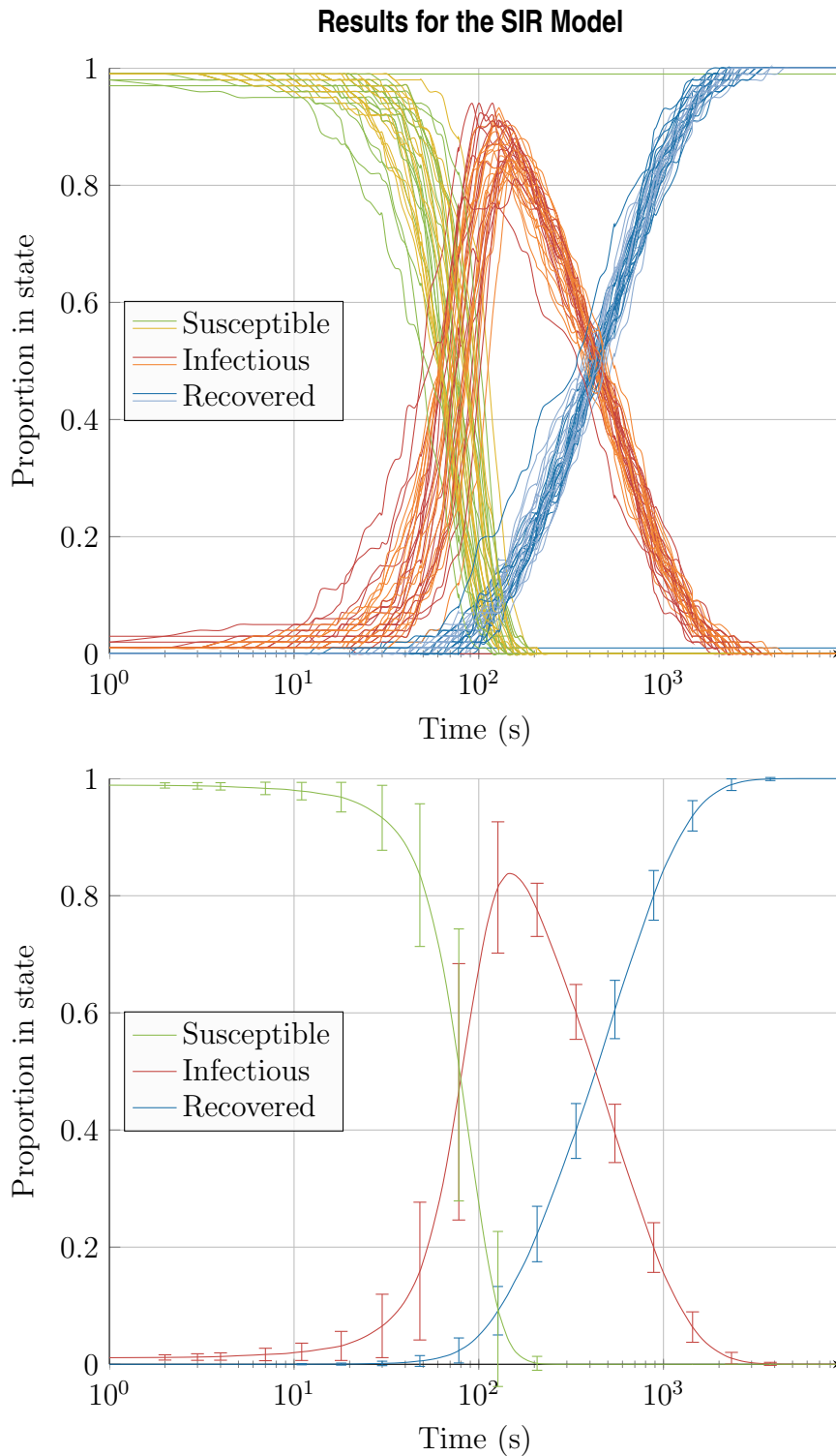
Figure 2.4: Graph to show the results of simulations using the SIR model. The individual results of 40 simulations are shown at the top; the average of 200 simulations is shown at the bottom with standard deviation error bars. 3% of results were not included in the averages as they led to the unstable equilibrium (an example of which can be seen in the upper plot). All simulations use an Urn model with the parameter values listed in Table 2.3 and $\gamma = 0$.

Setting $\dot{S}(t) = \dot{I}(t) = \dot{R}(t) = 0$ gives:

$$-\beta S(t)I(t) = 0,$$

$$\beta S(t)I(t) - \delta I(t) = 0,$$

$$\delta I(t) = 0.$$

From this, it is clear that a steady state occurs only when $I(t) = 0$. In this case, $S(t)$ and $R(t)$ can take any value that satisfies $S(t) + R(t) = 1$. This is to be expected as state changes can only occur if infectious particles are present.

Figure 2.4 shows the results of 40 and 200 simulations using the SIR model. From the results, it is clear that the number of infectious particles peaks then reduces to zero. Note that in some runs of the simulator, only one particle becomes infectious, namely the "source particle". Such cases occur when the initial infective undergoes a transition to the recovered state before it has infected any other particles.

## 2.2.5   SIS Model

In the SIS model, infectious particles cannot enter the recovered state, but they can revert to the susceptible state with probability $\delta$ per second. In this case, $\gamma = 1$ and $R = 0$. The following system of equations shows the evolution of the system state:

$$\dot{S}(t) = -\beta S(t)I(t) + \delta I(t),$$

$$\dot{I}(t) = \beta S(t)I(t) - \delta I(t),$$

$$\dot{R}(t) = 0.$$

Setting $\dot{S}(t) = \dot{I}(t) = 0$ gives

$$I(t)(\beta S(t) - \delta) = 0. \tag{2.3}$$

Therefore, either $I(t) = 0$ or $S(t) = \frac{\delta}{\beta}$. Substituting these values into Eq. (2.1) provides the following solutions:

$$\left(S(t), I(t)\right) = \begin{cases} (1, 0) & \text{(unstable equilibrium)} \\ \left(\frac{\delta}{\beta}, 1 - \frac{\delta}{\beta}\right) & \text{(stable equilibrium)} \end{cases}$$
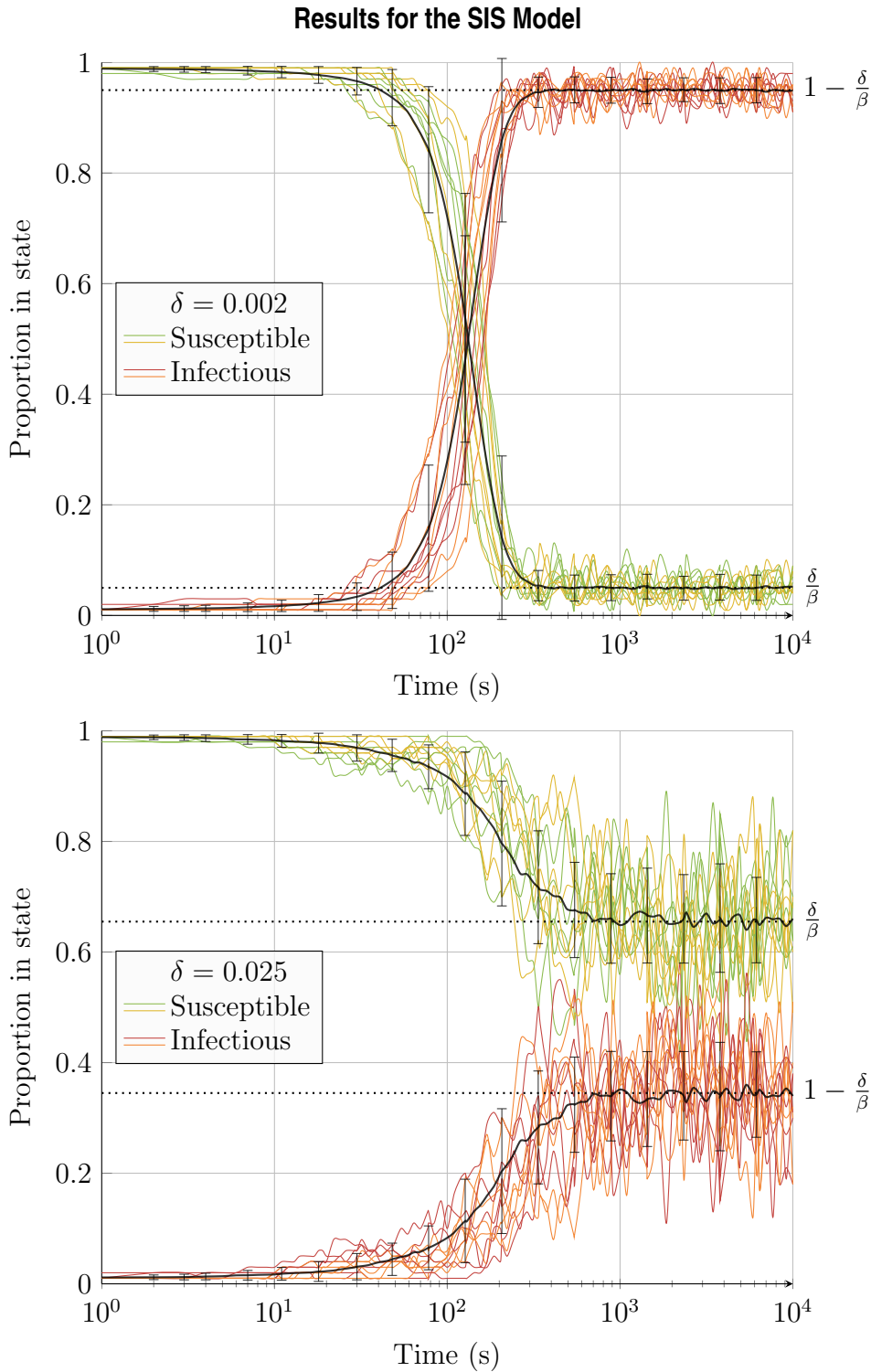
Figure 2.5: Graphs to show the stable equilibrium for an Urn model with the SIS interaction scheme. The upper plot uses the parameters listed in Table 2.3 (and $\gamma = 1$). The lower plot only deviates from these parameter values in that $\delta = 0.025$. Each plot shows 12 individual results with the average of 200 results overlaid in black (with standard deviation error bars). All simulations ending in the unstable equilibrium were discarded (5% and 65% for upper and lower plots, respectively) to prevent the mean being skewed. Dotted lines show theoretical model with $\beta = 0.040$ and 0.038 for upper and lower plots, respectively (approximated by eye).

As with the SI model from Section 2.2.3, the unstable equilibrium occurs when all particles are susceptible. However, unlike the SI model, the system can return to this state after the initial infectious particle has been introduced. The stable solution is achieved with the correct balance of susceptible and infectious particles. This solution is tested with computer simulation, the results of which can be seen in Fig. 2.5.

First, the upper plot of Fig. 2.5 are considered. Simulations for this plot use the parameter values listed in Table 2.3. The plot shows 12 individual simulation results with the average of 200 results overlaid in black (with standard deviation error bars). It is clear that there is a high proportion of infectious particles in the steady state, given the chosen parameter values.

> An engineer may wish to control the proportion of infectious devices in the steady state. In an OPNET, a lower proportion of infectious devices would save resources whilst maintaining the presence of the message in the system. To show how this can be achieved, $\delta$ is adjusted from 0.002 to 0.025 and the results are shown in the lower plot of Fig. 2.5.

From the plots, it can be seen that the state of the system oscillates around the steady state. Note that if a large value is set for $\frac{\delta}{\beta}$ (*i.e.* just below 1), the oscillations may cause $I(t)$ to return to zero. If so, the system will return to the unstable equilibrium and stay there. This was the case for many of the simulated results, however, these results were omitted from the plots, as discussed in the figure caption. In practice, an engineer might want to guard against this outcome by choosing a smaller value of $\delta$. Alternatively, $\delta$ could be adjusted as a function of time—slowly eradicating the message from the system as the message ages.

> The behaviour of the SIS model is more suitable for OPNETs than the SI model as devices are not required to carry messages indefinitely. Instead, there is a steady presence of the message in the network provided the deletion rate is chosen appropriately. However, it is possible for the same device to receive this message many times. This may waste resources, or it could be advantageous in the interest of keeping the message available in the network.

## 2.2.6  SIRS Model

In the SIRS model, infectious particles recover with probability $\delta > 0$ and remain immune to further infections for a certain time period. However, recovered particles return to the susceptible state with probability $\gamma > 0$ per time-step. The following system of equations describes the state transitions for continuous time:

$$\dot{S}(t) = -\beta S(t)I(t) + \gamma R(t),$$
$$\dot{I}(t) = \beta S(t)I(t) - \delta I(t),$$
$$\dot{R}(t) = \delta I(t) - \gamma R(t).$$

Setting $\dot{S}(t) = \dot{I}(t) = \dot{R}(t) = 0$ gives:

$$-\beta S(t)I(t) + \gamma R(t) = 0, \tag{2.4}$$
$$I(t) \cdot \big(\beta S(t) - \delta\big) = 0, \tag{2.5}$$
$$\delta I(t) - \gamma R(t) = 0. \tag{2.6}$$

There are two solutions to this system:

**Solution 1:**  Let $I(t) = 0$ to satisfy Eq. (2.5). From Eq. (2.6) it follows that $R(t) = 0$. From Eq. (2.1) it then follows that $S(t) = 1$; therefore, a steady state is $\big(S(t), I(t), R(t)\big) = (1, 0, 0)$.

**Solution 2:**  Let $S(t) = \frac{\delta}{\beta}$ to satisfy Eq. (2.5). Substituting this into Eq. (2.1) shows that $R(t) = \left(1 - \frac{\delta}{\beta}\right) - I(t)$. From Eq. (2.6) it follows that $R(t) = \frac{\delta}{\gamma}I(t)$. Equating these two expressions for $R(t)$ gives:

$$\left(1 - \frac{\delta}{\beta}\right) - I(t) = \frac{\delta}{\gamma}I(t)$$
$$\left(1 - \frac{\delta}{\beta}\right) = \left(1 + \frac{\delta}{\gamma}\right)I(t)$$
$$\frac{\beta - \delta}{\beta} = \frac{\gamma + \delta}{\gamma} \cdot I(t)$$
$$I(t) = \frac{\gamma(\beta - \delta)}{\beta(\gamma + \delta)}. \tag{2.7}$$
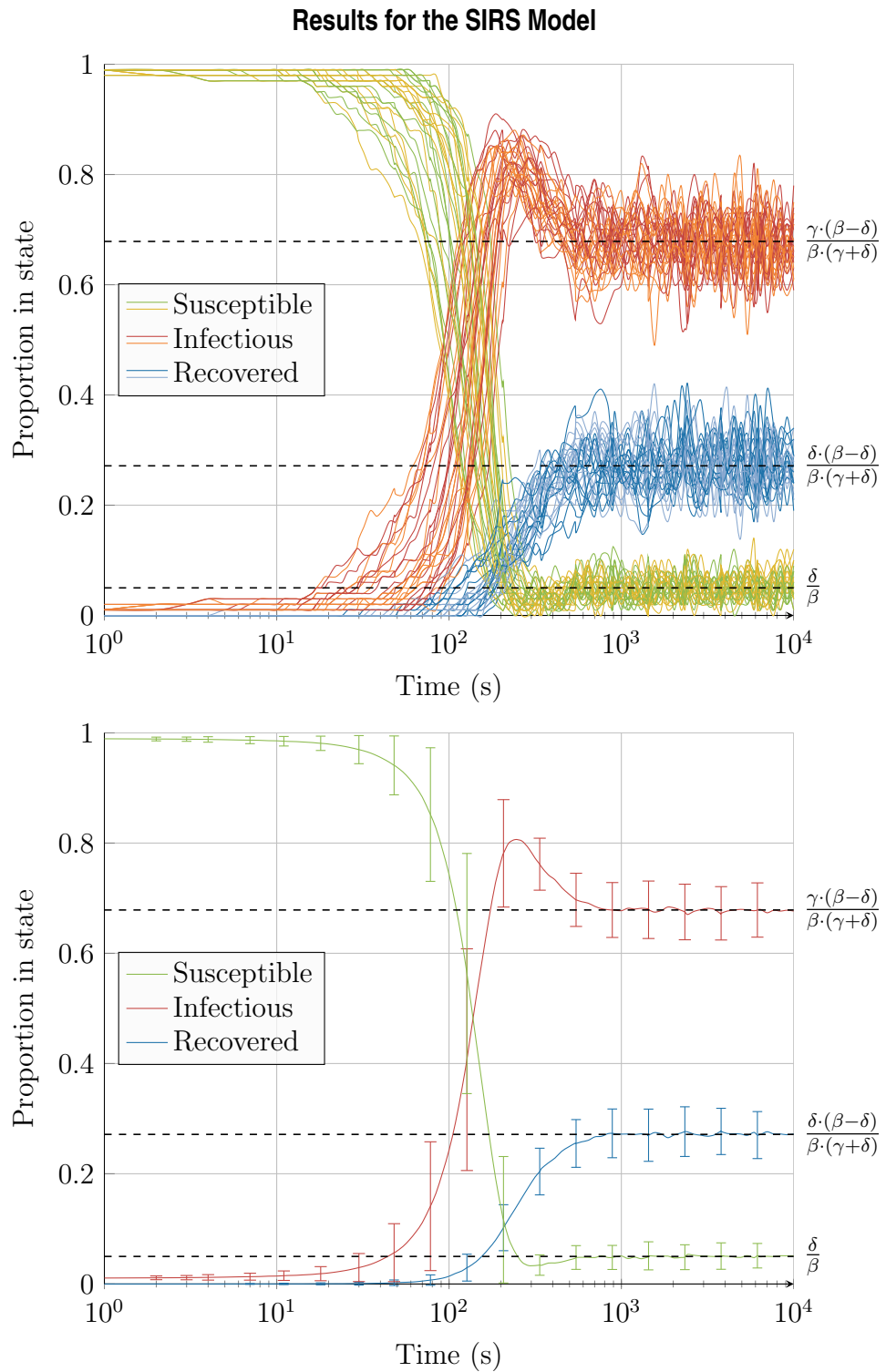
Figure 2.6: Graphs to show how the system converges to the stable equilibrium in the SIRS model. The individual results of 20 simulations are shown at the top; the average of 200 simulations is shown at the bottom with standard deviation error bars. 8% of results are discarded as they led to the unstable equilibrium. All simulations use an Urn model with the parameter values listed in Table 2.3. Dashed lines show theoretical estimates with $\beta = 0.04$ (approximated by eye).

Substituting Eq. (2.7) into Eq. (2.6) shows that $R(t) = \dfrac{\delta(\beta - \delta)}{\beta(\gamma + \delta)}$. Therefore, a steady state of the SIRS model is:

$$\big(S(t), I(t), R(t)\big) = \left( \frac{\delta}{\beta}, \frac{\gamma(\beta - \delta)}{\beta(\gamma + \delta)}, \frac{\delta(\beta - \delta)}{\beta(\gamma + \delta)} \right). \tag{2.8}$$

This solution is tested with computer simulations, the results of which can be seen in Fig. 2.6. Note that 8% of simulations led to the unstable equilibrium (see Section 2.2.1) and were omitted from the plots to prevent the mean being skewed. The results show a steady ratio of S, I and R particles. Like the SIS model, this interaction scheme is efficient on resources whilst maintaining the presence of the message in the network.

An OPNET engineer may benefit from an SIRS interaction scheme as it can be configured to create a steady presence of a message without overloading the network. Other interaction schemes, such as the SI and SIS models, require many infectious devices to maintain the presence of a message, which is resource intensive and may not be practical. It is impossible to maintain message presence in the SIR model as all infectious devices eventually become recovered. The SIRS model is better suited to maintaining the availability of a message in an OPNET.

## 2.3 Particle Movement

This section discusses the movement of devices in an OPNET. Firstly, the impact that device movement has on network behaviour is highlighted. Then, the way in which movement can be modelled is discussed, as well as the effects that movement has on device interaction. As explained in Section 1.5.1, devices will be referred to as particles throughout this thesis, unless discussed in context of a network.

### 2.3.1 Motivation

As stated by Jardosh *et al.* (2003), "simulation results obtained with unrealistic mobility models may not correctly reflect the true performance of the protocols". It is important to learn how significant an impact particle movement has on data propagation. This will help to decide which mobility models are appropriate for

use in the studies. In this section, some of the literature that explores the area of particle movement is reviewed.

## MANET Performance

A survey of mobility models, popularly used for MANET simulations, can be found in Camp *et al.* (2002). Several mobility models are tested to see how they affect the performance of a MANET. Various movement parameters are varied, and several metrics are analysed for a series of unicast transmissions. Concluding remarks state that "the performance of an ad-hoc network protocol can vary significantly with different mobility models" (Camp *et al.* 2002). It is also discovered that performance is significantly affected by the parameters of a mobility model.

Further studies on MANET performance are performed in Divecha *et al.* (2007) and Saad and Zukarnain (2009). Several mobility models are used in parameter studies on particle density and speed. Results are analysed against performance metrics such as throughput (the amount of data successfully transmitted from sender to receiver per second) and routing overhead (the number of intermediate particles used for a successful transmission). It is concluded that "empirical results illustrate that the performance of a routing protocol varies widely across different mobility models" (Divecha *et al.* 2007).

## Long-Distance Jumps

Buscarino *et al.* (2008) show how the spread of a disease is affected by long-distance jumps like train journeys or aeroplane flights. These jumps occur independently for each simulated individual with probability $p_j$ per second. Results show that an epidemic is greatly affected by $p_j$, with higher values increasing the rate at which the disease spreads. This is intuitive, as long-distance jumps quickly take the disease to new locations. Results also show that the epidemic threshold is dependent on $p_j$.

Prior to the work of Buscarino *et al.*, Frasca *et al.* (2006) show that epidemics are affected by the long-distance jumps of infectious individuals only. It is concluded that the movement of only the infected individuals should be restricted to increase the epidemic threshold.

Clearly, the impact of particle movement is significant, and care should be taken when deciding on which mobility models to use.

## 2.3.2 Movement Traces

Particle movement can be modelled empirically using movement traces of real-life objects. Traces can be recorded using tracking devices such as mobile phones or Global Positioning System (GPS) devices. This leads to accurate results, but these may not necessarily be typical. Traces show how an object moves at a certain instant of time. Before or after this time, the object may move in a different way. Indeed, the instance of captured movement could be a particularly unusual case.

Only a finite number of traces can be gathered. If insufficient data are collected, further trace gathering may be required, which can be expensive. Traces are of a finite length, so a model or simulation must stop when the end of the trace is reached. It may be possible to overcome the problems associated with the finite nature of traces. One potential solution is to quantify a set of traces and use their key properties to create synthetic traces with statistically similar features. This can be achieved by finding patterns of regularity.

By studying patterns in the traces of 100,000 mobile phone trajectories, Gonzalez *et al.* (2008) show that "human trajectories show a high degree of temporal and spatial regularity" (Gonzalez *et al.* 2008). The 100,000 mobile phone users were selected at random from a sample of 6 million anonymous users who were tracked over a 6 month period. By studying this dataset, it was shown that the mobile phone users tend to frequent particular places with a pattern of regularity. In Song *et al.* (2010), a similar study is performed that supports the finding of Gonzalez *et al.* Once again, human trajectories are found to be predictable, regardless of the distance travelled. Movement is also found to be predictable regardless of age, gender, home location, language group, population density and rural versus urban environments. It is even revealed that human trajectories are just as predictable during weekends as they are during weekdays.

### 2.3.3 Synthetic Mobility Models

Purely synthetic mobility models do not directly use any real-life data; rather, they are generated using an algorithm to approximate the movement of objects in the real-world. The algorithm can create an unlimited number of random trajectories, each of unlimited length. It is less expensive and less time-consuming to generate synthetic traces from simulations based on theoretical models than to gather a sufficient number of real-world traces. However, unlike traces, they can only *approximate* real-world movement.

The following sections explain several popular synthetic mobility models.

#### 2.3.3.1 Random Walk

An example of a simple synthetic mobility model is the Random Walk (Camp *et al.* 2002). The Random Walk is a discrete-time mobility model, meaning that time is divided into consecutive segments of equal size, known as *time-steps*. At each time-step, particles move independently from their current positions in a random direction for a fixed distance, called the *step size*. This distance is a parameter of the model, and is constant for all particles. Movement happens instantaneously: the position of each particle is not defined between two consecutive time-steps. A Random Walk is a Markov process (Janssen 2014), meaning that the next chosen movement depends only on the present position, not any past positions.

The way in which direction and step size are chosen depends on the simulation region. For example, in a 1D region of discrete space, the direction must be either left or right and the step size must be an integer. In a 2D region of continuous space, there are uncountably many possibilities for both direction and step size. Note that:

- A simple Random Walk is a Random Walk with a step size of 1.
- A symmetric Random Walk is a 1D Random Walk in which the direction of each movement is chosen with uniform probability.

**1D Discrete Space:** Suppose that a particle resides at the origin at time $t = 0$. The particle follows a simple Random Walk with a probability of $p$ and $q$ of moving left or right, respectively, where $p + q = 1$. After $n$ steps, the expected number of steps to the left is $np$, and $nq$ to the right (each with variance $npq$). Therefore, the

expected displacement of the particle after $n$ steps is $n(p - q)$. For a symmetric Random Walk ($p = q = 0.5$), the expected displacement is 0. However, the expected distance from the origin after $n$ steps (regardless of direction) is approximately $\sqrt{\frac{2n}{\pi}}$ for large values of $n$ (Weisstein 2010). Examples of 1D simple symmetric Random Walk trajectories can be seen in Fig. 2.7.

**Example Random Walk Trajectories**
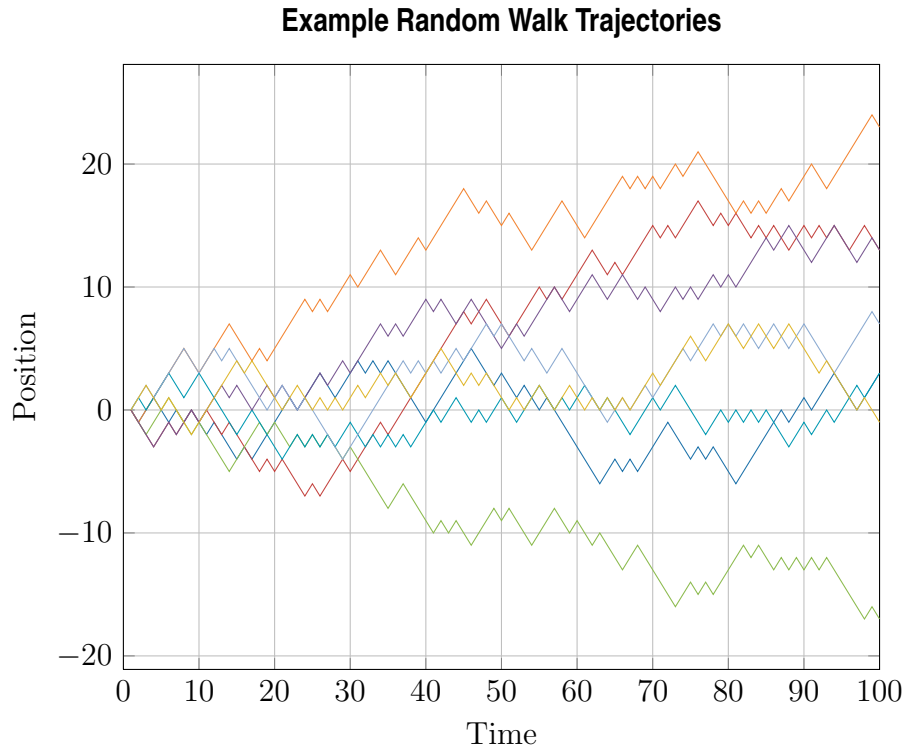


Figure 2.7: Eight examples of 1D simple symmetric Random Walk trajectories, each for 100 time-steps. Each plot is a separate trajectory.

#### 2.3.3.2 Levy Walk

A Levy Walk is a type of Random Walk in which the step size is not constant. It is instead chosen from a heavy-tailed probability distribution (Viswanathan *et al.* 1996). This means step size has a high probability of being small, but the probability of a very large step size cannot be ignored. Step size is chosen independently for each particle at each time-step. An example Levy Walk trajectory can be seen in Fig. 2.8.

It is found that the movement of many animals can be modelled with Levy Walks. This is shown for animals such as monkeys (Boyer *et al.* 2003), albatrosses (Viswanathan *et al.* 1996), reindeer (Viswanathan *et al.* 1996), jackals (Atkinson *et al.* 2002) and microzooplankton (Bartumeus *et al.* 2003). The movement of animals is an important consideration for the research of OPNETs as, already, several existing

**Example Levý Walk Trajectory**
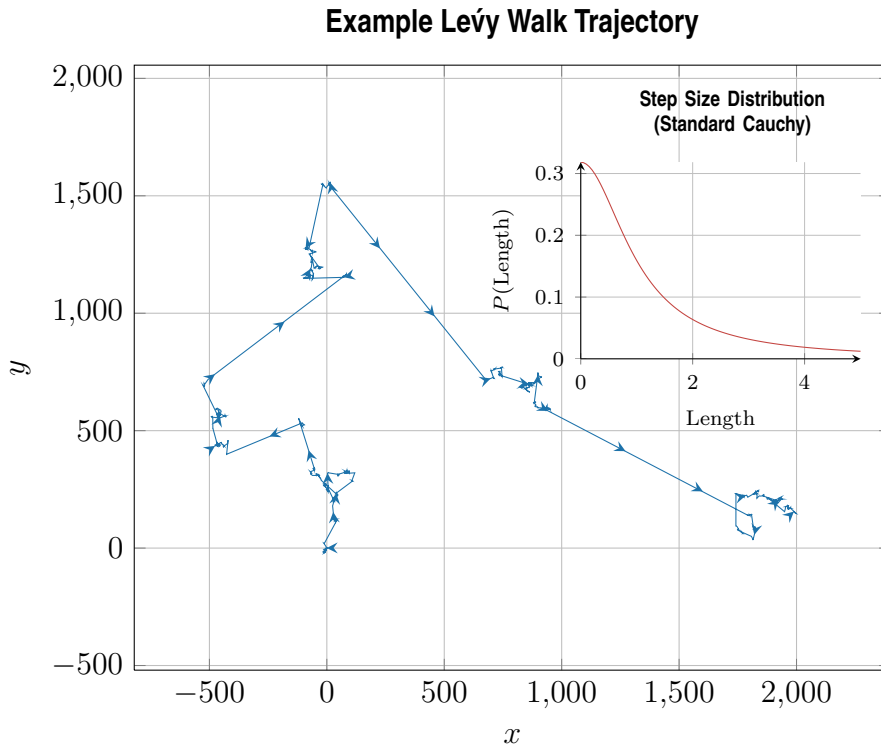
Figure 2.8: Example Levý Walk trajectory, consisting of 1000 time-steps. Arrows show the direction of travel. The sub-plot shows the distribution used to select step sizes (the standard Cauchy distribution).

OPNET applications use animals to carry the network devices. One example of such an application is Zebranet (Princeton University 2003), in which the behaviour of zebras is studied.

Levý Walks have the characteristic of *super-diffusive* behaviour, meaning that the step size has infinite variance (Kim *et al.* 2010). Kim *et al.* (2010) use real-world traces to show that such behaviour can be seen in the movement of humans. This gives evidence that, like animal movement, human movement can be modelled with Levý Walks. Similar propositions are made in other publications; for example, Rhee *et al.* (2011) draw a similar conclusion after analysing GPS traces of 44 volunteers. As another example, Brockmann *et al.* (2006) study human movement by tracking the circulation of bank notes in the United States. It is found that "the distribution of travelling distances decays as a power law" (Brockmann *et al.* 2006), leading to the conclusion that human movement can be modelled by Levý Walks.

On the other hand, Gonzalez *et al.* (2008) disagree with the findings of Brockmann *et al.* (2006). Specifically, the authors argue that human movement cannot be modelled with a random trajectory such as that of a Levý Walk. Instead, it is noted that human movement has regularity and periodicity. This conclusion is made after

analysing mobile telephone location traces. Such traces are more relevant to human mobility than bank notes as mobile telephones are largely carried by only one person. Bank notes diffuse as they are passed between many different people, therefore making it hard to see any periodic patterns. It is clear that random trajectories should not solely be relied upon, and this is discussed further in Section 5.7 in which real-world trajectories are studied.

### 2.3.3.3 Random Direction

The Random Direction mobility model (Camp *et al.* 2002) is a simple, yet versatile mobility model. In the model, particles move independently with periods of constant velocity. This velocity changes at certain time intervals which can be chosen at random. Traditionally, the model is implemented in 2D continuous space; however, the concept can be applied to other simulation regions.

Several definitions of the Random Direction model have been published (Bettstetter 2001; Camp *et al.* 2002; Klein *et al.* 2010; Saad and Zukarnain 2009); however, the following definition will be adopted for the remainder of this thesis:

### Parameters

- Velocity distribution, chosen in either of the following ways:
  - **Speed distribution for all spatial dimensions:** The speed for each spatial dimension is chosen independently. Speed distribution can be, for example, normally or uniformly distributed, or a constant value.
  - **Speed distribution for overall speed:** This is used together with a heading direction, $\theta$, chosen uniformly at random. Speed distribution can be, for example, normally or uniformly distributed, or a constant value. Depending on the system, $\theta$ may be, for example, $\pm 1$ for 1D space, or an angle on $[0, 2\pi)$ for 2D space.
- Path-length distribution. This defines the rate at which new velocities are chosen for a given particle. This is defined according to a *turning rate* parameter, $\lambda$, which is used as an absolute value or as the mean of an exponential distribution.
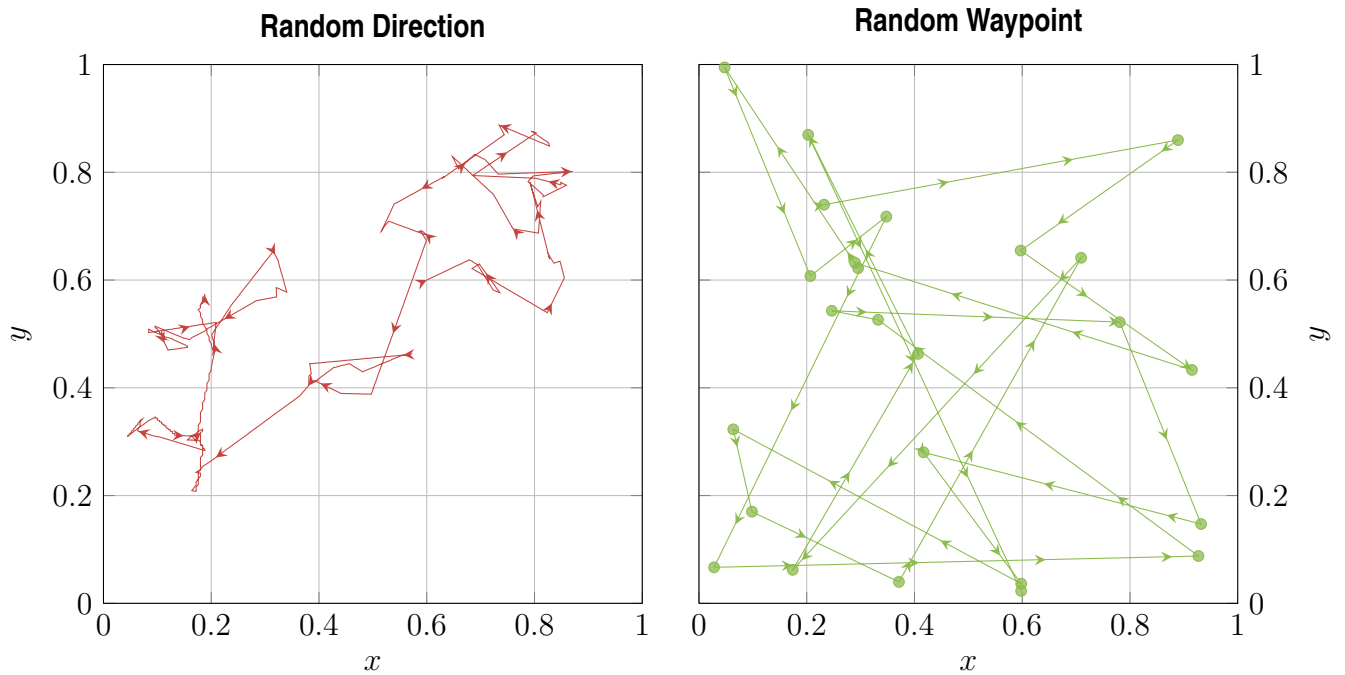
Figure 2.9: Example trajectories for the Random Direction (left) and Random Waypoint (right) mobility models. Arrows show direction of travel. The mean step size for the Random Direction trajectory is 1 (Normally distributed) and $\lambda = \frac{1}{10}$ (image scale: 1 : 250). Circles in Random Waypoint plot show positions of brief pauses in movement.

**Algorithm (for each particle)**

1. Choose a velocity according to the velocity distribution.

2. Choose a duration, $\tau$, for which to travel, according to the path-length distribution.

3. Travel at the chosen velocity for $\tau$ time units.

4. Go to step 1 and repeat the process.

The Random Direction model is versatile despite having few parameters. The model can be configured to match other mobility models. For example:

- **Simple Random Walk:** a constant speed for all particles and a constant turning rate of 1.

- **Levý Walk:** a heavy-tailed speed distribution (*e.g.* Levý distribution) with a constant turning rate of 1.

An example trajectory of a single particle following the Random Direction model can be seen in Fig. 2.9.

### 2.3.3.4 Random Waypoint

The Random Waypoint (RWP) model is commonly used for MANET simulations (Camp *et al.* 2002). This model consists of each particle choosing a random location to move towards at a randomly chosen speed. Once arrived at the destination, the particle may wait for a randomly chosen amount of time. This process is then repeated, each time with another random destination and speed.

The RWP model has received criticism due to its steadily decreasing average particle speed over time. However, this problem has since been overcome (Navidi *et al.* 2004).

Figure 2.9 shows an example trajectory of the RWP mobility model.

## 2.3.4 Human-Like Mobility Models

As discussed in Section 1.2, an interesting class of applications for OPNETs rely on the network devices being carried by people. It is clear that understanding the movement patterns of the network devices is important when studying OPNETs. Therefore, the study of human movement is an important aspect of this thesis.

Several models have been designed to match the movement of people. Bettstetter (2001) presents a modified Random Direction model that mimics the movement of cars and pedestrians. Key modifications include gradual changes in speed and direction. It is unclear how beneficial these modifications are and whether they are worth the extra computation required.

In Jardosh *et al.* (2003), in contrast to most synthetic models, it is argued that people do not move in straight lines nor in random directions. A mobility model is proposed in which particles travel to and from specific destinations using well-defined paths. A unique feature of this model is a set of obstacles such as buildings, which obstruct wireless signals.

In Lee *et al.* (2009), a mobility model called SLAW (Self-similar Least Action Walk) is proposed which matches the movement of people drawn to a common interest or meeting point. This is useful for modelling environments such as theme parks or university campuses. SLAW mimics patterns of regularity, as discussed in Gonzalez *et al.* (2008). Trajectories generated by SLAW are compared to traces recorded from

GPS devices. Comparisons reveal that SLAW has several true-to-life properties, such as a truncated power law distribution of step sizes (see Section 2.3.3.2).

Hsu *et al.* (2007) propose the *Time-Variant Community Model*, in which movement is non-homogeneous in both space and time. An example of a trajectory generated by this model can be seen in Fig. 2.10. The model is designed to be "mathematically manageable" (Hsu *et al.* 2007), meaning it is not too complex to be studied analytically. Indeed, theoretical models are provided for some aspects of particle interaction. Although the model uses regular patterns to mimic human travel, it is criticised by Lee *et al.* (2009) for not being statistically similar to real-life movement traces.
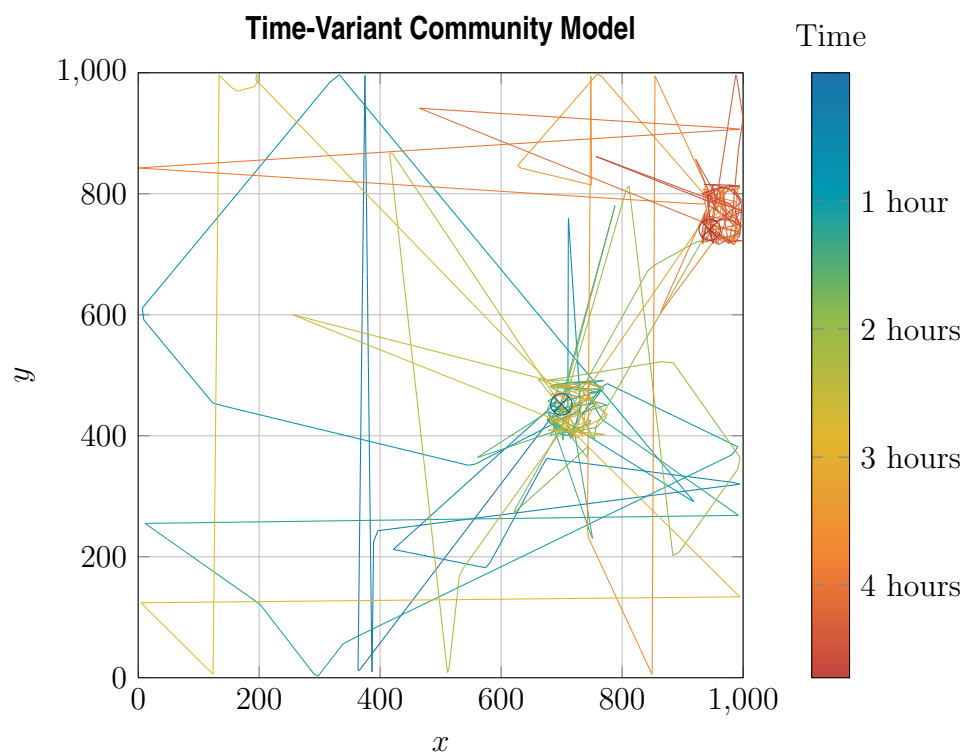


Figure 2.10: Example trajectory generated by the mobility model proposed in Hsu *et al.* (2007). All parameters use the default values provided by the simulator except the region boundaries are set to be reflective, rather than periodic. Colour indicates position time. Crossed circles represent start (blue) and end (red) points.

Other proposed models of human mobility can be found in Tuduce and Gross (2005); Kim *et al.* (2006); Kamal and Al-Karaki (2007) and Boldrini *et al.* (2008).

## 2.3.5  Group Movement

In group mobility models, the trajectory of a single particle is dependent on those of other particles. This is opposed to previously discussed mobility models, in

which each particle moves independently. Group mobility models may be useful for modelling how people move, for example, on a city tour, as a troop of soldiers or as groups of friends.

It is reported that "up to 70% of people in a crowd are actually moving in groups, such as friends, couples, or families walking together" (Moussaïd *et al.* 2010).

In Musolesi and Mascolo (2007), a group mobility model based on social network theory is presented. The model can be configured for temporal variance, to model different movement patterns on weekdays and weekends, for example. Particle interaction statistics are analysed, and found to be similar to those of real-world traces. Further studies are performed on how MANET performance is affected by the developed mobility model. It is found that the probability of a successful transmission is less affected by particle speed in the group mobility model than is the case in the RWP model, due to less frequent topology changes in the group model.

Despite their potential uses, group mobility models may not be of benefit when modelling OPNETs. In an OPNET, particles that form part of a group are likely to share their messages among the group. Therefore, all members of the group carry the same set of messages and the group can be treated as one entity. On the other hand, particles in a group may cause interesting behaviour if they split from the group or merge with other groups. However, little research has been done on this type of behaviour.

### 2.3.6 Regional Attributes

**Spatial Dimensions**

A simulation region may consist of 1–3 spatial dimensions. Fewer spatial dimensions are simpler to model but may not be adequate to represent certain environments. To provide some examples, a 1D model may be used for roads or corridors, a 2D model may be used for cities or shopping malls and a 3D model may be used for oceans or multi-storey buildings.

**Boundary Effects**

An infinite sized area is difficult to simulate, as an infinite number of particles would be required to ensure a non-zero particle density. Because of this, particles are usually restricted to movement within a finite region. There are several possibilities as to how a particle reacts when encountering the boundaries of this region. This behaviour is defined according to the boundary type, as explained in Table 2.4.

| Boundary Type | Behaviour |
|---|---|
| Reflective boundaries | Particles reflect off boundaries like billiard balls. |
| Periodic boundaries | Opposite boundaries join so that the region wraps around. A 1D region with periodic boundaries can be visualised as the edge of circle. A 2D region with periodic boundaries can be visualised as the surface of a torus. |
| Replacing boundaries | Particles leave the region when they move past the boundary edges. Whenever a particle leaves the region, a new particle is introduced at a random location. This keeps the number of particles in the region constant. |

Table 2.4: Table to explain the boundary types used for simulation regions.

Note that boundary effect considerations are not required for some types of movement. For example, particles never encounter region boundaries in the RWP model, although they may get close.

**Homogeneity vs. Heterogeneity**

**Density:**  A region may have a homogeneous distribution of particles, meaning that particles are spread evenly across the entire region. Alternatively, a region may be heterogeneous with respect to particle density. For example, in a shopping centre the density of people may vary between shops.

**Velocity:**  The velocity of particles may be homogeneous in space. For example, cars on a long, straight road move at roughly the same velocity regardless of their position. Alternatively, particle velocity may be heterogeneous in space, as particles move in different ways depending on their position. An example of this is a road network with different speed limits. Although heterogeneous density/velocity is to be expected in real life, most synthetic mobility models assume homogeneity for simplification.

**Temporal Properties:**   As well as potentially depending on location, particle density and velocity may also depend on time. For example, particle density in the suburbs may be low during the day, and high during the night as people commute to and from work in the city centre.

**Well-Mixed:**   If movement is homogeneously-mixed, each particle will proximate each other particle in the region with equal probability.

## 2.4   Particle Interaction

### 2.4.1   Contacts

In an OPNET, a pair of particles can only exchange data if they are within each other's wireless transmission range. When two particles come within range of each other, it is said that each particle has "made a new contact" (regardless of whether they have been within range of each other in the past). The pair of particles remain "in contact" with each other until they are no longer within range. In this section, terms relating to contacts between particles are defined.

#### Inter-Contact Times

The *inter-contact* time is the time between two consecutive new contacts. For example, if a particle makes a new contact at time $t$ then another at time $t'$, the inter-contact time is $t' - t$. Note that inter-contact time is not affected by the time two particles remain in contact. Neither is it affected by whether two particles have previously been in contact.

In La (2010), inter-contact time is studied for the Generalised Hybrid Random Walk mobility model. This is similar to a Random Walk on a toroidal region of discrete space. In the mobility model, space is divided into a grid of cells and each cell is divided into sub-cells. Movement occurs by selecting an adjacent cell in the same way as the Random Walk model, then moving to a sub-cell of this cell chosen uniformly at random. Analytic models are used to show that inter-contact time can be approximated by the exponential distribution. These models are verified using a simulation consisting of 2 mobile devices, with 449,949 inter-contact times

being recorded. It is also argued that the exponential distribution may approximate inter-contact times for other mobility models.

### Contact Rate

The *contact rate*, $\nu_c$, is the number of new contacts a particle makes per second. This is equal to the reciprocal of the inter-contact time. A higher contact rate means more opportunities to transfer a message. One would expect $\nu_c$ to increase as any of the following increase:

- Signal radius ($r$): In 2D or 3D space, a larger signal radius means that the wireless signal of a particle covers a larger area as the particle moves around. This increases the chances of making new contacts. Note that this is not the case for 1D space, as will be seen in Section 4.4.
- Particle density ($\rho$): more particles per unit area increases the chances of making new contacts.
- Particle speed ($s$): As particles travel faster, they are more likely to come within range of other particles for the first time.

### Contact Duration

The *contact duration*, $T_c$, is the length of time that two particles remain in contact. Studying $T_c$ is an essential step towards modelling non-instantaneous data transmission, which is a key contribution of this thesis (see Section 1.3.1). A longer contact duration means that larger messages can be transmitted between particles. One would expect $T_c$ to increase when any of the following occur:

- Signal radius ($r$) increases: A larger signal radius allows two particles that are within range to travel a further distance before moving out of range of each other.
- Particle speed ($s$) decreases: A pair of slower particles that are within range of each other take a longer time to move apart.

Note that particle density is not expected to affect contact duration as contact duration is measured for just two particular particles at a time, which are unaffected by the rest of the population.

Panisson *et al.* (2012) use real-world data to analyse $T_c$ for encounters between people. The data are collected using Radio-Frequency Identification (RFID) badges worn by conference attenders (SocioPatterns 2011). These badges collect information about the proximity of people and whether they are face-to-face (depending on the badge settings). The term $T_c$ is extracted from the gathered data and compared with the data artificially generated from the following synthetic mobility models:

- RWP (see Section 2.3.3.4),
- Truncated Lévy Walk (see Section 2.3.3.2).

Results show that the two synthetic models have near identical distributions of $T_c$, though in both cases these results are significantly different to the real-world data. This difference is emphasised with further studies regarding message propagation in a MANET. These findings highlight the importance of using a suitable mobility model for OPNET simulation (see Section 2.3.1). However, the article does not consider the possibility that the discrepancy may be due to the comparison of face-to-face contacts (real-world data) with proximity contacts (synthetic models).

**Little's Law**

In Jacquet *et al.* (2010), it is argued that contact rate ($\nu_c$) and contact duration ($T_c$) are related according to Little's Law:

> "Little's Law says that in the long-term, steady state of a production system, the average number of items $L$ in the system is the product of the average arrival rate $\lambda$ and the average time $W$ that an item spends in the system, that is, $L = \lambda W$" (Gustafson 2012).

In the context of OPNETs, the parameters of Little's Law can be interpreted as follows:

$$L = \nu_c \cdot T_c,$$

where $L$ is the number of particles that a given particle is in contact with at any given time.

In Jacquet *et al.* (2010), studies are performed using a Random Direction mobility model, with constant speed and exponential turning rate (see Section 2.3.3.3). An analytic expression is provided for $\nu_c$; this is combined with the average number of

particle contacts using Little's Law to derive the distribution of $T_c$. The findings of Jacquet *et al.* (2010) are further discussed later in this chapter in Section 2.8.2.

## 2.4.2 Link Models

As an alternative to using mobility models, link models can be used to represent interactions between particles. A link model is a dynamic graph that changes over time. Each vertex of the graph represents a particle in the network. An edge connecting a pair of vertices shows that the two corresponding particles are in contact at that time. This type of graph is known as a *contact graph* (Panisson *et al.* 2012).

Link models do not provide the spatial position of particles; however, they do provide all of the necessary information to simulate data propagation in an OPNET. A benefit of link models is that they are less computationally intensive than mobility models. An example of OPNET simulation using link models can be found in Becchetti *et al.* (2011).

*SocioPatterns* is a research project that makes use of real-world data to study the social dynamics of people (SocioPatterns 2011). The project offers a platform that can be used to generate link models from interactions between people. This platform makes use of RFID badges worn by individuals to collect information about their proximity with others. Badges can be configured to detect only short-range contacts, where individuals are face-to-face, or longer-range encounters of up to several metres.

## 2.4.3 Model Complexity

In Stehlé *et al.* (2011), a study is performed on how the complexity of a model affects the simulated spread of a disease. The study makes use of the SocioPatterns platform described in Section 2.4.2 (involving 405 volunteers over a 2-day conference) to construct a link model for a conference. The following variations of this link model are used in the study:

- Dynamic network (DYN): The fully-detailed link model is considered. This consists of a contact graph for every 20 seconds of the time period considered.
- Heterogeneous network (HET): A single, static graph for each day of the conference. Graph vertices represent each individual. Graph edges connect any

pair of individuals that were in contact at any time in the day. The weight of each edge represents the total time a pair remained in contact. The ordering of contacts and the time at which they occurred is lost.

- Homogeneous network (HOM): The same as HET, only all graph edges are weighted with a value equal to the average contact duration.

The spread of a disease is simulated on each of these network models. Results of the study include metrics such as the number of susceptible and recovered individuals over time, the final size of the epidemic, the size of the epidemic at its peak and the time at which this peak is reached. The results yielded by the DYN and HET networks were very similar, despite their difference in complexity. This means a detailed, high-resolution dataset may not be necessary to adequately describe disease propagation. On the other hand, the results yielded by the HOM network were significantly different, showing that contact duration is an important consideration. This makes sense as their model uses a probabilistic infection rate, where the chance of infection depends on contact duration.

Blower and Go (2011) reflect on Stehlé *et al.* (2011) with the following statement:

> "Complex models are based on many assumptions that are generally not evaluated to determine whether they are correct, and they can also include hundreds of parameters whose values are unknown or only imprecisely known. Consequently, complex models are not necessarily more accurate than simple models" (Blower and Go 2011).

## 2.4.4 Communications Protocol

Several decisions must be made before any communication can take place in an OPNET. Each device must decide whether to interact with any other device in the network using a set of rules known as the *communications protocol*. Many considerations must be made by the communications protocol, such as security, fairness and availability of resources. Each of these areas are discussed in this section.

### (a) Resource Saving

OPNET devices are mobile and are likely to have a limited power supply. It is important that energy is used efficiently to ensure devices can continue to participate.

An energy saving protocol is proposed in ElBatt *et al.* (2000). In this protocol, energy is conserved by adjusting the strength of the wireless transmitter depending on the number of nearby devices. This has the added benefit of reducing signal interference.

In Basu and Chau (2008), analytic expressions are developed to show that energy can be saved in a wireless ad hoc network by using *duty cycling*. Duty cycling means devices frequently turn off their wireless transmitters to conserve power. It is suggested that devices turn their transmitters on only at times selected by a pseudo random number generator (p-RNG). Devices would only have to synchronise clocks and p-RNG seeds to deterministically predict when another device is available for communication. Duty cycling would be well-suited to a sensor network, such as the ones described in Section 1.2. Simulations are used to verify the developed analytic expressions. A network of 10 and 100 devices (moving according to a Random Walk on a 2D plane) is used for the simulations. Simulations are repeated 1000 times with the average result being taken. Further reading on duty cycling with regards to broadcast transmissions can be found in Guo *et al.* (2009).

The Encounter Based Routing (EBR) protocol was proposed by Nelson *et al.* (2009). The protocol is intended for unicast transmissions, and designed to maximise the delivery ratio while minimising the use of resources such as energy and buffer space. The protocol is based on the idea that a higher contact rate implies a device is more likely to deliver a message to its destination. It is stated that the future contact rate of a device can be roughly predicted by past contact rate. The EBR protocol is tested using three different mobility models, namely, the RWP (see Section 2.3.3.4), an event-based disaster model and a street-map based vehicular model. Computer simulation is used to evaluate the protocol according to a set of metrics. The following metrics are captured: message delivery ratio, message delivery time-taken, and *goodput*, defined to be "the number of messages delivered divided by the total number of messages transferred (including those transfers that did not result in a delivery)." (Nelson *et al.* 2009). Despite economical use of resources, results show that EBR outperforms several other well-known protocols in terms of successful delivery ratio.

Several techniques for reducing device buffer occupancy are discussed in Zhang *et al.* (2007). This includes three buffer management systems which tell devices how and when to delete messages. It also includes mechanisms to inform devices that a

unicast transmission has been completed and propagation of the message is no longer required. This is achieved by spreading an *anti-packet*, which instructs devices to delete the message from their buffer and stops them accepting it again in the future.

## (b) Fairness

An OPNET can only work if enough users engage in message propagation. It is considered that "some kinds of incentive schemes might be necessary in opportunistic networks to encourage user participation" (Heinemann *et al.* 2008). Examples of such schemes are discussed in this section.

In Buttyan and Hubaux (2000), two counter-based mechanisms are proposed to reduce selfishness in a MANET. In this work, *nuggets* are used as a currency in the network. Each device has a nugget counter stored in an encrypted secure module (this requires tamper-proof hardware, such as some kind of chip or smart card). Devices have the incentive to collect nuggets to allow them to send/receive messages in the network. The two mechanisms are described below:

**Packet Purse Model (PPM):**  A source device attaches some of its nuggets to a message and introduces it to the network. Other devices take one of these nuggets on forwarding the message. The message is dropped if it has no nuggets left attached. A disadvantage of this mechanism is that nuggets are easily wasted if the source device over/under-estimates the amount required. However, the same authors attempt to resolve this problem in Buttyán and Hubaux (2003) by ensuring devices always get paid for forwarding a message, even if the initial number of nuggets was under-estimated.

**Packet Trade Model (PTM):**  In this model, nuggets are required to receive (rather than send) a message. Each device buys the message from the previous device for an increasing amount of nuggets. The destination device covers the cost of the entire transmission. A disadvantage of this mechanism is that the last intermediate device loses many nuggets if the destination device cannot be found.

In Li *et al.* (2010), a different approach is taken to tolerate (rather than punish) selfish devices. It is noted that devices are likely to be socially selfish and favour

doing tasks for devices of past encounters rather than a device never encountered before. This is especially interesting for social network applications (see Section 1.2).

> "Our underlying philosophy is that social selfishness is a kind of user demand that should be satisfied. It should be treated as a design metric to measure the user satisfaction, similar to other traditional performance metrics such as data delivery ratio and delay" (Li *et al.* 2010).

Using the proposed protocol, devices forward messages only to those who are willing to pass it on. Willingness depends on many factors, such as device resources and relationship with sender. There is no incentive to lie about intentions, meaning fewer security measures are required, such as tamper-proof hardware as seen in Buttyan and Hubaux (2000). When tested against other MANET protocols, results show improved performance despite the presence of selfish devices in the network.

### (c) Security

The two main security concerns for OPNETs are as follows:

- Eavesdropping of private information.
- Malicious behaviour of certain devices that disrupts the network.

As discussed in Section 1.1.3, OPNETs are most suited to broadcast transmissions. In this case, sent data are public and eavesdropping is not of concern. However, for unicast and multicast transmissions, eavesdropping is a difficult problem to overcome.

Several potential solutions for eavesdropping in a MANET are discussed in Hubaux *et al.* (2001) and Yang *et al.* (2004); however, they are not suitable for OPNETs. This is because some of the solutions require a form of infrastructure, like a security server, which cannot be included in an OPNET. Other solutions require the exchange of encryption keys between network devices using a two-way communication path, which are unlikely to occur in an OPNET. Furthermore, cryptography algorithms may require too much battery power from the mobile devices. With the current state of security technology, it is not recommended to transfer sensitive information in an OPNET.

An example of malicious behaviour is a virus spreading in the network. It is up to the operating system and applications on the device to prevent viruses causing

disruption (Yang *et al.* 2004). Another example is a DoS (Denial of Service) attack, in which devices may attempt to flood the network (Yang *et al.* 2004). It may be possible to prevent this type of behaviour with a reputation or friendship system, such as the ones described in the previous subsection.

## 2.5 Modelling Time

Time can be modelled as either a series of discrete events or a continuous progression (Bratley *et al.* 1987). Each of these models are discussed in this section.

### 2.5.1 Discrete-Event Simulation

In a discrete-event simulation, the state of the system changes over time according to a series of events. These events can be processed synchronously or asynchronously (Bratley *et al.* 1987), as described below.

**Synchronous Model**

In synchronous discrete-event simulation, time is divided into a set of consecutive snapshots, or *time-steps*, which occur at regular intervals. Between time-steps, the state of the system is undefined and any events that occur will not be realised until the following time-step. For all synchronous models in this thesis, it is assumed that each time-step is exactly one second, allowing the modelling of certain parameters, such as the deletion rate, as a *probability per time-step*.

Synchronous simulations are well-suited to regular or predictable events, such as message deletion after a fixed period of time. They are also the best way to simulate certain mobility models (such as the Random Walk of Levy Walk from Section 2.3). However, care must be taken when choosing the time-step size:

- if too large, many events may be grouped together to occur at the same time-step,
- if too small, much computation time can be wasted simulating time-steps over which no events occur.

Throughout this thesis, synchronous discrete-event simulation is used as it is easier to implement. Furthermore, there is less processing overhead required when events occur sufficiently frequently, and events are expected to occur frequently in the simulations.

**Asynchronous Model**

In this type of simulation, events are handled at the exact time of their occurrence. Simulations do not progress in time-steps; instead, the clock is incremented forward to the time of the next event. This is appropriate for situations where inter-event times are of high variance, as no computation time is wasted on simulation when no events occur. However, for frequent and regular events, the overhead of asynchronous simulation may make synchronous simulation a more efficient alternative.

### 2.5.2 Continuous-Time Model

In a continuous-time model, time is always defined and is not divided at all. The state of the system continually adjusts, allowing time to be drilled-down indefinitely into more detail (Bertsekas and Tsitsiklis 2002). Continuous-time models usually consist of a number of differential equations, which are to be solved numerically for time.

## 2.6 Real-World Experiments

From Section 2.3.4, it is clear that modelling human movement is a complex task. It is also clear that information propagation in an OPNET is greatly dependant on the movement of the particles. For these reasons, it can be difficult to accurately simulate a real-world OPNET. This section presents current research that helps to overcome this problem.

### 2.6.1 Link Models

Several simulations are performed on link models gathered using the SocioPatterns platform described in Section 2.4.2. In Panisson *et al.* (2012), broadcast transmissions

are simulated on several link models. Proximity detection of 10–12 meters is used to create one of the link models, while the other two use face-to-face interactions within a distance of 1.5 meters. Data from experiments based on all three link models are gathered at three day long conferences with over a thousand individuals participating in total. From the link models, a series of Fastest Route Trees (FRTs) are generated, showing the path of intermediate particles that must be taken for a message to reach any particular particle in the shortest possible time. An analysis of *delivery time* is also performed, showing the time it takes each particle to receive a message after it is first generated in the network.

### 2.6.2 Movement Traces

OPNET simulations are performed on movement traces in Zyba *et al.* (2011). Three traces are used in total, two of which come from real-world devices carried by people and one comes from avatar traces from a virtual world computer game called Second Life (Second Life 2011). Each simulation lasts for 2.5 days and is repeated until at least 95% confidence in the average result is reached. In the simulations, messages are disseminated as a broadcast using instantaneous transmissions. The main focus of the paper is to show how social behaviour of particles affects message propagation. It is found that, contrary to other research (see Section 2.3.2), the majority of particles are irregular and infrequent in their movement. Results of the simulations show that message dissemination is more effective when the particles in a network move with similar frequency and regularity, as opposed to a mixture of particles with different frequency or regularity of movement.

In Heinemann *et al.* (2008), movement trajectories are created with a combination of the following models:

- Traces of coarse granularity for movement on the macroscopic scale. This is taken from the Reality Mining dataset (Eagle and Pentland 2005), which consists of data collected from 100 mobile telephones over the course of 9 months.
- Synthetic models for movement on the microscopic scale. The following synthetic models are separately used and compared:
    - RWP model, see Section 2.3.3.4.

– Gauss-Markov Model, which is similar to the RWP model but yields smoother trajectories as future velocities are influenced by past velocities.

– Manhattan Grid Model, in which particles move only along predefined perpendicular paths. This mimics how people move in an American city.

OPNET message propagation is simulated on these trajectories with broadcast transmissions. Each simulation is repeated 100 times, with the average result being taken. Simulation results show that propagation is more effective with the addition of static devices known as *information sprinklers*, especially if they are connected with a backbone network. Information sprinklers are static devices that participate in the network. As these devices are static, they may include enhancements such as a large buffer size, or they may be mains powered. The benefits of information sprinklers are less significant if the mobile devices use a larger signal radius. Analysis is also performed on the number of intermediate devices used to get a message to each recipient. The main finding of this paper is that human movement is indeed suitable for effective OPNET communication.

### 2.6.3 Implementations

#### Serval Project

The Serval project is an implementation of a MANET that runs on smart phones (Gardner-Stephen 2011). The project aims to make mobile telephone communication (voice calls and SMS) available either by enhancing current cellular networks, or by replacing them. In Gardner-Stephen (2011), the implementation is tested in several locations that lack cellular infrastructure, such as the Australian outback and underground caves. Several test case scenarios were studied, including locating a lost party and re-establishing communication in a disaster situation.

#### Haggle

Haggle is a fully-functional implementation of an OPNET that runs on smart phones (Nordström *et al.* 2012). A key feature of Haggle is that it ranks content in terms of user interest; therefore, providing more relevant information. The ranking system works by matching network content to similar content on the individual devices. A range of content can be used with Haggle, such as audio files or social network

text updates. In Nordström *et al.* (2012), studies are performed on a real-world implementation of Haggle. Studies include analysis of power consumption, and delivery ratio analysis for various interest group sizes and content relevance.

**Pietiläinen and Diot (2009)**

An OPNET technology for smart phones was developed by Pietiläinen and Diot (2009). The technology was tested at conferences by providing attendees with suitably configured mobile phones. Bluetooth is used for transmissions, and the use of Wi-Fi is also discussed. During experimentation, devices make several attempts to transmit various file formats as a unicast or multicast transmission. Several metrics are recorded from the experiments, such as power consumption, contact rate and data throughput. Concluding remarks from the paper state that:

> "While the contact opportunities arise regularly in the type of environment we have studied, they are often simultaneous, short and limited by the available bandwidth and other resources on the mobile device such as battery and storage" (Pietiläinen and Diot 2009).

## 2.7   Non-Spatial Models for Data Propagation

This section discusses non-spatial models for data propagation. All research in this section assumes instantaneous data transmissions between particles. Unless otherwise stated, models use unicast transmissions, where there is a single source and a single destination particle.

### 2.7.1   Groenevelt *et al.* (2005)

Through the use of Markov chains, a stochastic model for unicast transmissions in a MANET is presented by Groenevelt *et al.* (2005). The following two protocols are considered:

- 2-hop multi-copy: the message is only ever transmitted from the source and/or to the destination.

- Unrestricted multi-copy: message copies are transmitted across as many intermediate particles as required.

Network delay is modelled with precise analytic expressions rather than simple scaling laws. Analytic expressions are also presented for the distribution of the number of message copies in the system (due to intermediate particles) at the time of delivery.

The models developed in Groenevelt *et al.* (2005) apply to arbitrary movement patterns in any number of spatial dimensions, provided contacts occur according to a Poisson process (meaning the inter-contact times are exponentially distributed). The models require only two parameters: the number of particles in the network and the contact rate. Contact rate encapsulates several features of the network on which propagation models are dependent, such as signal range and interference, as well as movement properties such as speed. After creating analytic expressions for contact rate, the models are validated with simulations for three synthetic mobility models. Results show that the theoretical models closely match simulated data for a small to moderate signal radius. Larger radii lead to inter-contact times that are not exponentially distributed, meaning they cannot be modelled by a Poisson process.

### 2.7.2 Zhang *et al.* (2007)

The work of Groenevelt *et al.* (2005) is extended by Zhang *et al.* (2007) where, once again, theoretical models are provided for network delay and the number of copies of the message in the network. This time, models are in the form of ODEs, which means derivation is simpler. Additionally, the probability of a message successfully reaching its destination is modelled. The following protocols are considered for the models:

- 2-hop multi-copy: identical to that of Groenevelt *et al.* (2005).
- Probabilistic multi-copy: message transmissions (when possible) occur with a certain probability. Multiple intermediate particles are allowed[1].
- Limited-time multi-copy: particles remove a message from its buffer after a certain time period.

These three protocols are compared with regard to performance and resource consumption. Further discussion of resource consumption includes several buffer management

---

[1]Although not mentioned in Zhang *et al.* (2007), the probability in this protocol could be configured to incorporate the average effects of factors such as interference and signal blocking.

systems that determine when particles delete messages. Buffer occupancy is theoretically modelled for each management system, revealing how resource consumption can be significantly reduced whilst maintaining an effective network. All theoretical models are verified with simulations using the Random Direction mobility model (see Section 2.3.3.3).

### 2.7.3 Jacquet *et al.* (2009a)

Jacquet *et al.* (2009a) derive a generic scaling law for lower-bounds on network delay using an asymptotic analysis. In contrast to other work surveyed here, this work also focuses on broadcast transmissions by providing a model for the time until all particles in the network receive the message. The scaling law is verified using simulation. Each simulation is repeated 10 times with the average result taken. Results show that the average delay and the average broadcast time are both of the same order. The authors discuss a discrepancy between their model and the model in Zhang *et al.* (2007), and claim that this discrepancy is due to the (allegedly incorrect) assumption that contact rate is independent for each particle in the network.

## 2.8 Spatial Models for Data Propagation

In this section, models of data propagation in both space and time are discussed. This means a message is modelled to progressively spread outwards from its source, rather than uniformly across the entire region. The work in this section assumes instantaneous message transmissions between particles, except for the two papers in the appropriate subsection.

### 2.8.1 Instantaneous Transmissions

Jacquet *et al.* (2007) use an asymptotic analysis to provide lower-bounds on network delay. The model concerns a MANET using an unrestricted multi-copy protocol, where message copies are transmitted across as many intermediate particles as required. The Random Direction mobility model is considered (with various values for turning rate, see Section 2.3.3.3) on a 2D region of infinite size. The destination of the transmission can be a mobile or static particle. Because of this flexibility, the destination can also

be modelled as a position, rather than a particle. The combination of this and the unrestricted multi-copy protocol means the model is applicable to broadcast as well as unicast transmissions. For example, the amount of time taken for a broadcast message to reach a certain distance from its source can be modelled.

The model from Jacquet *et al.* (2007) is extended in Jacquet *et al.* (2008) for (infinite) regions of one and three dimensions. It is also extended to model the success of a transmission between two particles as a function of the distance between those particles. This is useful for considerations such as signal fading and interference.

Jacquet *et al.* (2009b) is a similar paper to Jacquet *et al.* (2007) (indeed, they have the same title). However, in this paper, the model is extended for large regions of finite size, rather than infinite regions.

### 2.8.2 Non-Instantaneous Transmissions

The work of Jacquet *et al.* (2008, 2009b) is extended to consider non-instantaneous data transmissions in Jacquet *et al.* (2010). This work concerns the Random Direction mobility model in a 2D region of finite size. The authors present their work in terms of *journeys*, defined to be a path in space and time between a source and destination (*i.e.* as the network topology changes due to movement). A theoretical model is provided for *journey capacity* (the amount of data that can be transported through a journey). Furthermore, asymptotic analysis—approximating behaviour with functions as the parameters tend to infinity (Hildebrand 2009)—is used to provide upper and lower bounds of information propagation speed (applicable to unicast and broadcast transmissions) as a function of journey capacity. Theoretical models are verified using simulation. The theoretical models show that information propagation speed is of the same order as particle speed for large journey capacities.

Baccelli *et al.* (2011) consider information propagation speed in a vehicular ad hoc network (VANET)—essentially an OPNET where the network devices are carried by vehicles. The network is located on a motorway where vehicles travel in either direction. By repeatedly passing data to the vehicle in front, propagation speed can exceed that of the vehicles. If the vehicle in front is out-of-range, a vehicle travelling in the other direction may bridge the gap. A theoretical model is created for both instantaneous and non-instantaneous message transmissions. These models

are verified with simulations, with the total number of vehicles in the simulations varying from 1000 to 5000. The models show that data propagation speed (in terms of the distance a message travels along the road) is dependent on vehicular density. If density is below a certain threshold, propagation speed is the same as vehicular speed on average, otherwise, it is significantly higher.

### 2.8.3  Klein *et al.* (2010)

In Klein *et al.* (2010), non-spatial models (such as those in Section 2.7) are criticised as they assume well-mixed regimes (see Section 2.3.6). Theoretical and simulated modelling is used to show that this assumption only holds if contact rate is low enough, otherwise, spatial aspects become significant. Contact rate is affected by signal radius and particle density; by varying these parameters, a critical threshold is revealed, showing a transition between a well-mixed regime and when spatial effects become significant. Simulated models involve 200 mobile devices moving according to the Random Direction movement model on a 2D plane.

Klein *et al.* derive a partial differential equation (PDE) to model data propagation (for instantaneous transmissions only). This PDE is based on the reaction-diffusion equation developed by Kolmogorov *et al.* (1937) and Fisher (1937). Mathematical analysis is used to show that the model reduces to an ODE (like the non-spatial models in Section 2.7) when the system is adjusted to behave as well-mixed.

A travelling wave solution to the PDE is derived and used to create scaling laws for delay. The expected value of the delay is compared for a well-mixed regime and for when spatial aspects become significant. The theoretical and simulated models show that the well-mixed model becomes increasingly optimistic for larger signal radii and particle densities. This is because, for spatially significant regimes, particles closest to the source will receive the message first. Therefore, the message spreads from the source like a radial wave, rather than the uniform spread observed for well-mixed regimes.

Unlike the models of Jacquet *et al.*, the model presented in Klein *et al.* (2010) is non-asymptotic. This means that exact values are provided for delay rather than the bounds. The model is verified with simulations and a replica example can be seen in Fig. 2.11. A further study demonstrates how the model is affected by the

aspect ratio of the simulation region. Theoretical and simulated modelling is used to show that this behaviour is not captured by non-spatial models.
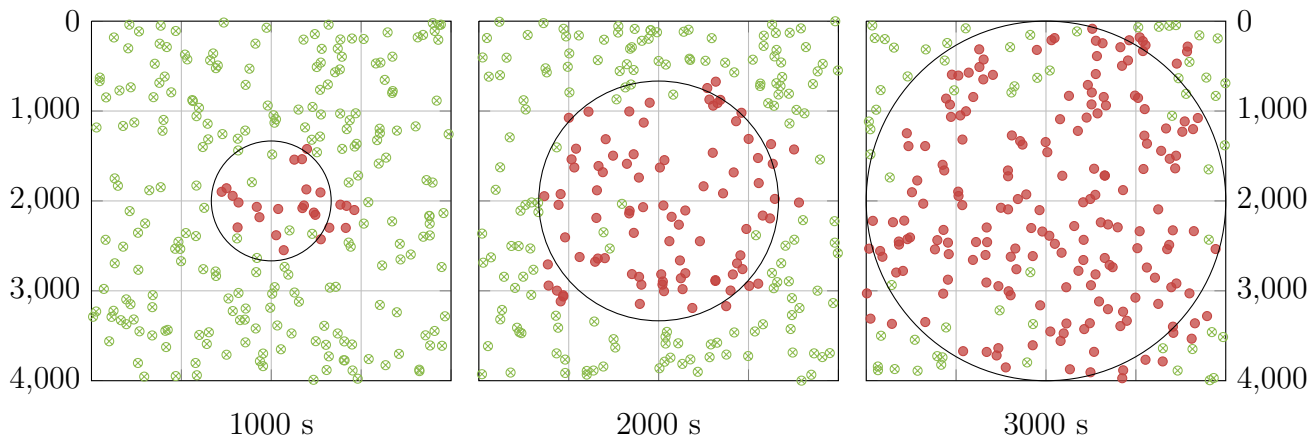


Figure 2.11: Replica of an experiment performed in Klein *et al.* (2010). A broadcast transmission is spread from the centre of a 16 km$^2$ 2D region. Red (filled) circles are infectious while green (crossed) circles are susceptible. The black ring shows the wave front as predicted by the reaction-diffusion model in Klein *et al.* (2010).

### 2.8.4 Summary (Spatial Models)

The work of Klein *et al.* and Jacquet *et al.* constitutes the state-of-the-art regarding models for data propagation in OPNETs. Their work is especially applicable to this thesis, as spatial considerations are incorporated into the models and, in the case of Jacquet *et al.*, non-instantaneous transmissions.

The key benefit of the model proposed by Klein *et al.* (2010) over those of Jacquet *et al.* is that it is based on an exact analysis, rather than on upper/lower bounds found through asymptotic analysis. This is more applicable to this thesis, and is most useful for the motivational topics discussed in Section 1.4.

The model of Klein *et al.* (2010) could be improved by adapting it to work with any mobility model, rather than just the Random Direction model. This could be achieved by defining the model in terms of contact rate/duration distributions, which encapsulates specific, mobility model dependent properties that are currently being used (such as particle speed and turning rate). In doing this, the model could be used in a wider variety of scenarios. For example, the model could be used with movement that is too complex to model analytically, such as real-world movement, as the contact rate and contact duration distributions could be captured empirically. Throughout this thesis, models have been defined to work with any mobility model

by defining the models in terms of contact rate/duration distributions. Furthermore, the same idea is used to extend the model of Klein *et al.* (2010) in Section 5.6.

Another way in which the model of Klein *et al.* (2010) might be improved is to include a message transmission time, as discussed in the key contributions (see Section 1.3.1). In real-world networks, it takes time to transfer data between particles; however, the model in Klein *et al.* (2010) assumes instantaneous transmissions. This assumption may affect the accuracy of the model. In Section 5.6, the model of Klein *et al.* (2010) is extended to include message transmission time.

## 2.9 Chapter Summary

In this chapter, relevant information relating to this thesis has been introduced. This chapter started with a literature review and study of epidemic models applied to OPNETs (Section 2.1). Several interaction schemes were discussed, such as the SI and SIS models, which are used later in this thesis in Section 4.2. Following epidemic models, particle movement was discussed. The mobility model primarily used in this thesis is the Random Direction model, discussed in Section 2.3.3.3. After particle movement, particle interaction was discussed (see Section 2.4.1). In this section, contact rate and contact duration models are introduced, which are used throughout this thesis, for example in Section 3.2. Models for time have also been discussed in this chapter (see Section 2.5). All simulations in this thesis use the synchronous discrete-event time model. Following time, real-world experiments were discussed in Section 2.6. This information comes in useful later in this thesis when real-world data are studied in Section 5.7. Finally, Spatial and non-spatial models are discussed in Sections 2.7 and 2.8. Non-spatial models are studied in Chapter 3 and spatial models are studied in Chapters 4 and 5.

This chapter has provided the reader with the necessary understanding of the underlying concepts on which this thesis builds upon. The context for the remainder of this thesis has been set and a clear indication has been given of the way in which it will proceed. The next chapter will be the first in this thesis to present an original contribution.

# CHAPTER 3

# Non-Spatial Models

This chapter starts by introducing a particle interaction model based on a transport graph. Following this, contact rate and contact duration is modelled for particles that interact on the transport graph. The contact rate and contact duration models are used to theoretically model message spread in the case of non-instantaneous transmission.

The models used for particle interaction in this chapter are not strictly non-spatial. However, the chapter earns its name as the chosen models simplify message spreading in an OPNET so that spatial aspects are not significant. In a truly spatial model, a message spreads from its source as a travelling wave through space, in a similar way to the spread of a drop of ink in water. This travelling wave causes difficulties when modelling message spread theoretically, as will be seen later in this thesis. The "non-spatial" models in this chapter avoid this complication and provide a straightforward starting point for the study on message spread.

## 3.1   Transport Graph

In this section, a transport graph for particle interaction is introduced. The transport graph is identical to the Urn models from Section 2.2.2 except for the following points:

**Use of Terms:** The terms *particles* and *sites* are used instead of *balls* and *urns*. As with the Urn models, there are $N$ particles and $n$ sites.

**Time Progression:** In the Urn models, $N$ pairs of balls are selected per second for potential interaction. However, in the transport graph, all particles can potentially interact with all other particles per second. This change is made as it allows for easier theoretical modelling and leads on to other models discussed later in this thesis.

**Message Transmissions:** In the Urn models, messages are transmitted with probability $\tau$ per second. This simplifying assumption was made due to the way in which time progresses in the model. It is an unrealistic assumption as it allows the possibility of a large message being completely transmitted in a short amount of time. In the transport graph, this idea is abandoned. Instead, message transmission occurs after exactly $\tau$ seconds of contact between particles, as illustrated in Fig. 3.1. If $\tau = 0$, susceptible particles become infected as soon as they make contact with an infectious particle.
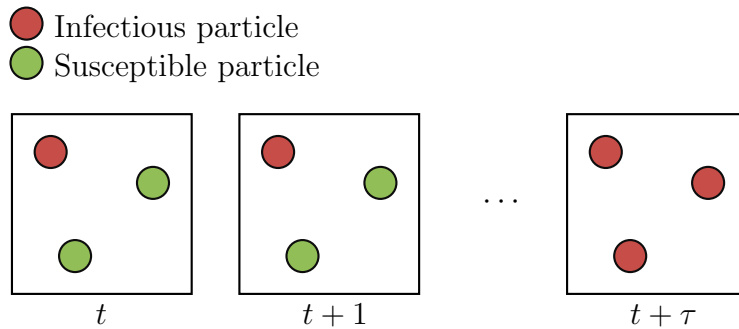


Figure 3.1: Diagram to show how several susceptible particles can be infected by a single infectious particle if and only if they remain in the same site for at least $\tau$ seconds.

In the transport graph, particles can simultaneously communicate with many particles that are in the same site (as shown in Fig. 3.1). All particles in other sites are considered to be out of range. Suppose a particle moves into a site that contains $k$ other particles. This particle makes contact with all $k$ particles in the site, and vice versa (see Fig. 3.2). Likewise, a pair of particles lose contact when one or both move out of their site.

> In the context of real-world OPNETs, it may be difficult for a device to communicate with multiple devices simultaneously. However, this could potentially be achieved with channel multiplexing or multiple antennae.
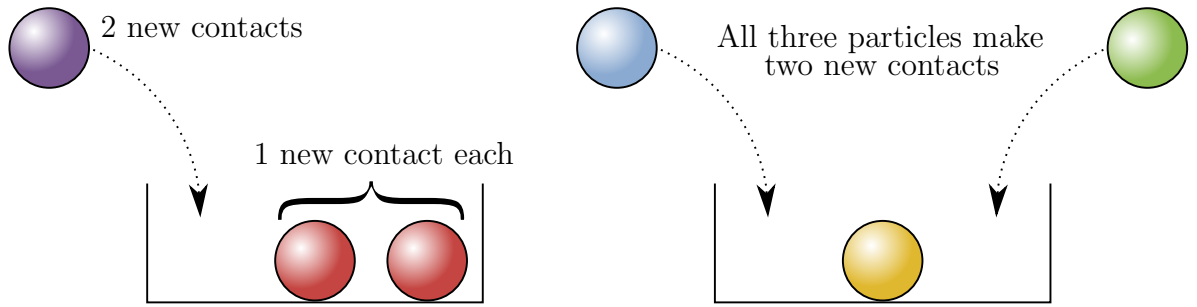
Figure 3.2: Diagrams to show how particles interact in the transport graph. The left site contains two particles and is about to receive a third. The right site contains one particle and is about to receive two more. The number of new contacts each particle makes is displayed in the figure.

As with the Urn models, each particle initially resides in a site chosen uniformly at random. At each time-step, each particle instantly moves, or *jumps*, to another site with probability $\theta$ (otherwise, it remains at the same site). The new site is chosen uniformly at random from the remaining $n - 1$ sites. The following assumption is made regarding jumps:

**Assumption** To simplify the development of theoretical models, it is assumed that at any given time-step, the probability that two particles simultaneously jump from site $i$ to site $j$ (where $i \neq j$) is zero. This is a reasonable assumption provided $n$ is sufficiently large and $\theta$ is sufficiently small.

The transport graph is illustrated in Fig. 3.3.

### 3.1.1 Distribution of Particles

Let $N_i$ be the number of particles at site $i$, where $N = \sum_{i=1}^{n} N_i$ is the total number of particles in the system. Given that the transition of particles between sites is equally weighted, the distribution of $N_i$ is the same for all values of $i$. This is true because all site transitions are chosen uniformly at random. However, if site transitions were unequally weighted (*e.g.* certain sites were favoured over others) then a steady state could still be reached, but the distribution of $N_i$ would depend on the site index $i$.

Let $k \in \{0, 1, \ldots, N\}$. The occupancy number $N_i = k$ if and only if exactly $k$ particles from the population are located at site $i$. Thus $N_i$ has binomial distribution

Figure 3.3: Diagram of the transport graph used for particle interaction. Each square is a site (numbered 1 to $n$). The red cir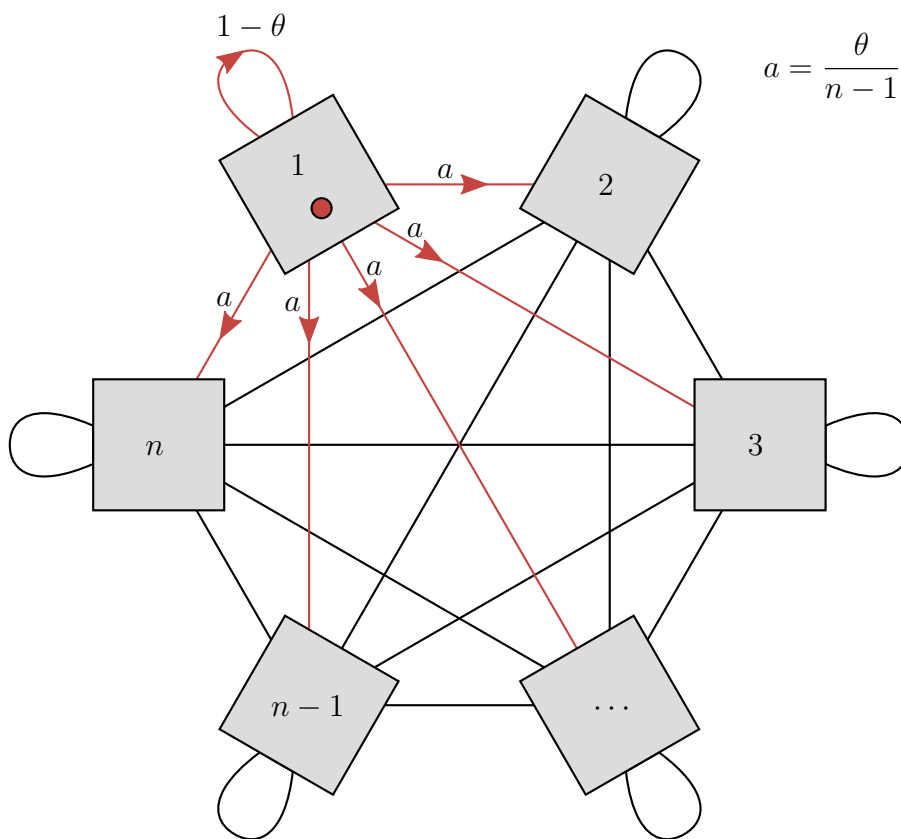cle is a particle within site 1. Edges between any pair of sites are equally weighted (with probability $a$). Self-loops represent the lack of movement to another site (occurring with probability $1 - \theta$).

with parameters $N$ and $\frac{1}{n}$:

$$N_i \sim \text{Binomial}\left(N, \frac{1}{n}\right), \tag{3.1}$$

which has probability mass function:

$$P(N_i = k) = \binom{N}{k}\left(\frac{1}{n}\right)^k \left(1 - \frac{1}{n}\right)^{N-k}. \tag{3.2}$$

Note that when $N$ and $n$ are both large, Eq. (3.2) can be approximated by the Poisson distribution with a parameter value of $N \cdot \frac{1}{n} = \rho$:

$$P(N_i = k) = \frac{\rho^k}{k!} \cdot e^{-\rho}. \tag{3.3}$$

Here, $\rho$ is the average number of particles per site. Despite the lack of a spatial aspect in the model, $\rho$ shall still be referred to as *particle density.*

Table 3.1 lists the symbols used to represent each variable in the model:

| Symbol | Meaning |
|--------|---------|
| $N$ | Number of particles in the system |
| $n$ | Number of sites in the transport graph |
| $\rho$ | Mean occupancy $\left(\frac{N}{n}\right)$ in steady state (particle density) |
| $\theta$ | Probability (per second) of moving to a new site |

Table 3.1: Description of the symbols used when discussing the transport model.

## 3.2  Contact Rate

In this section, particle contact rate $\nu_c$ is modelled. In Section 2.4.1, $\nu_c$ was defined to be the number of new contacts made by a particle per second. Generally speaking, one would expect $\nu_c$ to increase in the following situations:

- particle movement $(\theta)$ increases, making new contacts more likely;
- the number of particles $(N)$ increases, thus increasing particle density;
- the number of sites $(n)$ decreases, again increasing the particle density.

**Theorem 3.2.1** *The probability that an arbitrary particle makes exactly $k$ new*

*contacts in any given time-step is:*

$$P(\nu_c = k) = \theta \cdot \binom{N}{k}\left(\frac{1}{n}\right)^k \left(1 - \frac{1}{n}\right)^{N-k} + (1 - \theta) \cdot \binom{N}{k}\left(\frac{\theta}{n}\right)^k \left(1 - \frac{\theta}{n}\right)^{N-k}. \quad (3.4)$$

**Proof** The problem is firstly divided into two parts that are easier to solve:

- Contact rate is modelled for a particle that has just jumped to its current site. This means that the particle was in a different site at the previous time-step. This type of contact rate shall be denoted as $\nu_c^{\text{jump}}$.

- Contact rate is modelled for a particle that has not moved since the previous time-step. This shall be denoted as $\nu_c^{\text{stay}}$.

$\nu_c$ is simply a combination of $\nu_c^{\text{jump}}$ and $\nu_c^{\text{stay}}$ with respect to $\theta$ (the probability that a particle jumps at any given time-step):

$$P(\nu_c = k) = \theta \cdot P(\nu_c^{\text{jump}} = k) + (1 - \theta) \cdot P(\nu_c^{\text{stay}} = k). \quad (3.5)$$

The distributions of $\nu_c^{\text{jump}}$ and $\nu_c^{\text{stay}}$ are derived separately.

**Contact Rate Given a Jump:** Consider a particle that has just jumped to its current site. In this case, our particle makes a new contact with every other particle at the same site. Therefore, $\nu_c^{\text{jump}}$ is equal to the number of particles in the site just before our particle jumped to the site. The distribution of this number is given by Eq. (3.2), with $N$ replaced by $N - 1$ to exclude our jumping particle. Thus,

$$P(\nu_c^{\text{jump}} = k) = \binom{N-1}{k}\left(\frac{1}{n}\right)^k \left(1 - \frac{1}{n}\right)^{N-1-k}. \quad (3.6)$$

This is simply the binomial distribution with parameters $N-1$ and $\frac{1}{n}$. It is reasonable to assume that $N \approx N - 1$ for large values of $N$, hence,

$$\nu_c^{\text{jump}} \sim \text{Binomial}\left(N, \frac{1}{n}\right). \quad (3.7)$$

**Contact Rate Given No Jump:** Let us now look at $\nu_c^{\text{stay}}$, the contact rate of particles that did not jump to a new site at the previous time-step. Let $N_i^{\text{jump}}$ and $N_i^{\text{stay}}$ respectively denote the number of particles that did and did not move to site $i$ at the previous time-step. $N_i^{jump} = k$ if and only if any combination of $k$ particles at site $i$

jumped at the last time-step and the remaining $N_i - k$ particles did not. Therefore, $N_i^{\text{jump}}$ has binomial distribution with parameters $N_i$ and $\theta$. Any particle that did not move into its current site at the previous time-step will make new contacts with the $N_i^{\text{jump}}$ that did. Thus,

$$\nu_c^{\text{stay}} \equiv N_i^{\text{jump}} \sim Binomial\left(N_i, \theta\right). \tag{3.8}$$

The following Binomial distribution relationship is used: if $X \sim B\left(n, p\right)$ and $Y \sim B\left(X, q\right)$ then $Y \sim B\left(n, pq\right)$ (Bertsekas and Tsitsiklis 2002). This relationship can be used with Eqs. (3.1) and (3.8) to provide a simplified distribution for $\nu_c^{stay}$:

$$\nu_c^{\text{stay}} \sim Binomial\left(N, \frac{\theta}{n}\right).$$

Substituting Eqs. (3.7) and (3.8) into Eq. (3.5) provides the equation for $\nu_c$ regardless of whether a particle jumped:

$$P(\nu_c = k) = \theta \cdot \binom{N}{k}\left(\frac{1}{n}\right)^k\left(1 - \frac{1}{n}\right)^{N-k} + (1 - \theta) \cdot \binom{N}{k}\left(\frac{\theta}{n}\right)^k\left(1 - \frac{\theta}{n}\right)^{N-k}. \quad\blacksquare$$

Note that when $N$ and $n$ are large, the binomial distributions in Eq. (3.4) can be approximated Poisson distributions as follows:

$$P(\nu_c = k) = \theta \cdot \frac{\rho^k e^{-\rho}}{k!} + (1 - \theta) \cdot \frac{(\rho\theta)^k e^{-\rho\theta}}{k!}. \tag{3.9}$$

Figure 3.4 compares the developed theoretical and simulated models for contact rate. Clearly, the theoretical model matches the simulated results.

### 3.2.1 Expected Contact Rate

The mean value of the Binomial distribution with parameters $n$ and $p$ is $np$. By applying this property to both Binomial distributions in Eq. (3.4), the expected contact rate is found, as follows:

$$E(\nu_c) = \theta \cdot \rho + (1 - \theta) \cdot \theta\rho,$$
$$= \theta\rho(2 - \theta). \tag{3.10}$$

**Distribution of Contact Rate**
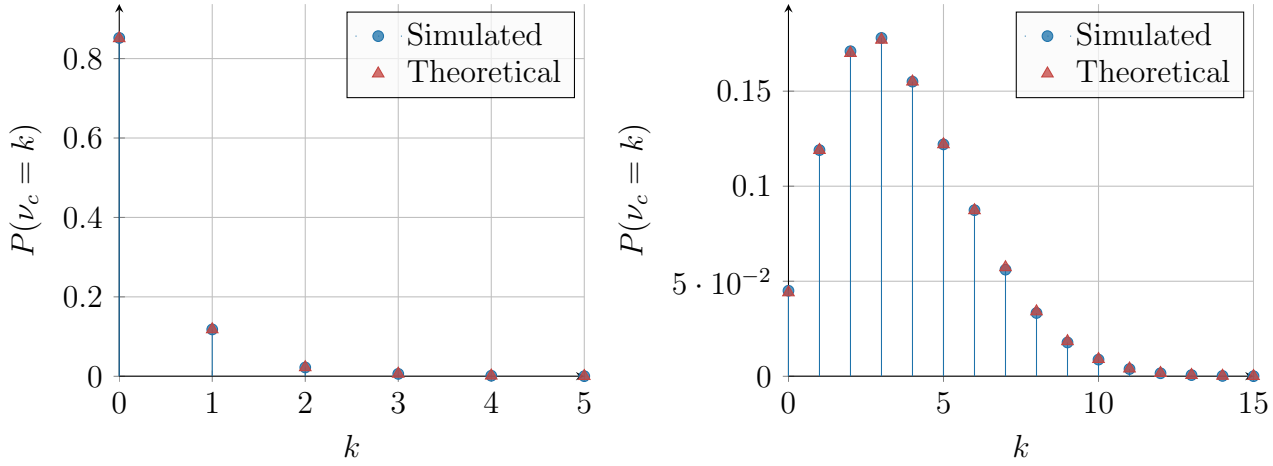
Figure 3.4: Theoretical/simulated model comparison for the contact rate distribution. Left plot parameter values: $N = 100$, $n = 100$, $\theta = 0.1$. Right plot parameter values: $N = 500$, $n = 100$, $\theta = 0.5$.

Figure 3.5 compares the theoretical expected contact rate model to a simulated model for various values of $\rho$ and $\theta$. From the results, it is clear that $E(\nu_c)$ linearly increases with $\rho$. This is confirmed in Eq. (3.10), from which it can be deduced that $E(\nu_c) \propto \rho$. This is not surprising, as a higher occupancy means more particles per site and hence more contact opportunities. It is also clear that $E(\nu_c)$ increases with $\theta$, as shown by the results and deduced from Eq. (3.10) as follows:

$$E(\nu_c) = 2\rho\theta - \rho\theta^2,$$
$$\frac{\mathrm{d}E(\nu_c)}{\mathrm{d}\theta} = 2\rho - 2\rho\theta,$$
$$= 2\rho(1 - \theta) \geq 0 \quad \text{as } 0 \leq \theta \leq 1.$$

Again, this is expected as a particle is likely to make more contacts if it moves around instead of waiting for others to come within range.

## 3.3   Contact Duration

In this section, contact duration $T_c$ is modelled for the transport graph model. Generally, one would expect $T_c$ to increase as particle movement ($\theta$) decreases. This is because decreased movement leads to particles remaining co-located for longer.

**Expected Contact Rate/Duration Against Particle Density/Jump Probability**

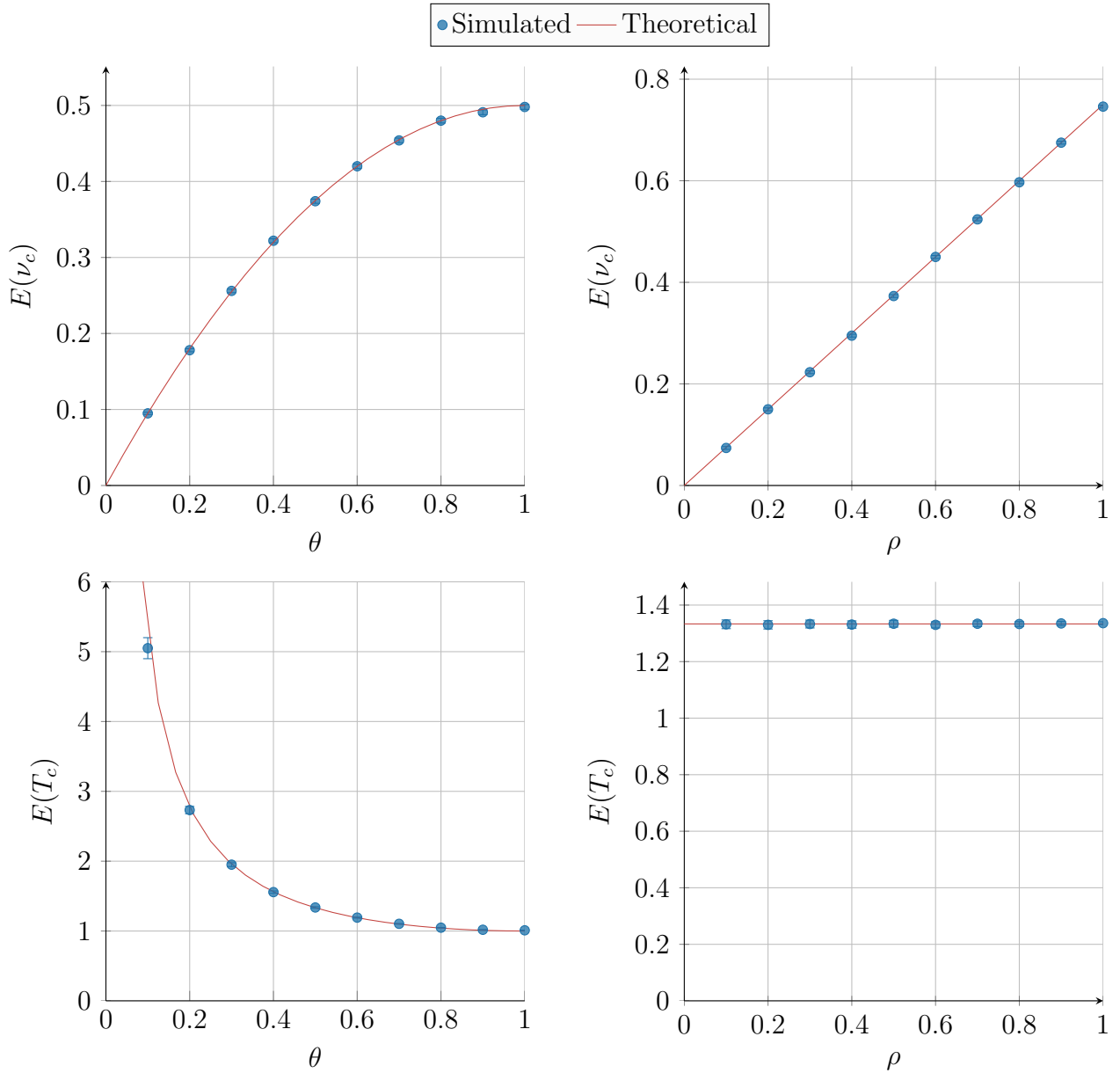Figure 3.5: Theoretical/simulated model comparisons for expected contact rate (top row) and expected contact duration (bottom row) against jump probability (left column) and particle density (right column). All error bars show standard error (some are too small to see). Parameter values: $N = 100$, $n = 100$, $\rho = \frac{N}{n} = 1$ (left column only); $\theta = 0.5$ (right column only).

**Theorem 3.3.1**

$$P(T_c \geq t) = (1 - \theta)^{2(t-1)}.$$

**Proof** For any pair of particles, $T_c = t$ if and only if the following are true:

- Both particles occupy the same site (*i.e.* neither jump) from time 0 to $t-1$. This occurs with probability $(1 - \theta)^{2(t-1)}$. The possibility of two co-located particles jumping together to the same site is ignored, as explained in Section 3.1.
- Both particles occupy different sites (*i.e.* one or both jump) at time $t$. This occurs with probability $1 - (1 - \theta)^2$.

Combining these two expressions provides the distribution of $T_c$:

$$P(T_c = t) = \left[(1 - \theta)^2\right]^{t-1} \left[1 - (1 - \theta)^2\right]. \qquad (3.11)$$

This is the probability mass function of the Geometric distribution with parameter value $1 - (1 - \theta)^2$; therefore, $T_c \sim \text{Geometric}\left(1 - (1 - \theta)^2\right)$.

The cumulative distribution function of the geometric distribution with parameter $p$ is $1 - (1 - p)^t$ for some $t \in \{1, 2, 3, \ldots\}$. Substituting $p$ with $1 - (1 - \theta)^2$ gives:

$$P(T_c \leq t) = 1 - (1 - (1 - (1 - \theta)^2))^t. \qquad (3.12)$$

Subtract this from 1 to get:

$$P(T_c > t) = 1 - (1 - (1 - (1 - (1 - \theta)^2))^t),$$
$$= \left[(1 - \theta)^2\right]^t.$$

Finally, substitute $t$ for $t - 1$ to get:

$$P(T_c \geq t) = (1 - \theta)^{2(t-1)}. \qquad \blacksquare$$

The probability mass function for $T_c$ for various values of $\theta$ is presented in Fig. 3.6. In Fig. 3.7, the developed theoretical model is compared to simulated results for two sets of parameter values. Clearly, the theoretical model matches the simulated results.
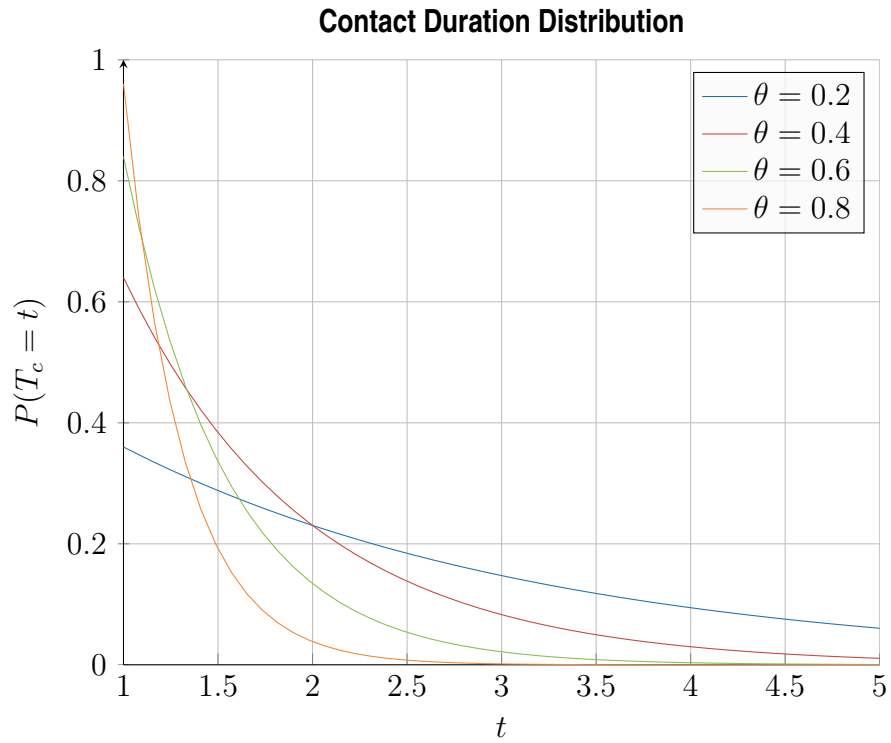
Figure 3.6: Plot to show the probability mass function of the contact duration for various values of $\theta$.
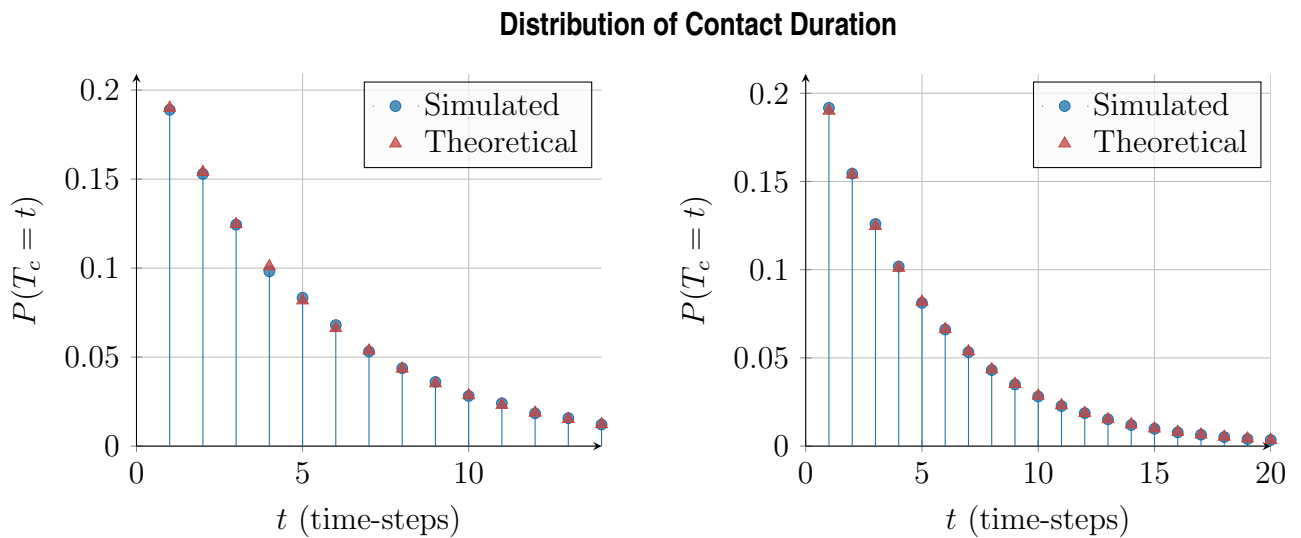


Figure 3.7: Theoretical/simulated model comparison for $T_c$. Left plot parameter values: $N = 10$, $n = 10$, $\theta = 0.1$. Right plot parameter values used: $N = 100$, $n = 100$, $\theta = 0.1$. Simulated results averaged over 50 simulations, each of 500 seconds.

### 3.3.1  Expected Contact Duration

As discussed, $T_c \sim$ Geometric $(1 - (1 - \theta)^2)$. The expected value of the Geometric distribution is the inverse of the parameter. Therefore, the expected value of $T_c$ is:

$$E(T_c) = \frac{1}{1 - (1 - \theta)^2} \tag{3.13}$$

From this equation, it is clear that $E(T_c) \to \infty$ as $\theta \to 0$, *i.e.* particles remain in contact indefinitely if they never move. Also, $E(T_c) \to 1$ as $\theta \to 1$, meaning particles stay in contact for only one second if they jump at every second.

Figure 3.5 compares the developed theoretical model for $T_c$ to simulated data for various values of $\rho$ and $\theta$. From the plots, it is clear that $\rho$ does not affect $T_c$. However, $\theta$ does affect $T_c$, which decreases at a rate inversely proportional to $\theta$. This can be seen in the polynomial Eq. (3.13). This polynomial decay is expected as contacts are terminated sooner if particles move more frequently.

## 3.4  Message Spread

In this section, a theoretical model is developed for message spread in the transport graph described in Section 3.1. In the transport graph, particles can only communicate with other particles in the same site. Each particle jumps to a new site with probability $\theta$ at each time-step. The used message spread model relies on the contact rate and contact duration distributions, derived in Sections 3.2 and 3.3 respectively. A single message is propagated for each experiment. Despite not being most suited to OPNET technology (as discussed in Section 2.2.3), the SI interaction scheme is used to simplify the theoretical models.

**Definition** Let $I(t)$ be the proportion of infectious particles (particles which are carrying the message) in the system at time $t$. Only one particle has the message at time 0, therefore, $I(0) = N^{-1}$. Let $S(t) = 1 - I(t)$ be the proportion of susceptible particles in the network at time $t$.

Let $\Delta_\tau(t)$ be the increase in the proportion of infectious particles at time $t$, given a message transmission time of $\tau$. Note that $\Delta_0(t)$ corresponds to instantaneous

transmissions. Let $T_c$ be the contact duration for any two particles in the system (see Section 3.3).

**Theorem 3.4.1**

$$\Delta_\tau(t) = P(T_c \geq \tau) \cdot \Delta_0(t)$$

**Proof** If transmission time is instantaneous, a successful transmission occurs with every infectious–susceptible contact. For non-instantaneous transmissions, only a certain proportion of the infectious–susceptible contacts result in successful transmissions— those of a duration of at least $\tau$. ∎

Let us now proceed to create a model for $\Delta_0(t)$.

**Definition** Let $\nu_c$ be the number of new contacts a particle makes in a given second (see Section 3.2).

**Theorem 3.4.2**

$$\Delta_0(t) = S(t) \cdot \sum_{k=0}^{\infty} P(\nu_c = k) \cdot (1 - S(t)^k)$$

**Proof** At time $t$, a particle is susceptible and makes $k$ new contacts with probability $S(t) \cdot P(\nu_c = k)$. This susceptible particle becomes infected unless all $k$ new contacts are not infectious, which occurs with probability $S(t)^k$. Therefore, the probability that our susceptible particle is infected at time $t$ (given that it made $k$ new contacts) can be expressed as follows:

$$S(t) \cdot P(\nu_c = k) \cdot (1 - S(t)^k).$$

The sum of this expression over all possible values of $k$ provides the probability of infection regardless of the number of new contacts made. This is equal to $\Delta_0(t)$, the proportion of particles that become infected at time $t$:

$$\Delta_0(t) = S(t) \cdot \sum_{k=0}^{\infty} P(\nu_c = k) \cdot (1 - S(t)^k). \quad ∎$$

**Theorem 3.4.3**

$$\Delta_\tau(t) = P(T_c \geq \tau) \cdot S(t) \cdot \sum_{k=0}^{\infty} P(\nu_c = k) \cdot (1 - S(t)^k)$$

**Proof** Follows from Theorem 3.4.1 and Theorem 3.4.2. ∎

## 3.4.1 Experimental Results

Figure 3.8 presents a comparison of simulated results with the theoretical model developed in this section. The top-left plot is the *control plot* which presents the results of a control experiment. The three other plots each present the results of an experiment which differs from the control experiment by a single parameter value. This makes it easy to see how each parameter affects the accuracy of the developed theoretical model. Table 3.2 shows the parameter values used for the control plot. The deviated parameter values are indicated at the bottom-right of each other axis in the figure.

| Parameter | Value |
| --- | --- |
| Number of particles ($N$) | 100 |
| Number of sites ($n$) | 1000 |
| Jump probability ($\theta$) | 0.1 |
| Transmission time ($\tau$) | 0 |

Table 3.2: List of parameter values used for the control plot in Fig. 3.8.

**Control Plot:** Looking at the control plot (a), it can be seen that the developed model is accurate as it falls within the error bars of the simulated results. The developed model fits perfectly for the first 100 seconds or so, after which the proportion of infectious particles starts to be overestimated. The reasoning for this is speculated upon later in this section.

**High Particle Density:** The results in plot (b) use a higher particle density than the control experiment. This is achieved by decreasing $n$ from 1000 to 100, giving a density of 1 instead of 0.1. It is clear that this has little effect on the developed model, reducing the accuracy only slightly. The model still falls within the empirical error bars, but not as much as with the control plot. Looking at the $x$ axis scale, it is clear that the rate of message spread has increased. This is due to a higher contact rate, resulting from the increased particle density.

Figure 3.8: Plots to compare simulated/theoretical models of message spread for the transport graph model using an SI interaction scheme. Table 3.2 shows the parameter values used for the control plot. All other plots have one parameter value adjusted (indicated in the bottom-right of the axis). All markers represent the averaged empirical data of 100 simulations; all errorbars show standard deviation. Note the different scales used on the x-axis.

**Non-Instantaneous Transmissions:** The results for non-instantaneous transmissions can be seen in plot (c). This experiment differs from the control experiment in that the transmission time is 5 rather than 0. It is clear that the model is still accurate for the first 100 or so seconds. Beyond this, accuracy starts to deteriorate and the model eventually falls outside of the empirical error bars. Nevertheless, the model still provides a fair estimate of message spread. Both the empirical results and the theoretical model show that propagation is slower than the control experiment, which is due to the longer transmission time.

**High Jump Probability:** In plot (d), jump probability is set to 0.5 instead of 0.1. By looking at the scale of the x-axis, it is clear that increasing the jump probability increases the rate of message spread. This is due to an increased contact rate. Although contact duration is decreased, this does not affect message spread as instantaneous transmissions are used. It is clear that increasing the jump probability has had little effect on the accuracy of the developed model.

## 3.4.2  Evaluation

Overall, the developed model appears to provide a good estimate for message spread in the transport graph. However, a consistent over-estimation of the proportion of infectious particles in the system is observed. This may be because the theoretical model is deterministic, while the simulations are non-deterministic. This may be causing small discrepancies between the models in the early stages which are subsequently amplified in the ensuing evolution of the system. It can sometimes take a long time for a message to start propagating in a simulation, due to how fortunate the source particle is to contacting other particles. Conversely, fractional proportions of particles become infected straight away in the theoretical model (continuous time), leading to a slightly higher value in the early stages. Each value of the theoretical model is dependent on the previous, so a small deviation in the early stages has a snowball effect, leading to a large discrepancy in the later stages. Eventually, all particles become infectious and the model matches simulated results once again.

## 3.5   Chapter Summary

In this chapter, OPNETs have been studied where the particles move on a graph-based transport model. The particle contact rate for such a transport model has been theoretically modelled in Section 3.2. This informs subsequent chapters of this thesis as contact duration is modelled for more complex systems in Sections 4.4 and 5.4. Similarly, contact duration has been modelled for a graph-based transport model in Section 3.3, which informs Sections 4.6 and 5.5 later in this thesis. The models for contact rate and contact duration were combined and built upon to model the spread of a message in an OPNET in Section 3.4. This informs Sections 4.7 and 5.6 later in this thesis, which also aim to model message spread. In the next chapter, focus is shifted from graph-based regions to regions of discrete space.

# Discrete Spatial Models

In this chapter, discrete spatial models are considered. Empirical studies are performed to find how the behaviour of OPNETs is affected by the fundamental parameters in 1D and 2D space. Following this, theoretical models are created for contact rate and contact duration in 1D space. Finally, an empirical study is performed on message spread and the results are discussed with regard to the developed models for contact rate and contact duration.

## 4.1 Mobility Model

This chapter starts by introducing a discrete-space mobility model for 1D and 2D space. The mobility model is based on the Random Direction model, as discussed in Section 2.3.3.3. Synchronous, discrete-event simulation is used as described in Section 2.5.1. This section gives details of the mobility model for 1D and 2D space.

### 1D Space

Consider a lattice consisting of $n$ of vertices, or *sites*, sequentially connected by edges. Particles reside in a single site at any time. Edges are used only for movement, which occurs instantaneously. At every time-step, each particle moves to an adjacent site (chosen at random) with probability $\theta$, which shall be referred to as the *jump probability*. Periodic boundaries are used for the region, which can be visualised as
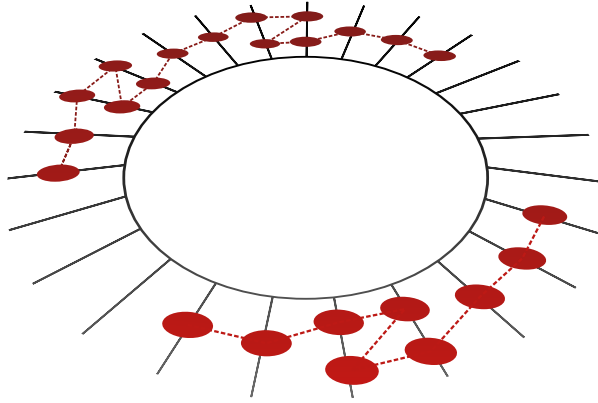
Figure 4.1: Diagram of the 1D lattice used for particle movement. Each black line emerging from the black circle is a site. The sites have no dimensions and only appear long so that the particles can be drawn onto them. The red dots are particles and the dotted line between them shows an example path that a particle may take.

a circle. Figure 4.1 shows an example of such a region. Note that this model is identical to the transport graph described in Chapter 3 with all chords removed.

## 2D Space

Consider a 2D lattice consisting of $n$ uniformly distributed sites. Edges connect all sites along the vertical and horizontal axes and there are no diagonal edges. Particles reside in a single site at any time. Edges are used only for movement, which occurs instantaneously. For every time-step, each particle moves to an adjacent site (chosen at random) with probability $\theta$. It is assumed that the width and height of the lattice is equal. The lattice is periodic in both directions, meaning it *wraps around* to form the surface of a torus. Figure 4.2 illustrates this region and shows how distance is measured within the region.

For 1D and 2D space, only *closed systems* is considered, meaning that no particle may enter or leave the region. It is assumed each edge is of unit length and each site has no dimensions. This allows the following definition of particle density: $\rho = \frac{N}{n}$, where $N$ is the total number of particles and $n$ is the total number of sites. It also allows the definition of particle speed as the number of sites travelled along per second.
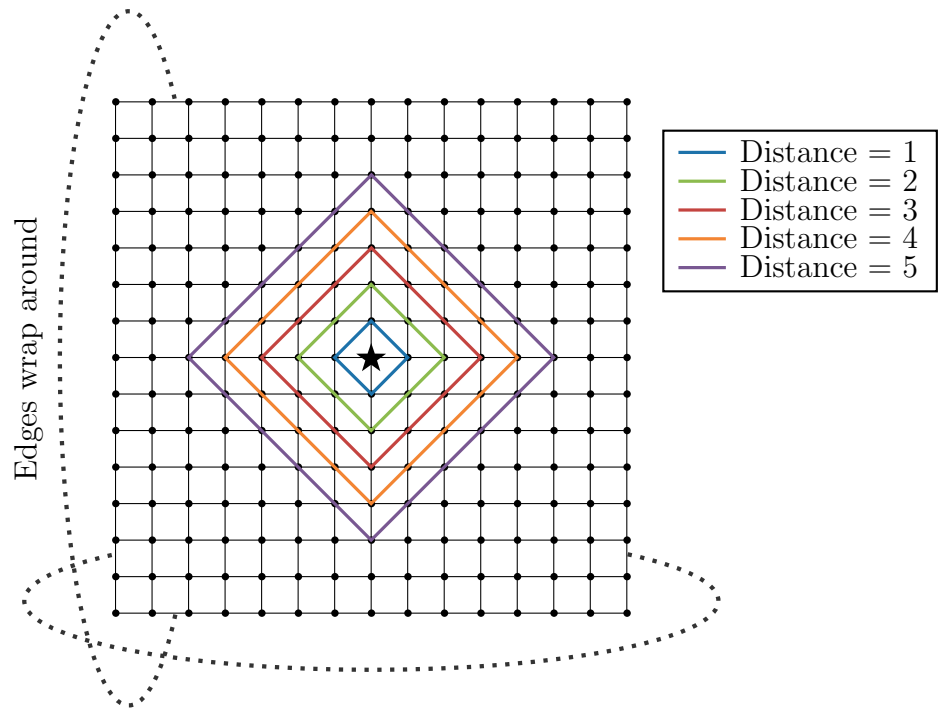
Figure 4.2: Diagram to illustrate how distance is measured in the 2D region. Instead of Euclidean distance, Manhattan distance is considered. This means distance is measured as the shortest path across the grid edges, rather than a straight line that is not restricted to the grid. In the figure, distance is being measured from the star in the centre.

## 4.2   Fundamental Parameter Study

In this section, a methodical study is performed on each of the fundamental parameters:

- particle density ($\rho$),
- transmission time ($\tau$),
- signal radius ($r$),
- particle speed, in this case defined by jump probability ($\theta$).

Each parameter will be studied to find how it affects message propagation in an OPNET. All studies are performed using the discrete space mobility model described in Section 4.1 for both 1D and 2D space.

### 4.2.1   Approach

The Monte Carlo method is to be used for all studies. This involves stochastic simulations that are repeated many times and the accuracy of the conclusions depends on the number of trials performed. Preliminary simulations showed that 200

simulation trials for each experiment provides a good compromise between confidence and computation time, given the considered parameter ranges. Therefore, 200 trials will be used for each study. Averaged results with standard deviations will be taken from each set of trials.

## 4.2.2  Parameter Values

Table 4.1 shows the values that will be used for each parameter study. All parameters except for the one being studied will use the default values. All parameter values were decided by running preliminary experiments to find a suitable combination. The preliminary experiments were the same as the actual experiments in the study, except only the minimum and maximum values were tested. Each preliminary experiment was repeated 100 times.

| Parameter | Default | Min. | Max. | Increment |
|-----------|---------|------|------|-----------|
| $\rho$    | 0.1     | 0.05 | 0.5  | 0.05      |
| $\tau$    | 10      | 0    | 100  | 10        |
| $r$       | 0       | 0    | 100  | 10        |
| $\theta$  | 0.1     | 0.1  | 1.0  | 0.1       |

Table 4.1: Range of parameter values used in the studies. The value of just one parameter is scaled at a time (from the minimum to maximum values shown in this table) while the other three parameters are set to their default values.

**Signal Radius:**  A signal radius of $r = 0$ means that particles can only interact with co-located particles, *i.e.* in the same site. A signal radius of $r > 0$ means that particles can interact with particles in sites up to $r$ jumps away in any direction. This concept is illustrated in Fig. 4.3. See also Fig. 4.2 for understanding how distance is measured in 2D space. Note that $r$ is a member of the set of positive integers.

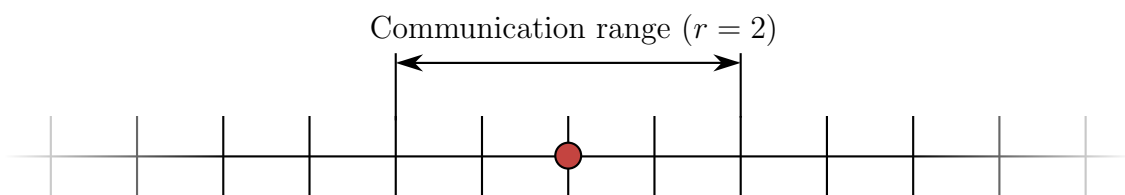Communication range ($r = 2$)



Figure 4.3: Diagram to show which sites (vertical lines) are within range of the particle (red circle) given $r = 2$. The illustrated particle can communicate with any particle in the same site or in sites that are 1 or 2 steps to the left/right.

| Region | $n$ | Default $N$ | Min. $N$ | Max $N$ | Increment |
|---|---|---|---|---|---|
| 1D | 1000 | 100 | 50 | 500 | 50 |
| 2D | 10000 | 1000 | 500 | 5000 | 500 |

Table 4.2: Range of values used for particle density.

**Transmission Time:**  Particles can transmit data at a rate of 1 bit per second. A message of 10 bits would, therefore, require a transmission time of 10 seconds. Note that a value of $\tau = 0$ means instantaneous transmissions (rather than a non-existent message).

**Particle Density:**  Note that $\rho$ will be adjusted by varying the number of particles in a region of fixed size. This is shown in Table 4.2. Note that the 2D region is square, so $n = 100 \times 100$.

### 4.2.3   Metrics

There are many ways in which the performance of an OPNET can be measured. It is difficult to know which metrics will provide the most useful results before they are recorded. Some metrics may produce uninteresting results due to high variation or high sensitivity to extreme circumstances. For example, the time taken for the message to be received by all particles in the network may vary greatly due to some particles residing in particularly hard-to-reach locations. To increase the chances of gaining useful insights into the behaviour of OPNETs, several performance metrics will be recorded. Each of the chosen metrics are described below. To the best of the author's knowledge, these particular metrics are original concepts.

$T_{50}^{Q}$:  The time until a certain quota of the particles have received a particular message. A quota of 50% shall be used for all studies as this is plenty of particles and results will not be skewed by waiting for the last few to receive the message. For example, waiting for all particles to receive the message may take a particularly long time due to one or two particles that do not receive the message for an abnormally long amount of time. This metric will provide insight into how fast a message spreads among the particles. A low value of $T_{50}^{Q}$ implies the message has spread quickly.

$T_{50}^D$: The time until a message reaches a certain distance (in any direction) away from its origin. A distance of 50 units shall be used as this is the largest distance possible in the 2D region, which is of size $100 \times 100$. The Manhattan distance will be taken when using 2D space, as illustrated in Fig. 4.2. The term $T_{50}^D$ will provide insight as to the way in which information spreads with respect to geographical space. A low value of $T_{50}^D$ would suggest that the message has spread quickly across a region.

$SP_{60}$: The probability that a message survives in the network for at least 60 minutes. A duration of 60 minutes is chosen as the relevance of a typical message may start to lose relevance beyond this time. A message survives, or *persists*, until its final copy is deleted from the network. Figure 4.4 shows how the probability that a message persists in an OPNET varies depending on the age of the message. In this figure, $SP_{60}$ is highlighted for 1D and 2D space. This metric will provide understanding of the length of time that a message is available in an OPNET.
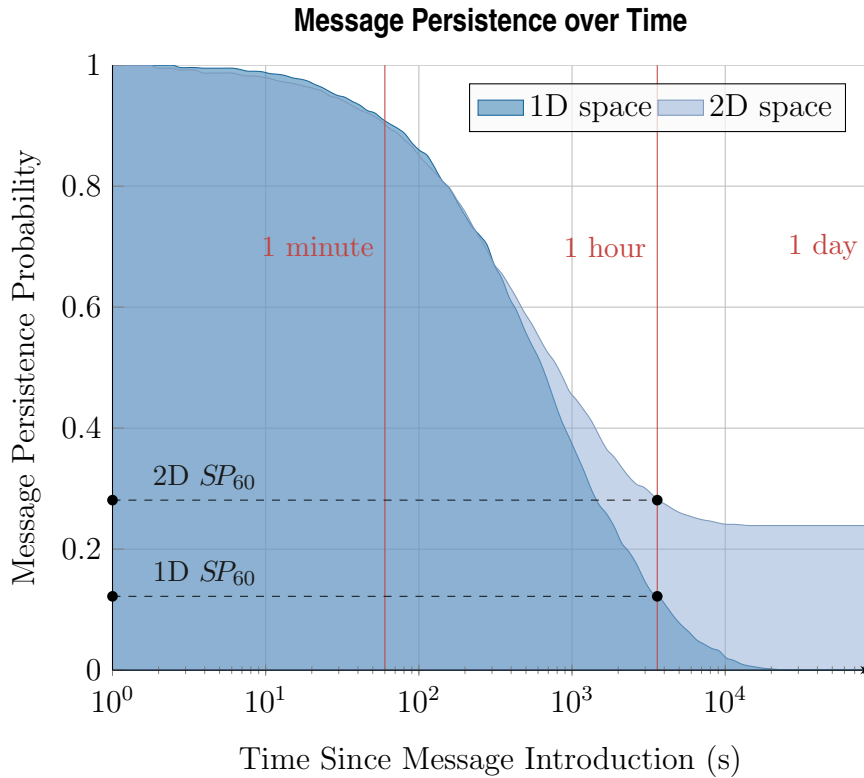


Figure 4.4: Plot to show the probability that a message persists given its age. Results averaged for 1000 simulations, all using the discrete space mobility model described in Section 4.1. Parameter values used: $\rho = 0.1$, $s = 5$, $r = 0$, $\tau = 10$. From the graph, it is clear that $SP_{60} = 0.28$ in the 2D region and 0.12 in the 1D region.

86

The terms $T_{50}^Q$ and $T_{50}^D$ shall be collectively referred to as the *temporal metrics*. These metrics are subject to a 24 hour cut-off time. Therefore, data are not recorded if it takes longer than 24 hours for the message to reach 50% of particles or a distance of 50 units.

## 4.2.4 Communications Protocol

In all simulations, there is one source particle and one message. This message is propagated as a broadcast transmission meaning that each particle, having received the message, attempts to forward it to as many other particles as possible. The source particle introduces the message as soon as the simulation begins.

For simplicity, an SI interaction scheme (as described in Sections 2.1 and 2.2) will be used when recording the temporal metrics ($T_{50}^Q$ and $T_{50}^D$). This will reveal the purest behaviour of OPNETs, minimally affected by communication protocol. This makes sense when recording the temporal metrics as another interaction scheme, such as the SIS, may cause the thresholds of the metrics to never be reached. However, the message persistence metric ($SP_{60}$) measures whether the message has become extinct at a certain time. The protocol used must, therefore, allow deletion of the message. For a closed system, it is important that particles can become infected with the same message more than once, otherwise the message persistence duration is greatly limited. Because of this, an SIS interaction scheme is used for simulations in which $SP_{60}$ is recorded.

For all SIS simulations, the rate at which infectious particles delete the message ($\delta$) will be set to 0.0035 per second, so that each infectious particle is expected to carry the message for $\delta^{-1} \approx 5$ minutes. This value was decided semi-arbitrarily as it is a reasonable amount of time to carry a message. As a sanity check, preliminary experiments each consisting of 100 simulation runs were used to confirm that the value of $\delta$ is appropriate. The preliminary experiments were much like the final experiments presented here, except only the maximum/minimum parameter values were studied, rather than the whole range.

### 4.2.5 Expected Outcome

One might anticipate that the message will spread more quickly and persist for longer in 2D space rather than 1D space as there is more surface area between infectious and susceptible particles. In 2D space, particles have more choice of where to move. This is beneficial for message spread as infectious particles tend to be tightly coupled in space as a group. Hence, if particles have more choice of where to move, they are more likely to jump outside of the group and find a susceptible particle. This concept is illustrated in Fig. 4.5.
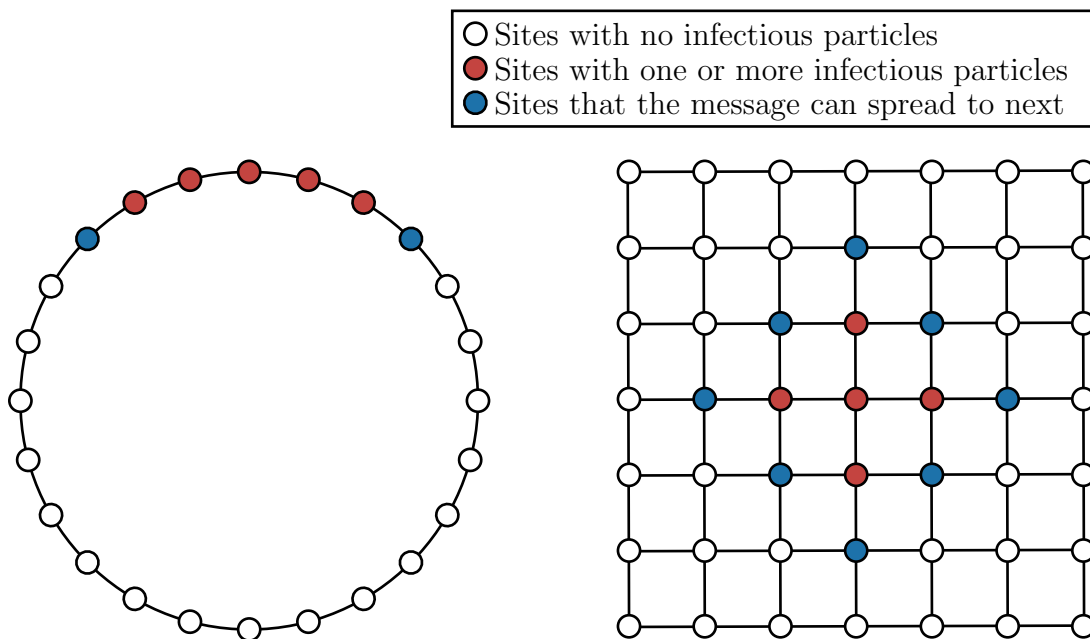


Figure 4.5: Diagram to show the size difference of the susceptible/infectious boundary in 1D space (left) and 2D space (right). It is assumed that $r = 1$ and $\rho$ is large. It is clear that the message can spread to many more sites in the 2D region, despite having the same number of infectious particles (which are grouped as tightly as possible). This accounts for why propagation is faster in 2D space.

### 4.2.6 Experimental Results

#### 4.2.6.1 Particle Density

Figure 4.6 shows the results of the study on particle density. The results are very similar in both regions (with smaller values for the temporal metrics in the 2D region, as predicted in Section 4.2.5). It is clear that both the time taken for 50% of particles to receive the message, and the time taken for the message to travel a distance of 50

units, decreases as particle density increases. This rate of decrease appears to reduce as the particle density gets higher.

## 1D Space—Particle Density Study



## 2D Space—Particle Density Study
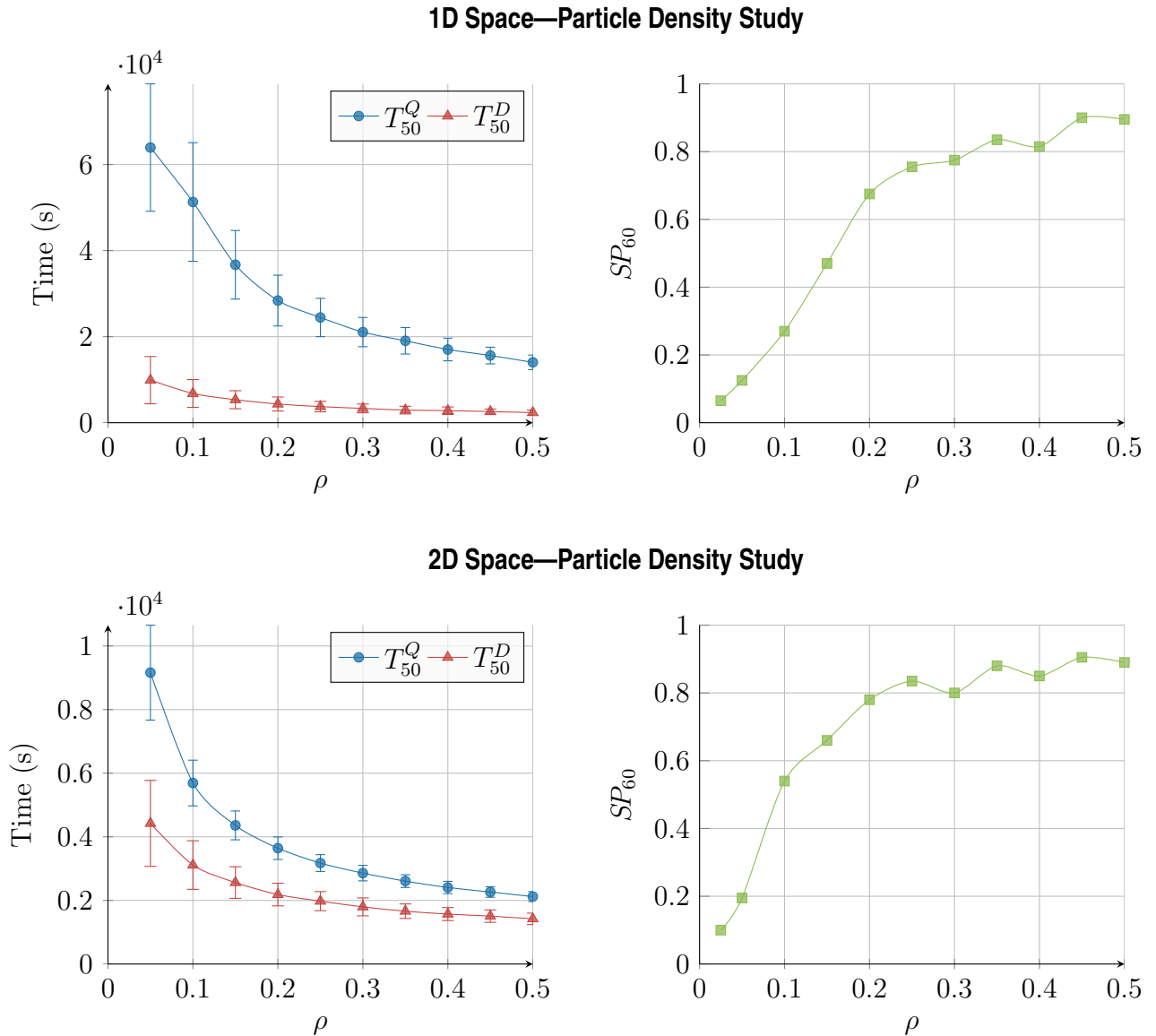


Figure 4.6: Parameter study on particle density, $\rho$. The first/second row shows results for 1D/2D space, respectively. All markers represent the averaged empirical data of 200 simulations; all errorbars show standard deviation. The results show that the message propagates faster and persists for longer as $\rho$ increases. Note that $\tau = 10$ for all simulations.

Looking at the right-hand column of Fig. 4.6, it is clear that the persistence probability of the message increases as particle density increases. As with the temporal metrics, the rate of increase appears to reduce as the particle density gets higher.

In summary, it is concluded that increasing particle density is beneficial to message propagation. This is expected, as a higher density of particles means more interactions and more transmissions.

> Note that in the context of OPNETs, there may also be drawbacks to a high
> device density. Depending on the hardware, a high density of devices may cause
> signal interference, leading to a reduction in channel capacity.

### 4.2.6.2 Transmission Time

Figure 4.7 shows the results of the study on transmission time. For 1D and 2D space,
it is clear that the time taken for 50% of particles to receive the message increases as
transmission time increases. This rate of increase appears to be sharper for 2D space.
This may be due to the fact that particles are less likely to simultaneously jump to
the same site in 2D space as they have additional options of moving up/down rather
than just left/right.

It is clear that the message takes longer to travel a given distance as transmission
time increases. The rate of increase appears to be the same for 1D and 2D space;
it is slow and perhaps reduces to zero for larger messages. The term $T_{50}^D$ certainly
seems less affected by transmission time than $T_{50}^Q$. This may be because $T_{50}^D$ relies
more on particle movement whereas $T_{50}^Q$ relies more on message passing—only the
latter is affected by transmission time. Perhaps this effect becomes more prominent
as transmission time increases, explaining why $T_{50}^D$ appears to stabilise for longer
transmission times.

The persistence probability decreases as the transmission time increases. Results are
similar for 1D and 2D space. The probability that the message persists for at least
an hour sharply decreases to near-zero for a transmission time of about 20 units.

In summary, it is concluded that larger messages do not propagate as quickly, or
persist for as long as smaller messages. This is expected as larger messages take
longer to transmit and can, therefore, lead to more unsuccessful transmissions.

### 4.2.6.3 Signal Radius

Figure 4.8 shows the results of the study on signal radius. It is clear that both the
time taken for 50% of particles to receive the message, and the time taken for the
message to travel a distance of 50 units, decreases as signal radius increases. The
rate of decrease appears to be approximately linear for 1D space and polynomial

Figure 4.7: Parameter study on transmission time ($\tau$) for 1D and 2D space. All markers represent the averaged empirical data of 200 simulations; all errorbars show standard deviation. Not all results are shown for $T_{50}^Q$ as they go beyond the 24 hour cut-off time. The results show that the message propagates slower and persists for less time as $\tau$ increases.

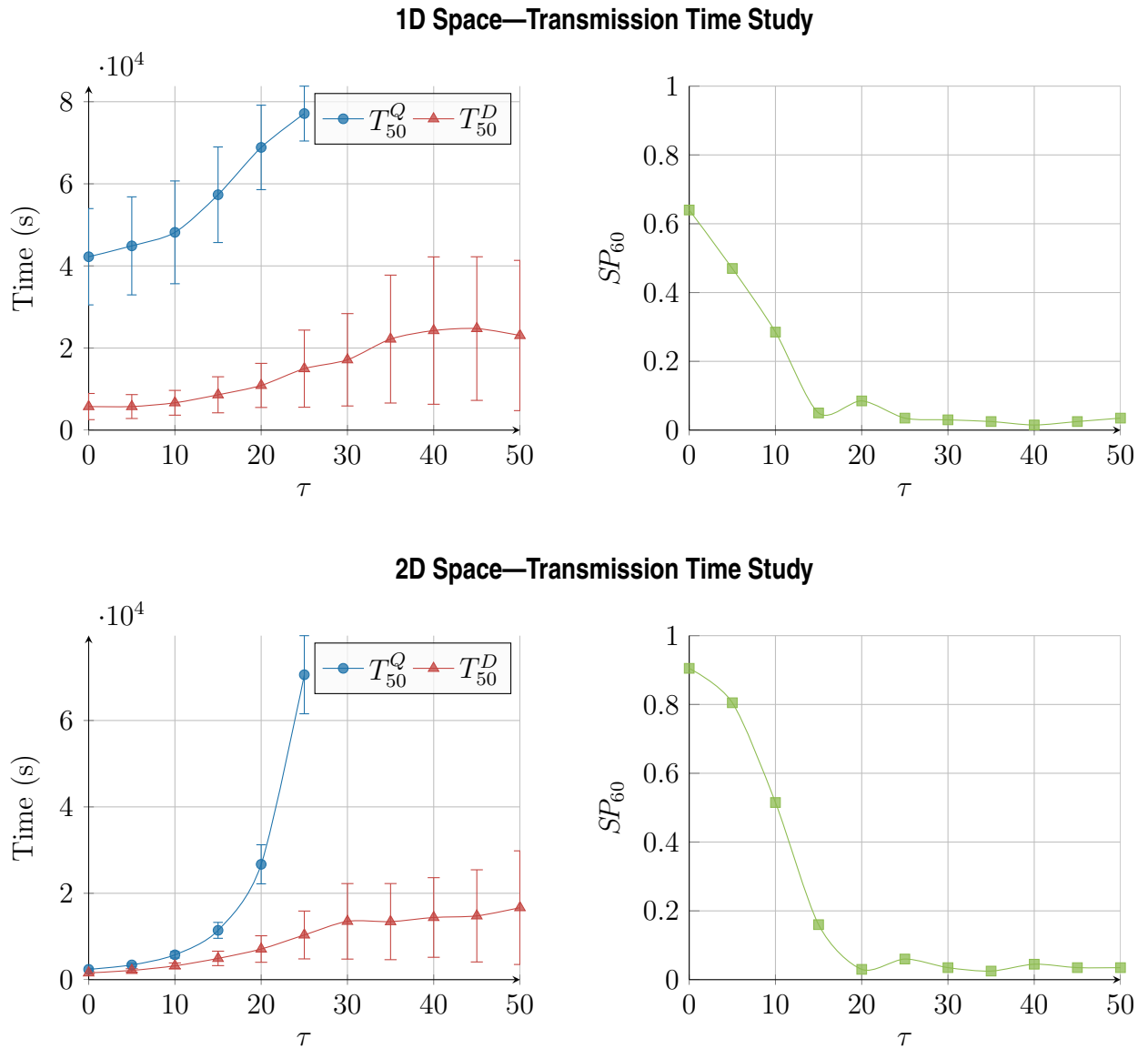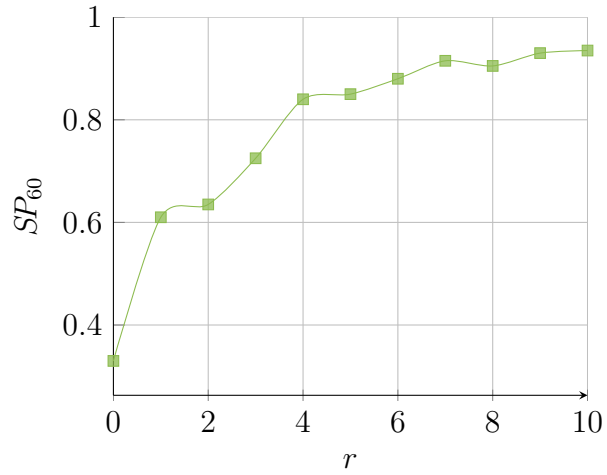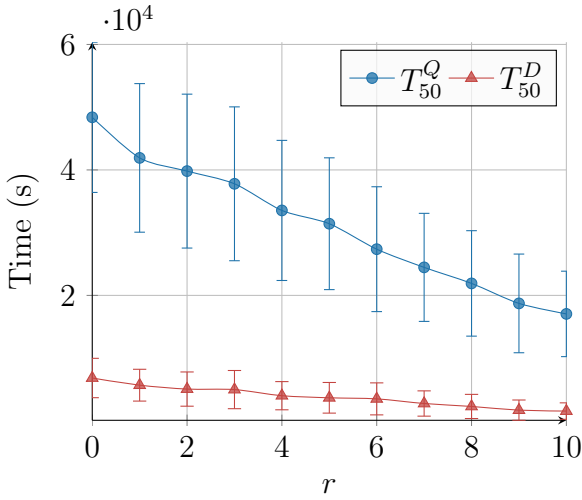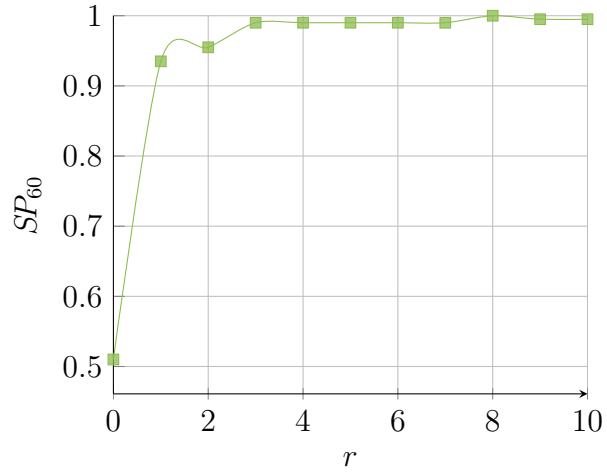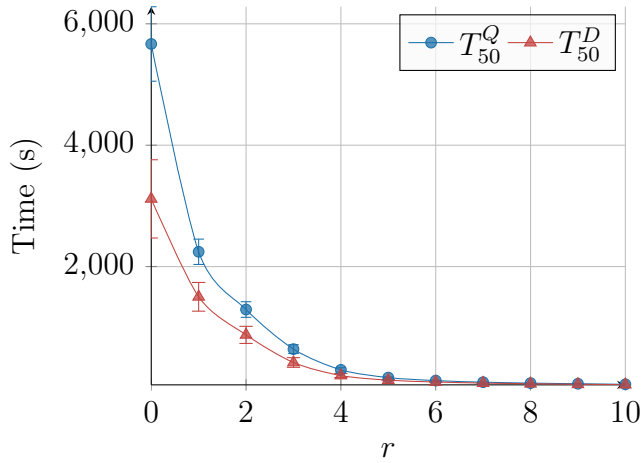Figure 4.8: Parameter study on signal radius ($r$) for 1D and 2D space. All markers represent the averaged empirical data of 200 simulations; all errorbars show standard deviation. The results show that the message propagates more quickly and survives for longer as the signal radius increases. Note that $\tau = 10$ for all simulations.

for 2D space. This is expected as signal area is proportional to $r$ in 1D space and proportional to $r^2$ in 2D space.

The probability that the message persists for at least an hour increases as signal radius increases. Once again, this effect is sharper for 2D space, where it quickly rises until the message almost always persists for at least an hour.

In summary, it is concluded that a larger signal radius causes the message to spread more quickly and to survive for longer. This is expected as a larger signal radius leads to more particle interactions and, therefore, more message transmissions.

### 4.2.6.4 Jump Probability

Fig. 4.9 shows the results of the study on jump probability. Results show that the time taken for the message to spread to 50% of the particle increases sharply as the jump probability increases, in both 1D and 2D space. The rate of increase is so large that it quickly exceeds the 24 hour cut-off. Similarly, the probability that the message persists for more than 1 hour quickly decreases as the jump probability increases. These results are to be expected as a higher jump probability means fewer particles remain co-located for the entire 10 second message transmission.

Results show that jump probability has little overall effect on the distance travelled by the message. This may be related to the point discussed in Section 4.2.6.2: as there are fewer particles carrying the message, the speed at which the message travels is reduced. However, this is countered by the fact that the particles are moving faster, so overall the message travels at a fairly constant speed. Note that the system may be affected more significantly by particle movement for other values of transmission time, as will be seen in the following chapter.

## 4.3    Asymmetric Particle Movement

As well as jump probability, it is interesting to study bias in the direction of the jump. Until now, it has been assumed that particles move in all directions with equal probability. Now, the possibility of particles tending to favour a certain direction over others is discussed. A brief study is performed with a 1D space experiment in
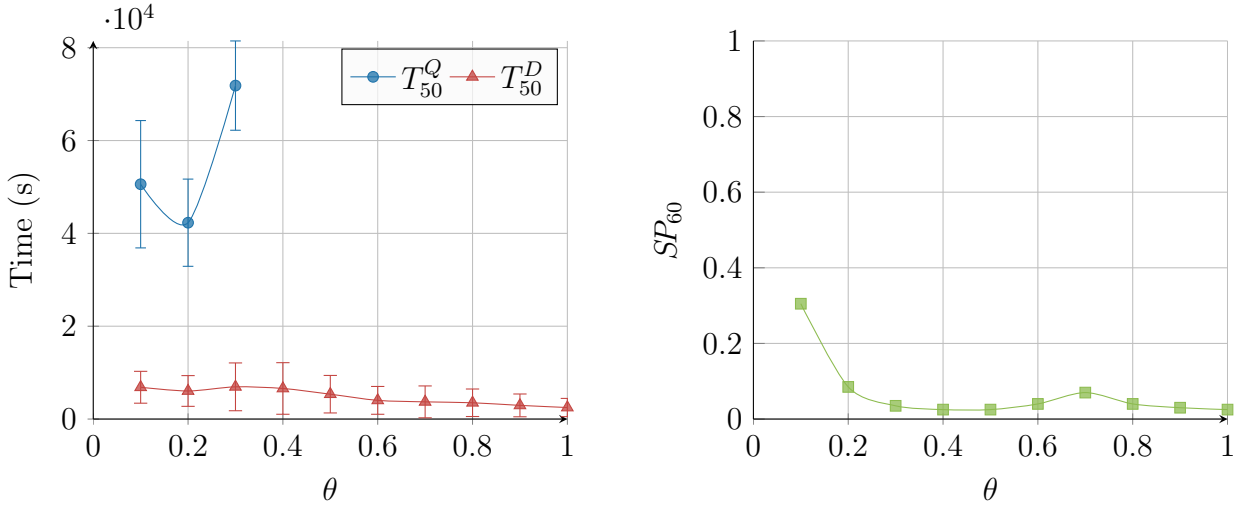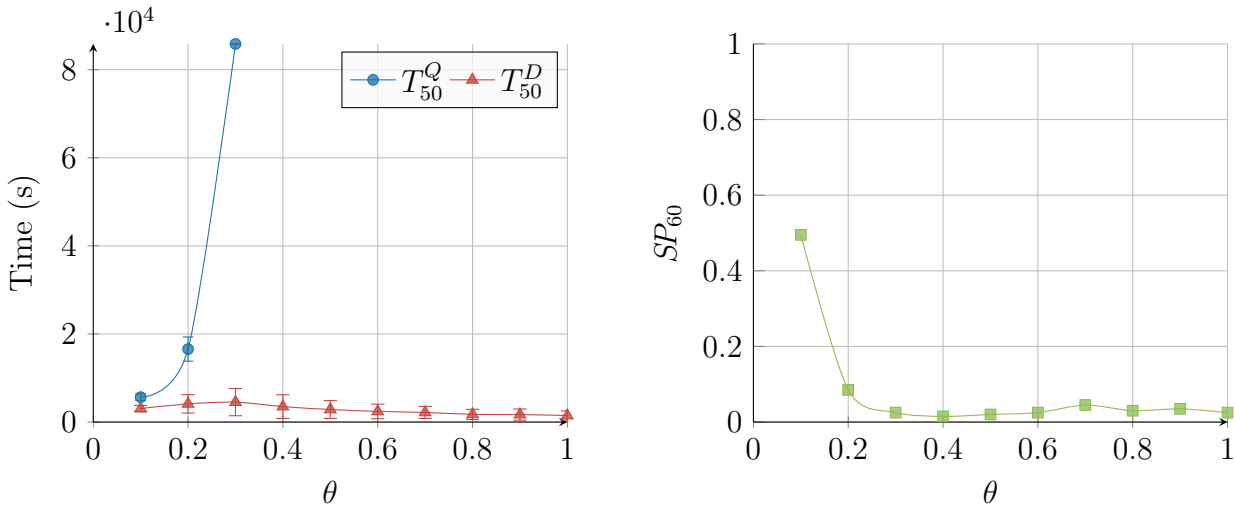
Figure 4.9: Parameter study on jump probability ($\theta$) for 1D and 2D space. All markers represent the averaged empirical data of 200 simulations; all errorbars show standard deviation. Not all results are shown for $T_{50}^Q$ as they go beyond the 24 hour cut-off time. The results show that jump probability does not affect the speed at which the message travels. However, the message does not survive for as long, and it takes longer for particles to receive the message for larger jump probabilities. Note that $\tau = 10$ for all simulations.

which particles only move to the right (never to the left). The following parameter values are used:

- jump probability, $\theta = 0.1$;
- particle density, $\rho = 0.1$;
- transmission time, $\tau = 10$;
- signal radius, $r = 12$.

Rather than recording the metrics used in previous studies, simply the spatial spread of the message is looked at over time.

The results of this study can be seen in the upper plot of Fig. 4.10 (see note[1]). As expected, the message spreads from left to right at roughly the average speed of the particles (0.1 sites per second). However, notice that the message spreads slightly to the left, even though particles are moving only to the right. This is due to the signal radius being 12 units. This allows the message to *hop* wirelessly to particles at positions to the left (without a particle carrying it there). For the same reason, the spatial extent of infectious particles increases as more particles become infected over time.

It became clear that the message can spread against the movement of the particles. Now, certain parameter values are adjusted to emphasise this behaviour. The lower plot in Fig. 4.10 (see Footnote 1) shows the same results as before, but with $\theta = 0.01$ and $r = 20$. It is clear that the message now spreads a lot further to the left, giving an almost symmetrical profile. The message also stays to the left of the origin for a longer period of time.

> It may be useful for engineers to configure OPNETs to encourage message spread against the movement of the devices. For example, it may be desirable to pass a message backwards to cars on a motorway to warn of high congestion ahead.

---

[1]It should be noted that the data displayed in Fig. 4.10 have been normalised in order to display it correctly. To be able to produce such a plot, the message must be released from the same position in all 200 trials (or, the start positions must be aligned after simulation). In doing this, an artificially high particle density appears around the origin. This is due to the fact that there is always a particle at this position (the message source) in all 200 trials. Although this effect fades over time, the plots still remain affected. To counter this artefact, each bar of the histogram has been individually scaled according to the particle density at that time and position. This eradicates the artificially high peak of infectious particles at the mode.
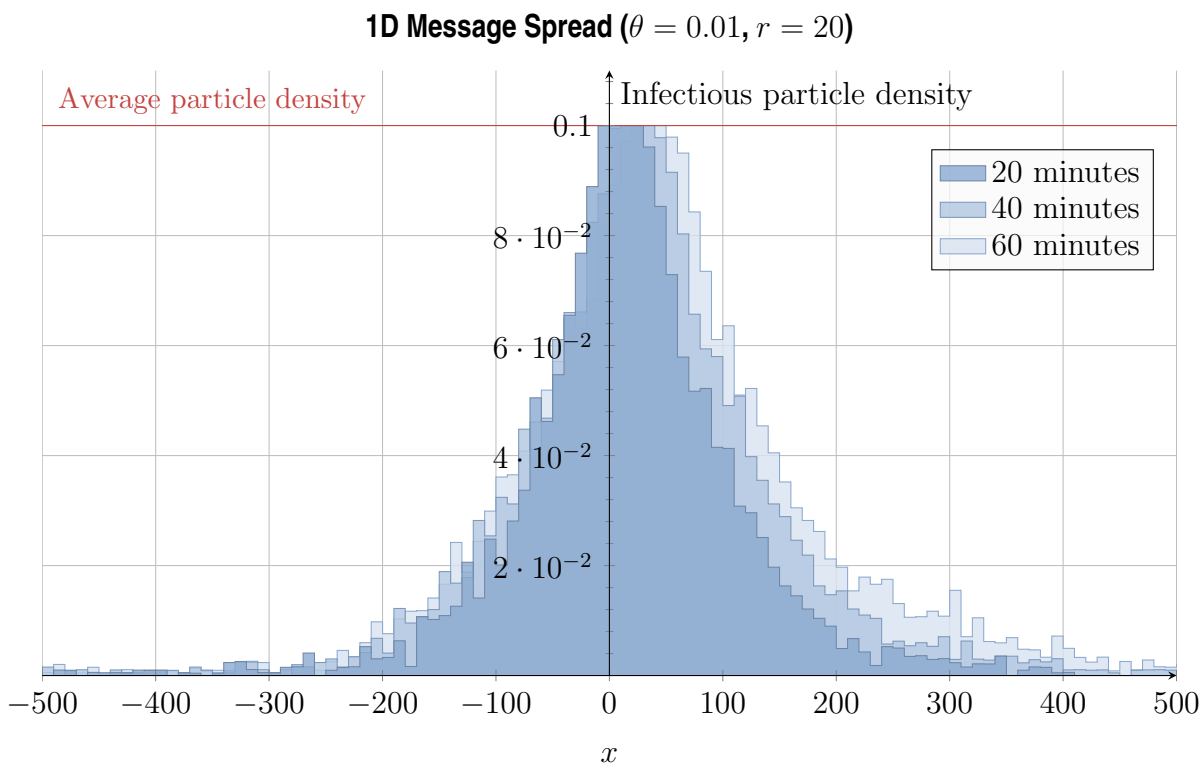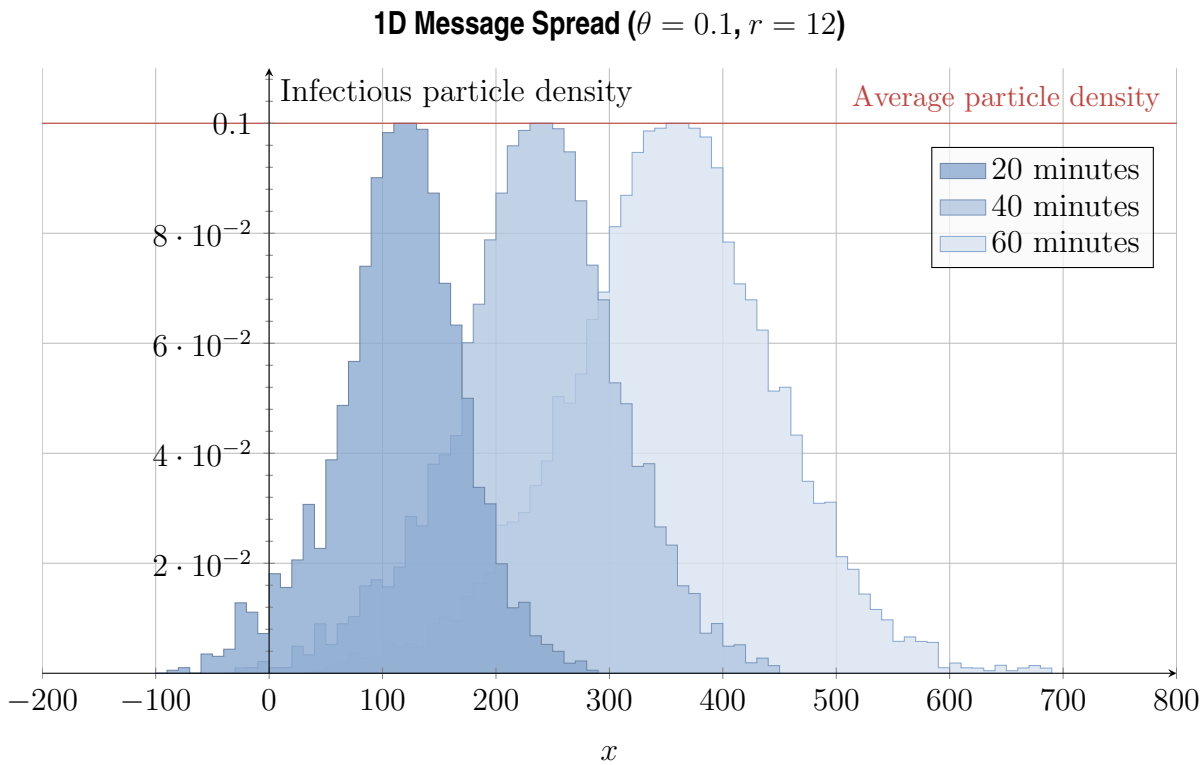
Figure 4.10: Histogram to show the message spread profile in 1D space with uni-directional movement. For both plots, $\rho = 0.1$, $\tau = 10$ and particles move only to the right. The values of $r$ and $\theta$ are indicated in the plot titles. In the upper plot, the message appears to spread primarily in the direction of particle movement, but the signal radius of the particles allows the message to travel slightly in the other direction. This behaviour is emphasised in the lower plot because of the adjustment to the parameter values. Both plots have been normalised as described in Footnote 1.

## 4.4 Contact Rate Theoretical Model

In this section, a theoretical model is created for particle contact rate, $\nu_c$. The 1D discrete space mobility model described in Section 4.1 is considered. Due to time constraints, theoretical models are not developed for 2D discrete space. However, a contact rate theoretical model for 2D continuous space is developed in Section 5.4.

The same assumption is made from Section 3.1, which is:

**Assumption** At any given time-step, the probability that two particles simultaneously move from site $i$ to site $j$ (where $i \neq j$) is zero. This is a fair assumption to make provided $n$ is sufficiently large and $\theta$ is sufficiently small.[2]

Given this assumption, the contact rate distribution of the 1D mobility model is equal to that of the transport network studied in Chapter 3. Therefore, the same contact rate model developed in Section 3.2 is adopted:

$$P(\nu_c = k) = \theta \cdot \binom{N}{k}\left(\frac{1}{n}\right)^k\left(1 - \frac{1}{n}\right)^{N-k} + (1 - \theta) \cdot \binom{N}{k}\left(\frac{\theta}{n}\right)^k\left(1 - \frac{\theta}{n}\right)^{N-k} \quad (4.1)$$

and

$$E(\nu_c) = \theta\rho(2 - \theta). \quad (4.2)$$

Contact rate for the 1D mobility model is unaffected by signal radius. This is because particles only ever move one site at a time left or right. Hence, this contact rate model holds regardless of signal radius. Figure 4.11 shows that the developed theoretical model matches simulated results. It is clear that the results are the same, regardless of signal radius. A theoretical model for contact rate in a 2D region is not considered.

## 4.5 Contact Duration Theoretical Model (Coarse-Grained)

Note that, due to time constraints, theoretical models are not developed for 2D discrete space. However, a contact duration theoretical model for 2D continuous

---

[2]This assumption is less likely to hold true for the discrete-space mobility models described in this chapter than the non-spatial models described in Chapter 3. This is because each particle has far fewer options of which site to move to next. To overcome this, the time-scale in the developed models is adjusted. For example, each time-step may be considered to be a millisecond rather than a second, and $\theta$ is to be scaled accordingly. This significantly reduces the chances of two co-located particles jumping together in a single time-step.
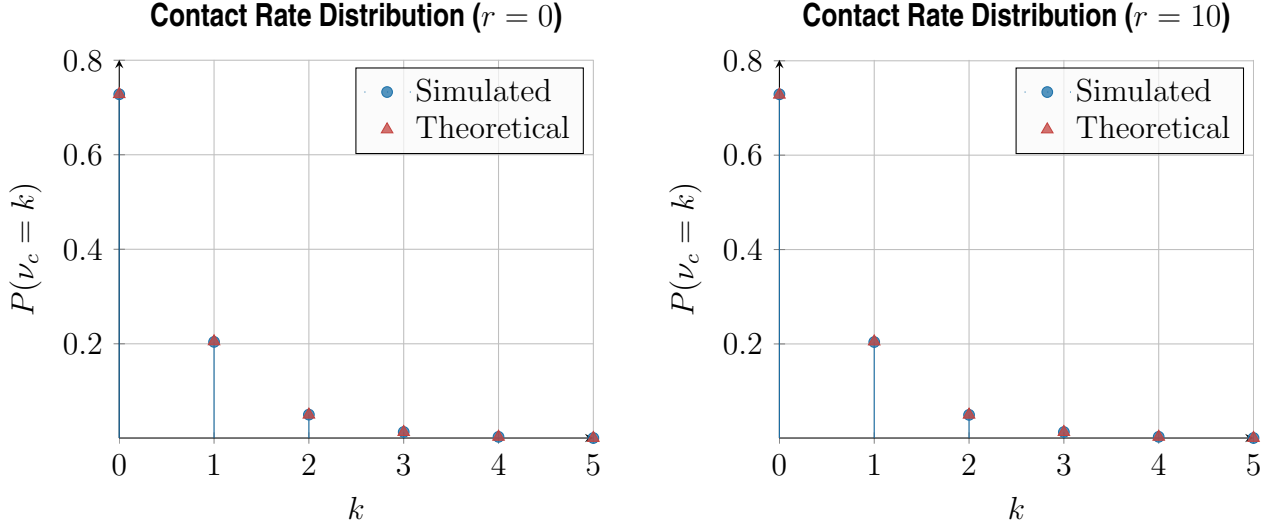
Figure 4.11: Plot to compare theoretical model with simulated results for particle contact rate. Simulated results show the contact rate distribution after 1 hour of simulation time. The following parameter values are used: $N = n = 500$, $\theta = 0.2$. Signal radius is indicated in the title of each plot and it is clear that it does not affect the results.

space is developed in Section 5.5.

When $r = 0$, the chosen mobility model shall be described as *coarse-grained*, otherwise, *fine-grained*. A contact duration $(T_c)$ theoretical model is developed for the coarse-grained model in this section and the fine-grained model is considered in the following section.

As with contact rate, contact duration in 1D space (coarse-grained) is identical to that of the transport network studied in Chapter 3. Therefore, the theoretical models derived in Section 3.3 is used:

$$P(T_c \geq t) = \left[(1 - \theta)^2\right]^{t-1},$$
$$P(T_c = t) = \left[(1 - \theta)^2\right]^{t-1} \left[1 - (1 - \theta)^2\right],$$
$$E(T_c) = \frac{1}{1 - (1 - \theta)^2}.$$

Results are produced to compare the developed 1D simulated/theoretical models in Fig. 4.12. It is clear from the plots that the theoretical model appears to match the empirical data closely.
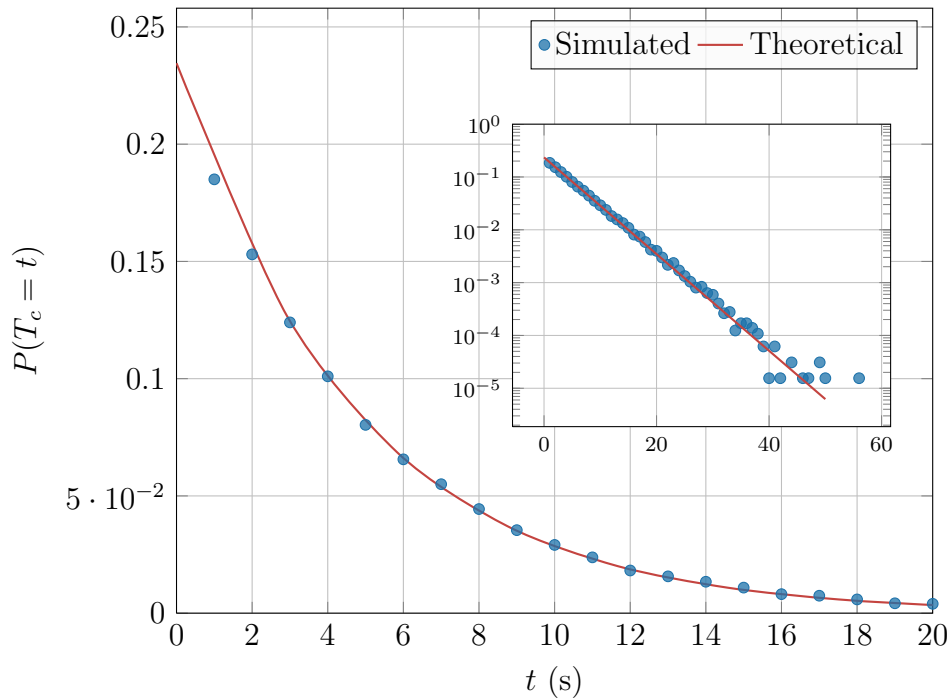
Figure 4.12: Plot to compare the developed theoretical model with simulated results for particle contact duration in 1D space (coarse-grained). The following parameter values are used: $N = 200$, $n = 1000$, $\theta = 0.1$. Simulated results show the average after 5 hours of simulation time.

## 4.6 Contact Duration Theoretical Model (Fine-Grained)

Now, contact duration $(T_c)$ is considered in the fine-grained 1D mobility model in which $r > 0$ and particles can communicate with other particles up to $r$ jumps away. Let $d$ be the number of jumps separating a pair of particles. For a successful transmission, $d \leq r$ must hold true for at least $\tau$ seconds. Therefore, in order to model contact duration when $r > 0$, the length of time for which $d \leq r$ holds true must be modelled. Gambler's Ruin theory is used to solve this problem. In this section, Gambler's Ruin theory is described and, as an original contribution, its application to the developed contact duration model is explained.

### 4.6.1 Gambler's Ruin (with draws)

A typical Gambler's Ruin problem (with draws allowed) consists of a gambler with an initial finite capital of $m$ pennies, playing an opponent with an initial capital of $a - m$ pennies (therefore, a combined capital of $a$ pennies). For each trial, our gambler wins, loses or draws with probabilities $\alpha$, $\beta$ and $\gamma$ respectively, where $\alpha + \beta + \gamma = 1$. Therefore, the opponent wins, loses or draws a trial with probabilities $\beta$, $\alpha$ and $\gamma$

respectively. For each trial, the winner gains a penny from the loser. If a trial results in a draw, no pennies change hands. Our gambler continues to play his opponent until he has won the entire combined capital $a$ (he wins the game), or until his capital reaches zero (he is ruined) (Bertsekas and Tsitsiklis 2002).

## 4.6.2  Particles as Gamblers

Gambler's Ruin theory can be applied to the 1D mobility model described Section 4.1 in order to find the length of time two particles remain within range of each other. In this case, each particle can be seen as a gambler and the relative positions of each particle is represented by the gambler's capital. A game begins as soon as two particles move within range of each other. Our gambler (one of the two particles) always begins with an initial capital of 1. The game ends when the particles have moved out of range, *i.e.* when our gambler's capital reaches either of the absorbing barriers, 0 or $a$. In our case $a = 2(r+1)$, where $r$ is the signal radius of the particles. This is shown in Fig. 4.13. The contact duration of two particles is represented by the duration of the game.
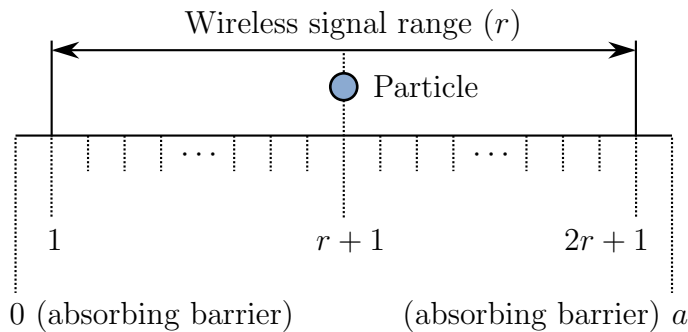


Figure 4.13: Figure to show the absorbing barriers of a Gambler's Ruin game and how a game can be applied to a particular particle in 1D space. The blue circle is our particle (or gambler). Each dotted vertical line is a site (or capital of the opponent). A game begins when a previously out-of-range particle moves within range of our particle. The game ends once that particle moves to either of the absorbing barriers. Note that the absorbing barriers are relative to the position of our particle, and therefore move with our particle.

## 4.6.3  Generating Functions

In the following section, it is necessary for the reader to understand generating functions. For this reason, a brief introduction is provided in this section.

A generating function is a series of numbers presented as the coefficients of a random variable in a power series (Weisstein 2014b). The index of each coefficient is determined by the power to which the variable is raised. Therefore, the generating function for sequence $\{a_0, a_1, a_2, \ldots\}$ is $G(z)$ (where $z$ is a random variable), defined as follows:

$$G(z) = a_0 z^0 + a_1 z^1 + a_2 z^2 + \ldots = \sum_{k=0}^{\infty} a_k z^k.$$

Generating functions can be used to solve recurrence relations, such as the Fibonacci Sequence (Johnston 1940). As a simple example, the following generating function is considered:

$$G(z) = 1 + z + z^2 + z^3 + z^4 + \ldots$$

In this case, the coefficient is always 1, therefore, the series produced by this generating function is 1, 1, 1, ... This power series can also be expressed in its closed form:

$$G(z) = \sum_{k=0}^{\infty} z^k = \frac{1}{1-z}.$$

As a more general case, we can multiply $z$ by some constant $c$:

$$G(z) = \sum_{k=0}^{\infty} (cz)^k = \frac{1}{1-cz}. \tag{4.3}$$

### 4.6.4   Specific Worked Example of a Generating Function

As a more detailed example, a recurrence relation similar to the Fibonacci Sequence is considered. We denote this sequence $a = \{a_0, a_1, a_2, \ldots\}$ and we express it algebraically as follows:

$$a_k = a_{k-1} + 2a_{k-2}, \tag{4.4}$$
$$a_1 = 1,$$
$$a_0 = 1.$$

This gives the sequence $\{1, 1, 3, 5, 11, 21, 43, \ldots\}$. Using these equations, it would take a long time to calculate $a_k$ for a large value of $k$. However, generating functions can be used to create a formula for each value without needing to know the previous values.

Let $G(z)$ be the generating function for our sequence. This means that the coefficient of each power is the corresponding value from the sequence.

$$G(z) = 1 + z + 3z^2 + 5z^3 + 11z^4 + 21z^5 + 43z^6 + \ldots$$

Now, use algebraic manipulation to find the closed form of this equation.

$$
\begin{aligned}
G(z) &= a_0 + a_1 z + a_2 z^2 + a_3 z^3 + \ldots \\
-z \times G(z) &= \quad - a_0 z - a_1 z^2 - a_2 z^3 - \ldots \\
-2z^2 \times G(z) &= \qquad\quad - 2a_0 z^2 - 2a_1 z^3 - \ldots
\end{aligned}
$$

Taking the sum of these three equations gives:

$$
\begin{aligned}
G(z) - zG(z) - 2z^2 G(z) = a_0 &+ (a_1 - a_0)z + \\
&(a_2 - a_1 - 2a_0)z^2 + \\
&(a_3 - a_2 - 2a_1)z^3 + \ldots
\end{aligned}
$$

From Eq. (4.4), we know that $a_k - a_{k-1} - 2a_{k-2} = 0$, and the value of $a_0$ and $a_1$ are also known. Thus,

$$
\begin{aligned}
(1 - z - 2z^2) \times G(z) &= a_0 + (a_1 - a_0)z, \\
G(z) &= \frac{1}{1 - z - 2z^2}, \\
G(z) &= \frac{1}{(1 - 2z)(1 + z)}.
\end{aligned}
$$

Now we use methods of partial fractions to change the expression for $G(z)$ to be of the form of Eq. (4.3).

$$
\begin{aligned}
\frac{1}{(1 - 2z)(1 + z)} &= \frac{A}{(1 - 2z)} + \frac{B}{(1 + z)} \\
\frac{1}{(1 - 2z)(1 + z)} &= \frac{A(1 + z)}{(1 - 2z)(1 + z)} + \frac{B(1 - 2z)}{(1 - 2z)(1 + z)} \\
\frac{1}{(1 - 2z)(1 + z)} &= \frac{A + Az + B - 2Bz}{(1 - 2z)(1 + z)} \\
\frac{1}{(1 - 2z)(1 + z)} &= \frac{(A + B) + (A - 2B)z}{(1 - 2z)(1 + z)}
\end{aligned}
$$

So $A + B = 1$ and $A - 2B = 0$. Therefore, $A = \frac{2}{3}$ and $B = \frac{1}{3}$. Thus,

$$G(z) = \frac{2}{3} \times \frac{1}{1 - 2z} + \frac{1}{3} \times \frac{1}{1 + z}.$$

Now we have fractions in the form of Eq. (4.3), so now we can extract the coefficients of our generating function, giving us a formula for each number in the original sequence:

$$a_k = \frac{2}{3} 2^k + \frac{1}{3}(-1)^k.$$

We verify this equation by calculating the first four numbers in our sequence:

$$
\begin{aligned}
a_0 &= \frac{2}{3} 2^0 + \frac{1}{3}(-1)^0 = 1, \\
a_1 &= \frac{2}{3} 2^1 + \frac{1}{3}(-1)^1 = 1, \\
a_2 &= \frac{2}{3} 2^2 + \frac{1}{3}(-1)^2 = 3, \\
a_3 &= \frac{2}{3} 2^3 + \frac{1}{3}(-1)^3 = 5, \\
a_4 &= \frac{2}{3} 2^4 + \frac{1}{3}(-1)^4 = 11.
\end{aligned}
$$

Indeed, this matches the sequence from the start of this section, demonstrated for the first five terms.

### 4.6.5 Gambler's Ruin Game Duration

In this section, the theoretical model of Gambler's Ruin game duration is described according to the work of Feller (1957); Heyman and Sobel (2003) and Lengyel (2009).

Let $p_{m,n}$ denote the probability that a game will end with our gambler ruined at the $n$th trial, given an initial capital of $m$. After the first trial, our gambler's capital is $m + 1$, $m - 1$ or $m$ with probabilities $\alpha$, $\beta$ and $\gamma$ respectively. Therefore, we have the following difference equation:

$$p_{m,n+1} = \alpha p_{m+1,n} + \beta p_{m-1,n} + \gamma p_{m,n}. \tag{4.5}$$

with boundary conditions:

$$p_{0,n} = p_{a,n} = 0 \quad \text{when } n > 0$$

$$p_{0,0} = 1, p_{m,0} = 0 \quad \text{when } m > 0$$
(4.6)

Generating functions are now introduced. Let

$$G_m(z) = \sum_{n=0}^{\infty} p_{m,n} z^n$$
(4.7)

be the generating function for the probability that a game will end with our gambler ruined at the $n$th trial (given an initial capital of $m$). Multiply Eq. (4.5) by $z^{n+1}$ and sum for $n = 0, 1, 2, \dots$ to get

$$\sum_{n=0}^{\infty} p_{m,n+1} z^{n+1} = \alpha \sum_{n=0}^{\infty} p_{m+1,n} z^{n+1} + \beta \sum_{n=0}^{\infty} p_{m-1,n} z^{n+1} + \gamma \sum_{n=0}^{\infty} p_{m,n} z^{n+1}.$$

Now we re-arrange to get formats similar to Eq. (4.7):

$$-p_{m,0} z^0 + \sum_{n=0}^{\infty} p_{m,n} z^n = \alpha z \sum_{n=0}^{\infty} p_{m+1,n} z^n + \beta z \sum_{n=0}^{\infty} p_{m-1,n} z^n + \gamma z \sum_{n=0}^{\infty} p_{m,n} z^n.$$

Finally, we substitute Eq. (4.7) to get the difference equation:

$$G_m(z) = \alpha z G_{m+1}(z) + \beta z G_{m-1}(z) + \gamma z G_m(z), \ 0 < m < a. \quad (4.8)$$

Doing the same to Eq. (4.6) leads to the boundary conditions of Eq. (4.8):

$$G_0(z) = p_{0,0} + p_{0,1} z + p_{0,2} z^2 + \dots = 1$$

$$G_a(z) = p_{a,0} + p_{a,1} z + p_{a,2} z^2 + \dots = 0$$
(4.9)

Given a capital of $m$, our gambler would have to lose $m$ times to become ruined. A loss occurs with probability $p_{1,n}$, hence, $G_m(z) = p_{1,n}^m$. Therefore, we can expect a solution for Eq. (4.8) of the form $f^m(z)$ for some function $f(z)$ taking values in $[0, 1]$. We solve $f(z)$ by substituting it into Eq. (4.8) to create a quadratic equation

as follows:

$$f(z) = \alpha z f^2(z) + \beta z + \gamma z f(z), \tag{4.10}$$

$$0 = \alpha z f^2(z) + (\gamma z - 1) f(z) + \beta z.$$

Using the quadratic formula, we find the following two solutions (taking the positive square root where $0 < z < 1$):

$$f_\pm(z) = \frac{1 - \gamma z \pm \sqrt{(\gamma z - 1)^2 - 4\alpha\beta z^2}}{2\alpha z}. \tag{4.11}$$

Eq. (4.10) is the characteristic equation with roots as given in Eq. (4.11). These roots are distinct, therefore, according to the superposition principle, we have the following general solution for Eq. (4.8):

$$G_m(z) = A(z) f_+^m(z) + B(z) f_-^m(z), \tag{4.12}$$

where $A(z)$ and $B(z)$ are arbitrary functions. We now solve Eq. (4.12) using the boundary conditions of Eq. (4.9) to get simultaneous equations:

$$G_0(z) = A(z) + B(z) = 1,$$

$$G_a(z) = A(z) f_+^a(z) + B(z) f_-^a(z) = 0. \tag{4.13}$$

Now we solve for $A(z)$ and $B(z)$ by substituting $A(z) = 1 - B(z)$ in Eq. (4.13) as follows:

$$0 = [1 - B(z)] f_+^a(z) + B(z) f_-^a(z),$$

$$0 = f_+^a(z) - B(z)[f_+^a(z) - f_-^a(z)],$$

$$B(z) = \frac{f_+^a(z)}{f_+^a(z) - f_-^a(z)}, \tag{4.14}$$

$$A(z) = 1 - B(z) = \frac{-f_-^a(z)}{f_+^a(z) - f_-^a(z)}. \tag{4.15}$$

Substituting Eqs. (4.14) and (4.15) into Eq. (4.12) gives:

$$G_m(z) = \frac{f_+^a(z) f_-^m(z) - f_+^m(z) f_-^a(z)}{f_+^a(z) - f_-^a(z)}. \tag{4.16}$$

This equation is simplified using $f_+(z)f_-(z) = \frac{\beta}{\alpha}$ from Vieta's formulas (Weisstein 2014c):

$$G_m(z) = \left(\frac{\beta}{\alpha}\right)^m \frac{f_+^{a-m}(z) - f_-^{a-m}(z)}{f_+^a(z) - f_-^a(z)}. \tag{4.17}$$

This generating function is used to find the probability that a game ends with our gambler ruined at the $n$th trial. The probability that the game ends at the $n$th trial with our player winning (the opponent is ruined) is found by substituting $\alpha$, $\beta$ and $m$ with $\beta$, $\alpha$ and $a - m$, respectively, as follows:

$$\left(\frac{\alpha}{\beta}\right)^{a-m} \frac{f_+^m(z) - f_-^m(z)}{f_+^a(z) - f_-^a(z)}. \tag{4.18}$$

The generating function for the game duration (regardless of who wins) is the sum of Eqs. (4.17) and (4.18):

$$G_m(z) = \left(\frac{\beta}{\alpha}\right)^m \frac{f_+^{a-m}(z) - f_-^{a-m}(z)}{f_+^a(z) - f_-^a(z)} + \left(\frac{\alpha}{\beta}\right)^{a-m} \frac{f_+^m(z) - f_-^m(z)}{f_+^a(z) - f_-^a(z)}. \tag{4.19}$$

### 4.6.6  Particle Movement as Gambler's Capital

Recall that $\alpha$, $\beta$ and $\gamma$ are the respective probabilities of our gambler winning, losing or drawing a trial. Now, the relation of these probabilities to particle movement is discussed. Let $\theta_L$, $\theta_R$ and $1 - \theta$ be the probability that each particle independently moves left, right or remains still at any given time-step. Let $\Delta d$ be the change in distance between two particles at a given time-step. The term $\Delta d = 0$ in the following cases:

- $[\times, \times]$ Neither particle jumps $\left(\text{probability } (1 - \theta)^2\right)$
- $[<, <]$ Both particles jump left (probability $\theta_L^2$)
- $[>, >]$ Both particles jump right (probability $\theta_R^2$)

Therefore, the probability that the outcome of a trial is a draw, $\gamma$, is $(1-\theta)^2 + \theta_L^2 + \theta_R^2$.

If $\Delta d \neq 0$ then $\Delta d$ is equally likely to be positive/negative (this does not affect the magnitude). Therefore, $\alpha = \beta = (1 - \gamma)/2$ regardless of $\theta_L$, $\theta_R$ and $(1 - \theta)$ as each particle moves independently. The term $\Delta d > 0$ in the following cases:

- $[<, \times]$ One particle jumps to the left and the other particle remains still, with probability $(1 - \theta)\theta_L$

- [×, >] One particle jumps to the right and the other particle remains still, with probability $(1 - \theta)\theta_R$
- [<, >] One particle moves to the left and the other particle moves to the right, with probability $\theta_L\theta_R$

Therefore, we have $\alpha = (1 - \theta)(\theta_L + \theta_R) + \theta_L\theta_R$. Note that the $[<, >]$ case listed above gives $|\Delta d| = 2$, when usually $|\Delta d| = 1$. This causes problems as it is not included in the Gamber's Ruin model. We solve this problem in the following section.

### 4.6.7  Adapting Gambler's Ruin Model

If both particles jump in opposite directions, $|\Delta d| = 2$ rather than 1. This means that in the Gambler's Ruin problem, two pennies change hands rather than one. This is not included in the standard Gambler's Ruin model, therefore, such moves cause inaccuracy to the developed model. There are several ways in which this can be avoided and they are now discussed as an original contribution of this thesis.

**Totally Asymmetric Movement**   Setting $\theta_L$ or $\theta_R = 0$ means that all particles move in the same direction. This makes it impossible for particles to jump in opposite directions, therefore eradicating the chance that $|\Delta d| = 2$.

**Particles Rarely Jump**   Setting $(1 - \theta) \gg 0$ reduces the chances of two particles jumping at once. If $1 - \theta$ is large enough, $P(|\Delta d| = 2)$ is negligible.

**Particles Always Jump**   Setting $1 - \theta = 0$ means that all particles jump every second. Although this does not exclude $|\Delta d| = 2$, it does exclude $|\Delta d| = 1$. Now we can use the developed Gambler's Ruin model as before, only we must adjust the absorbing barriers by halving $a$. Note that roughly half of particle contacts will start with an initial distance of $r - 1$ rather than $r$; however, this does not not affect the integrity of the model.

**Unrestricted Approximation**   Building on the method used for when particles always jump, an unrestricted approximation is created. Instead of simply halving $a$, we divide $a$ by $E(\Delta d|\Delta d > 0)$. As $P(\Delta d = 1) = (1-\theta)(\theta_L +\theta_R)$ and $P(\Delta d = 2) = \theta_L\theta_R$,

we get

$$E(\Delta d|\Delta d > 0) = \frac{1 \cdot (1 - \theta)(\theta_L + \theta_R) + 2 \cdot \theta_L\theta_R}{\alpha} = \frac{\alpha + \theta_L\theta_R}{\alpha}. \qquad (4.20)$$

Recall that $a = 2(r + 1)$. Dividing $a$ by Eq. (4.20) and rounding gives

$$a = \left\lfloor \frac{2\alpha(r + 1)}{\alpha + \theta_L\theta_R} \right\rfloor.$$

Note that the model becomes an approximation for some values of $\theta$ as $a$ must be rounded and sometimes the initial distance between particles is $r - 1$ rather than $r$.

### 4.6.8  Final General Model

The contact duration, $T_c$, of any pair of particles can be modelled by Eq. (4.19). Given our initial capital of 1 and recalling that $\alpha = \beta$, this becomes:

$$G(z) = \frac{f_+^{a-1}(z) - f_-^{a-1}(z) + f_+(z) - f_-(z)}{f_+^a(z) - f_-^a(z),} \qquad (4.21)$$

where $a = \left\lfloor \dfrac{2\alpha(r + 1)}{\alpha + \theta_L\theta_R} \right\rfloor$ and $f_\pm(s) = \dfrac{1 - \gamma s \pm \sqrt{(\gamma s - 1)^2 - (2\alpha s)^2}}{2\alpha s}$,

where $\gamma = (1 - \theta)^2 + \theta_L^2 + \theta_R^2$ and $\alpha = (1 - \gamma)/2$.

Eq. (4.21) is the required generating function for $P(T_c = n)$. Note that, to the best of the author's knowledge, this is the first time that Gambler's Ruin theory has been applied to OPNET technology. A message with transmission time $\tau$ can be transferred given any $T_c \geq \tau$; therefore, it is useful to point out $P(T_c \geq \tau) = 1 - \sum_{\tau=0}^{\tau-1} P(T_c = \tau)$.

### 4.6.9  Experimental Results

Experimental results are produced for all four adaptations in Section 4.6.7. Figure 4.14 shows results for asymmetric movement and for when particles always/rarely jump.

Results for unrestricted approximations can be seen in Fig. 4.15. All of these results combine theoretical and empirical models for 1D discrete space (fine-grained). Although not theoretically modelled, empirical results are included for 2D space in Fig. 4.16 for the reader's interest. All results show that the probability of a longer

Figure 4.14: Contact duration distribution for 1D discrete space. All markers represent the averaged empirical data of simulations; all line plots represent theoretical models. The inset axis presents the same data on a log-log scale. Results shown for asymmetric particle movement and for when particles always/rarely jump. The term $r = 10$ for all simulations.
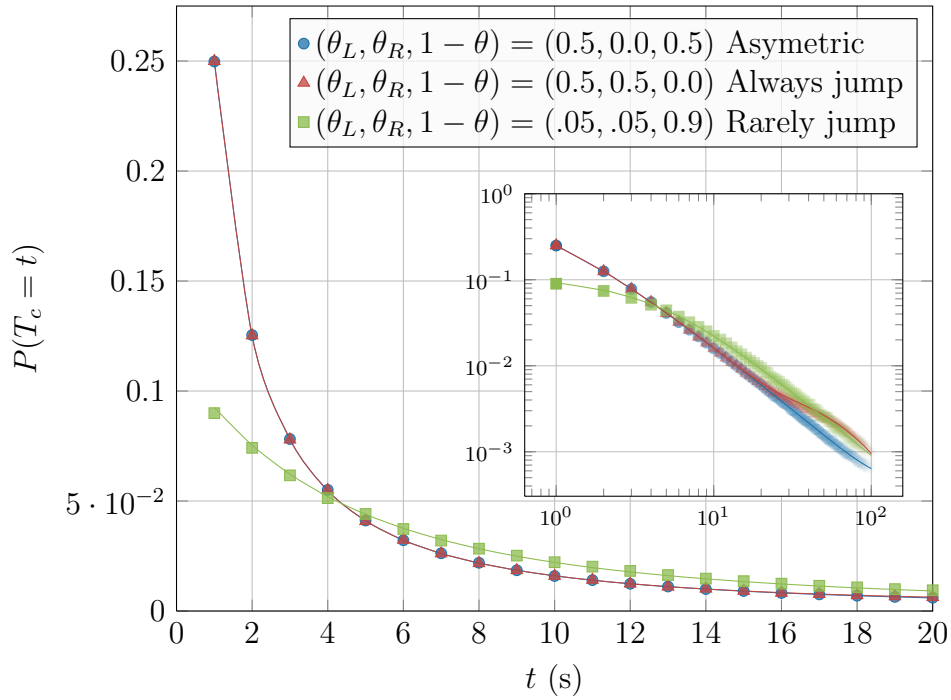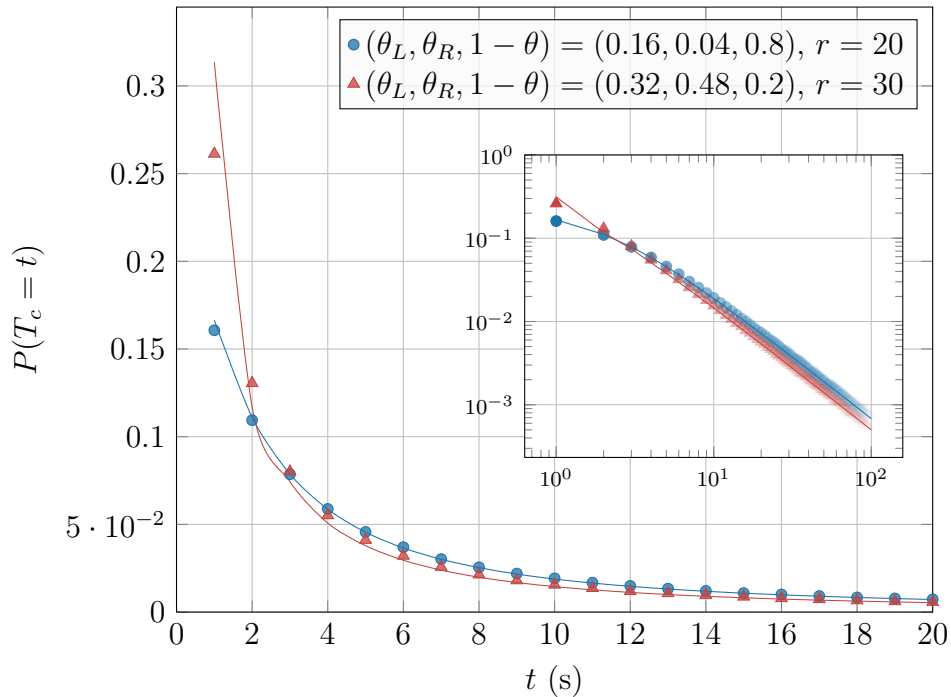


Figure 4.15: Contact duration distribution for 1D discrete space. All markers represent the averaged empirical data of simulations; all line plots represent theoretical models. The inset axis presents the same data on a log-log scale. Results shown for two examples of unrestricted approximation. Different values of $r$ are used, as shown in the legend.
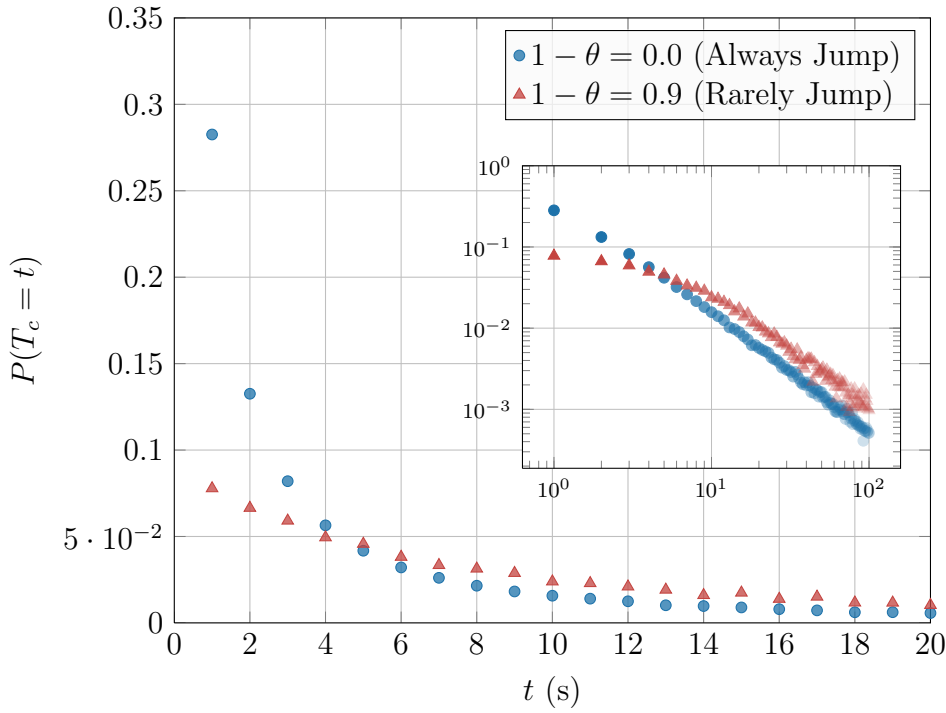
Figure 4.16: Contact duration distribution for 2D discrete space. All markers represent the averaged empirical data of simulations. The inset axis presents the same data on a log-log scale. Results shown for when particles always/rarely jump. The term $r = 40$ for all simulations.

contact duration sharply decreases. It is clear from the plots that the theoretical model appears to match the empirical data closely.

## 4.7 Message Spread Empirical Model

The creation of a theoretical message spread model for discrete space is left to future work. However, the current author believes that such a model will consist of some combination of the developed models for contact rate and contact duration. In this section, empirical results are produced for message spread and their relation to the theoretical models derived in this chapter is discussed.

**1D Spatio-Temporal Spread:**  As a basic starting point, the spatio-temporal infection density is looked at for 1D space. Results are displayed as a histogram in Fig. 4.17.

It is clear that there is only a small concentration (depicted by colour) of infectious particles near the origin at the start of the simulation. Over time, this concentration increases until the infection density reaches the average particle density of 0.15. It
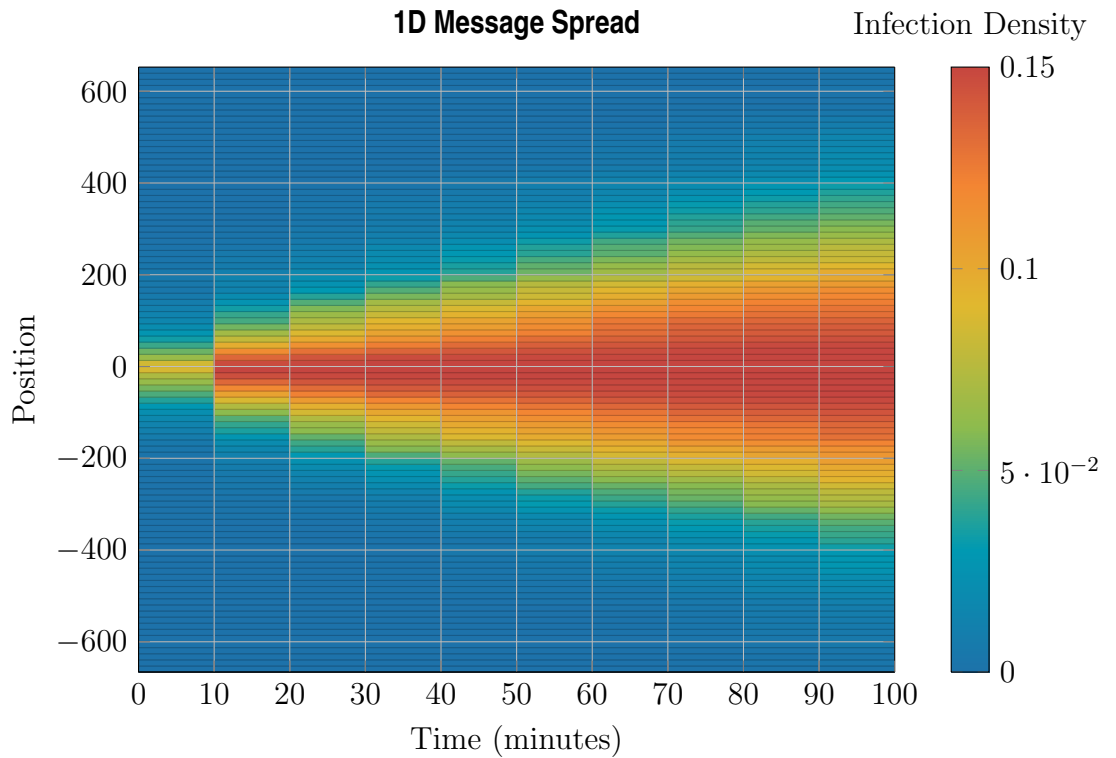
Figure 4.17: Histogram to show how a message spreads in 1D discrete space. Figure was generated from the averaged results of 200 simulations with the following parameter values: $\rho = 0.15$, $r = 10$, $\theta = 0.1$, $\tau = 0$. Note that results have been normalised as described in Footnote 1 on Page 95.

is clear that the message also spreads throughout space, across the region in both directions.

**2D Spatio-Temporal Spread:** Similar empirical results are produced for 2D space in Fig. 4.18. The state of the system is displayed after 15 minutes and 30 minutes in the two plots. Results show that the system behaves similarly in 1D and 2D space, with the message spreading in all directions over time.

**Effects of Transmission Time:** Non-instantaneous data transmissions are now considered to see how the transmission time, $\tau$, affects message spread. Figure 4.19 shows the message spread profile for 1D space after 100 simulation minutes for various values of $\tau$. From the results, it is clear that a larger $\tau$ inhibits message spread. This is to be expected as fewer particle contacts last for $\tau$ seconds if $\tau$ is large. This behaviour is captured in the developed model for contact duration in Section 4.6.
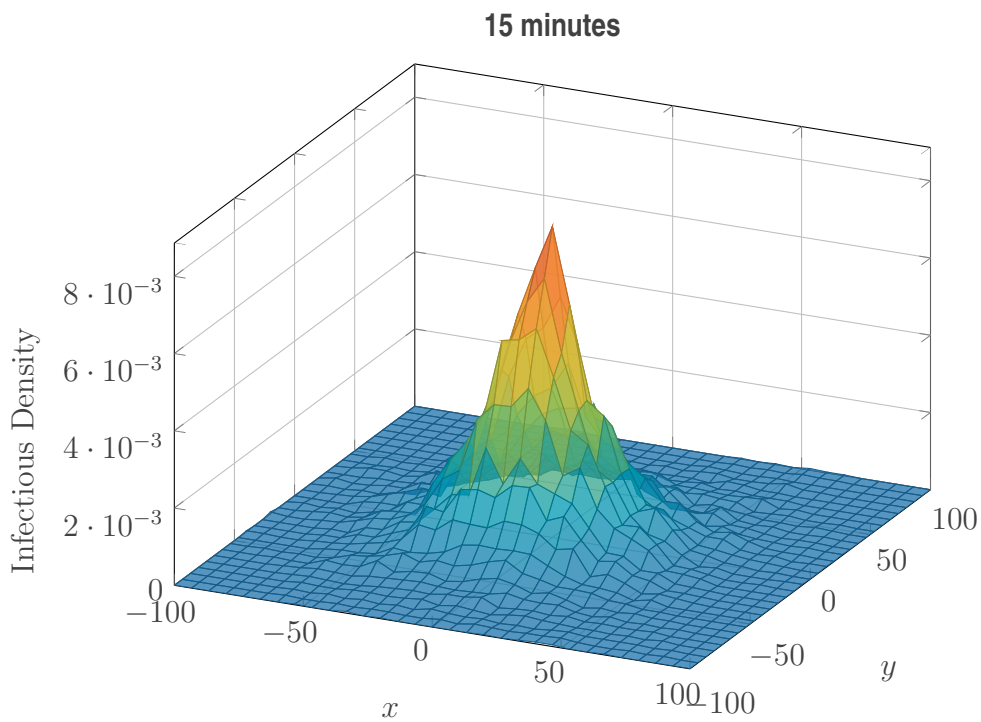
Figure 4.18: Surface plot to show how a message spreads in 2D space. Results were generated from the averaged results of 1000 simulations with the following parameter values: $\rho = 0.005$, $r = 10$, $\theta = 0.1$, $\tau = 0$. Note that results are not normalised as described in Footnote 1 on Page 95, hence why the infectious density mode is higher than the average particle density ($\rho$).

Figure 4.19: Message spread profile after 100 minutes in 1D space for various transmission times. Results show the average of 200 simulations with the following parameter values: $\rho = 0.15$, $r = 10$, $\theta = 0.1$.

**Effects of Signal Radius:**   Signal radius is now varied for instantaneous transmissions. From Fig. 4.20, it is clear that a larger signal radius is beneficial for message spread. However, this behaviour is not captured in the theoretical models developed in this chapter. To prove this, the contact rate model derived in Section 4.4 is looked at (models for contact duration can be discarded as $\tau = 0$). The term $r$ does not appear in the developed model for contact rate, therefore, $r$ must appear separately in any model derived for message spread. This means that such a model is more complex than a simple combination of contact rate and contact duration models, as previously expected. This is why a theoretical model for message spread has been left to future work. Perhaps message spread is affected by $r$ only because of initial conditions. For instance, a larger value of $r$ means that more devices will be within range of the source device when the message is first released, in turn leading to more devices spreading the message in the network.
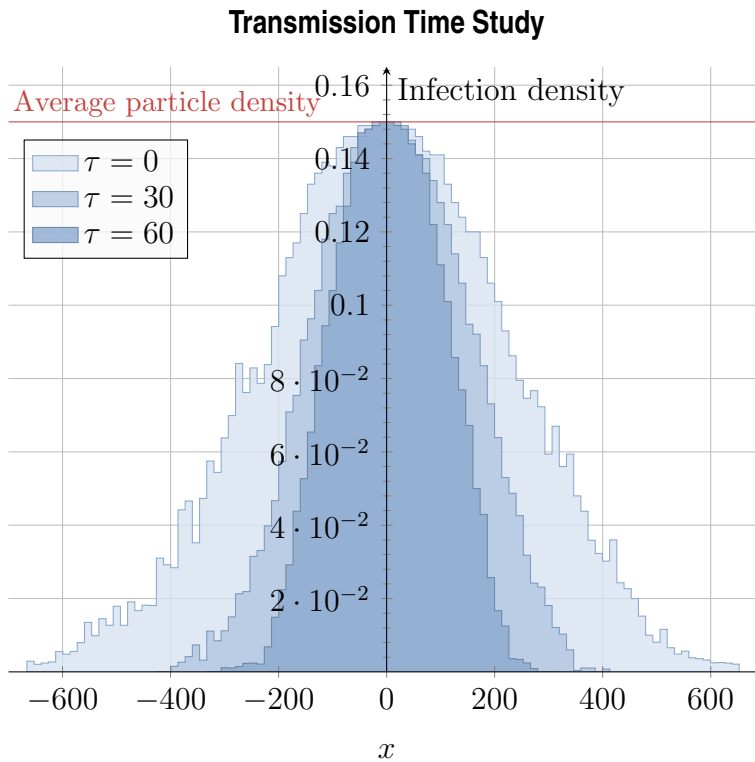
113
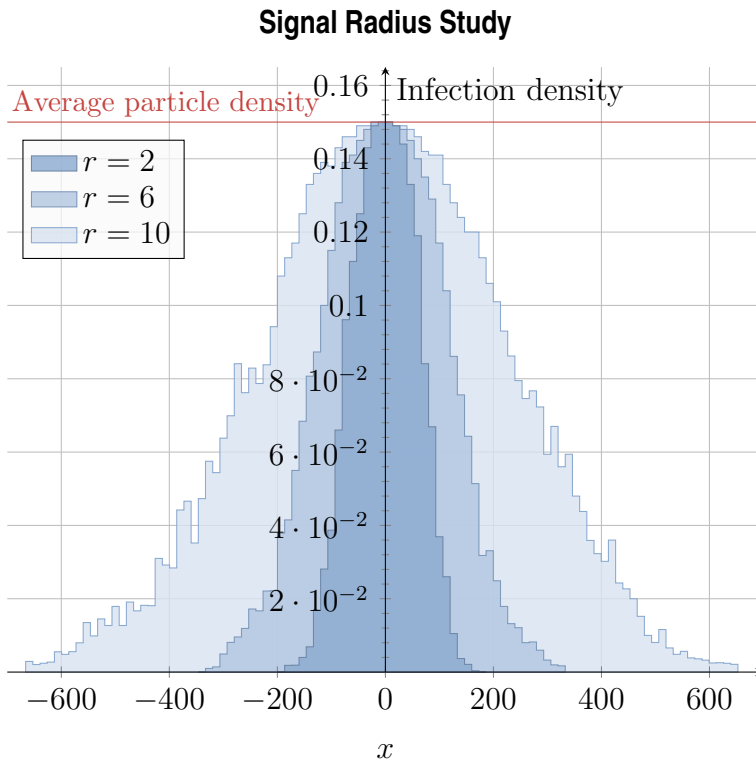
Figure 4.20: Message spread profile after 100 minutes in 1D space for various signal radii. Results show the average of 200 simulations. Parameter values: $\rho = 0.15$, $\theta = 0.1$, $\tau = 0$.

## 4.8   Chapter Summary

In this chapter the focus has been on OPNETs deployed in regions of discrete space. A methodical study has been performed on the fundamental parameters in Section 4.2 to better understand the behaviour of OPNETs. The approach and findings of this study inform Section 5.2 in which a similar study is performed. A theoretical model has been created for contact rate in Section 4.4. This will prove useful in Section 5.4 where contact rate is studied for 2D continuous space. Similarly, the theoretically model for contact duration (Section 4.6) will inform Section 5.5. In Section 4.7 it was discussed how the developed models for contact rate and contact duration could be used to model message spread. The discussion and empirical study from this section will inform Section 5.6 later in this thesis.

In the next chapter, focus is shifted from 1D discrete space to 2D continuous space.

## CHAPTER 5

# Continuous Spatial Models

## 5.1 Mobility Model

This chapter considers continuous space in one and two dimensions. As with the previous chapter, synchronous discrete-event simulation with the Random Direction mobility model is used throughout (see Section 2.5.1 and Section 2.3.3.3). Firstly, specific details about the movement of particles is provided.

### 1D Space

In the 1D continuous space model, particles move independently along a line. The line is periodic, meaning that any particle which moves past the left edge of the line will appear at the right edge and vice versa. The starting positions of the particles are randomly distributed along the line. Each particle assumes a velocity chosen at random from the Normal distribution, denoted $\mathcal{N}(\mu, \sigma^2)$, with the mean value $\mu$ set to zero. Therefore, there is an equal chance of moving left or right. Each particle independently chooses another velocity at random after a certain time period. This time period is determined according to a *turning rate*, which is chosen at random from the Exponential distribution for every velocity change, with mean value $\lambda$.

### 2D Space

The following property of the Normal distribution is used in this section:

**Definition 1:** *Given two independent Normally distributed random variables, $X \sim \mathcal{N}(0, \sigma^2)$ and $Y \sim \mathcal{N}(0, \sigma^2)$, $\sqrt{X^2 + Y^2} \sim \text{Rayleigh}(\sigma)$ (Siegrist 2014).*

In the 2D continuous space model, particles move independently on a periodic plane of equal height and width. The region can be visualised as the surface of a torus, as illustrated in Fig. 5.1.
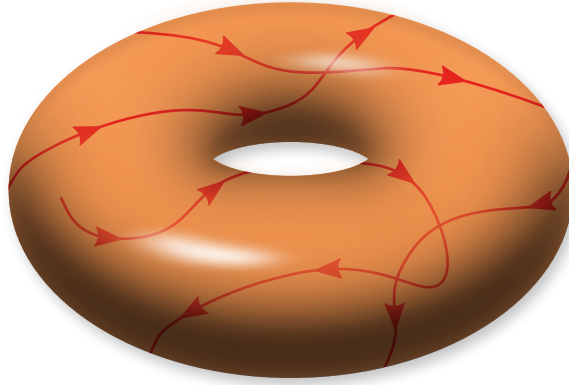


Figure 5.1: Diagram of 2D continuous-space plane used for particle movement.

The following parameters are used for the Random Direction mobility model:

- An exponential turning rate with mean value $\lambda$. It is assumed that $\lambda$ is sufficiently small so that it is unlikely for particles to change direction during interaction.
- A velocity with components $u, v \sim \mathcal{N}(0, \sigma^2)$, where $\sigma = \sqrt{\frac{2}{\pi}} E(s)$. According to Definition 1, this gives an overall speed distributed according to $\text{Rayleigh}(\sigma)$. This has a mean value of $\sigma \sqrt{\frac{\pi}{2}}$, therefore the mean speed is $E(s)$.

**Relative Speed**

Consider two particles moving independently, each with velocity components chosen at random from $\mathcal{N}(0, \sigma^2)$, where $\sigma = \sqrt{\frac{2}{\pi}} E(s)$. Each component of the relative velocity of our two particles is calculated as follows: $v_1 - v_2 \sim \mathcal{N}(0, 2\sigma^2)$, where $v_1$ and $v_2$ are corresponding velocity components from our particles. Using Definition 1, it is found that the particles have a relative speed of $\tilde{s} \sim \text{Rayleigh}(\sigma\sqrt{2}) = \text{Rayleigh}(\frac{2E(s)}{\sqrt{\pi}})$, with mean value $E(s)\sqrt{2}$ and the following density function:

$$h(\tilde{s}) = \frac{\pi \tilde{s}}{4E(s)^2} \cdot \exp\left(\frac{-\pi \tilde{s}^2}{8E(s)^2}\right).$$

116

where exp is the exponential distribution.

## 5.2 Fundamental Parameter Lookup Table

In this section, the empirical study on the fundamental parameters from Section 4.2 is extended. Recall that the four fundamental parameters are:

- particle density ($\rho$),
- transmission time ($\tau$),
- signal radius ($r$),
- particle speed ($s$).

As an addition to the fundamental parameters, the deletion rate $\delta$ is included in the experiment, giving a total of five parameters to be studied. Instead of studying each parameter individually, their combined behaviour is now looked at. This is achieved by creating a multi-dimensional lookup table of simulation results. Each cell of this table is indexed by five values, one for each parameter, and holds the value of a certain performance metric for those parameter values. The metric chosen for this study is $SP_{60}$, defined in Section 4.2.3 to be the probability that an information epidemic persists for at least 60 minutes.

The lookup table may provide a useful tool to OPNET engineers as it can be used to find suitable parameter values. For example, let us assume an engineer knows the value of four out of five parameters, (say $\delta$, $E(s)$, $\rho$ and $r$), and would like to spread a message that will persist for at least an hour with high probability. The lookup table can be used to find the maximum value of the fifth parameter, $\tau$. To do this, the engineer would use the four known parameter values to index a single row of the lookup table. This row will hold metrics results for the known parameter values and a range of transmission times. The engineer can use this information to decide on the size of the message to introduce into the network.

### 5.2.1 Experimental Description

All simulations are performed using the 2D mobility model described in Section 5.1, with a region size of 1 km × 1 km. The only deviation from the described mobility model is that all particles move with the same constant speed and the turning rate

is an absolute value of 1 $s^{-1}$. As the focus of this chapter is on 2D space, and due to time constraints, the 1D region is not included in this study. We focus on the 2D model in this chapter as this thesis progresses towards more true-to-life mobility models.

A single broadcast message is disseminated using an SIS interaction scheme (see Section 2.1). The SIS scheme is used as this is required when recording the $SP_{60}$ metric (as explained in Section 4.2).

A lookup table is created with five dimensions—one for each parameter studied. These dimensions correspond to a range of values for each parameter, as stated in Table 5.1. Each of these ranges (*i.e.* dimension of the table) is uniformly split into 10 bands, creating a total number of $10^5$ cells. Each cell contains an (empirical) estimate of $SP_{60}$ for the corresponding parameter values. These values are computed by performing many simulations, each with randomly chosen parameter values. Simulation results are mapped (according to parameter values) to the correct table cell where an average is taken. The aim is to have an average of 100 simulated results for each cell in the table, therefore, a total of $100 \times 10^5 = 10^7$ simulations shall be performed[1]. The method in which the lookup table is filled at random is chosen as it allows an average to be taken for each cell in the table. The alternative is to repeat a single experiment with the same parameter values 100 times for each cell, but this would not be a true average value for the corresponding cell.

| Parameter | Minimum | Maximum |
|---|---|---|
| $\rho$ (particles/m$^2$) | $5 \times 10^{-5}$ | $5 \times 10^{-4}$ |
| $s$ (m/s) | 1 | 10 |
| $r$ (m) | 10 | 100 |
| $\tau$ (s) | 0 | 100 |
| $\delta$ (s$^{-1}$) | 0.0 | 0.1 |

Table 5.1: Table of parameter values used in simulations for the lookup table.

## 5.2.2 Experimental Results

Figure 5.2 presents several example datasets from the lookup table. Four histogram plots are presented, each comparing two fundamental parameters. The value range for the other three parameters are displayed in a text-box inside each axis. Colour

---

[1]These simulations were performed on Cardiff University's High Performance Computer: Merlin.
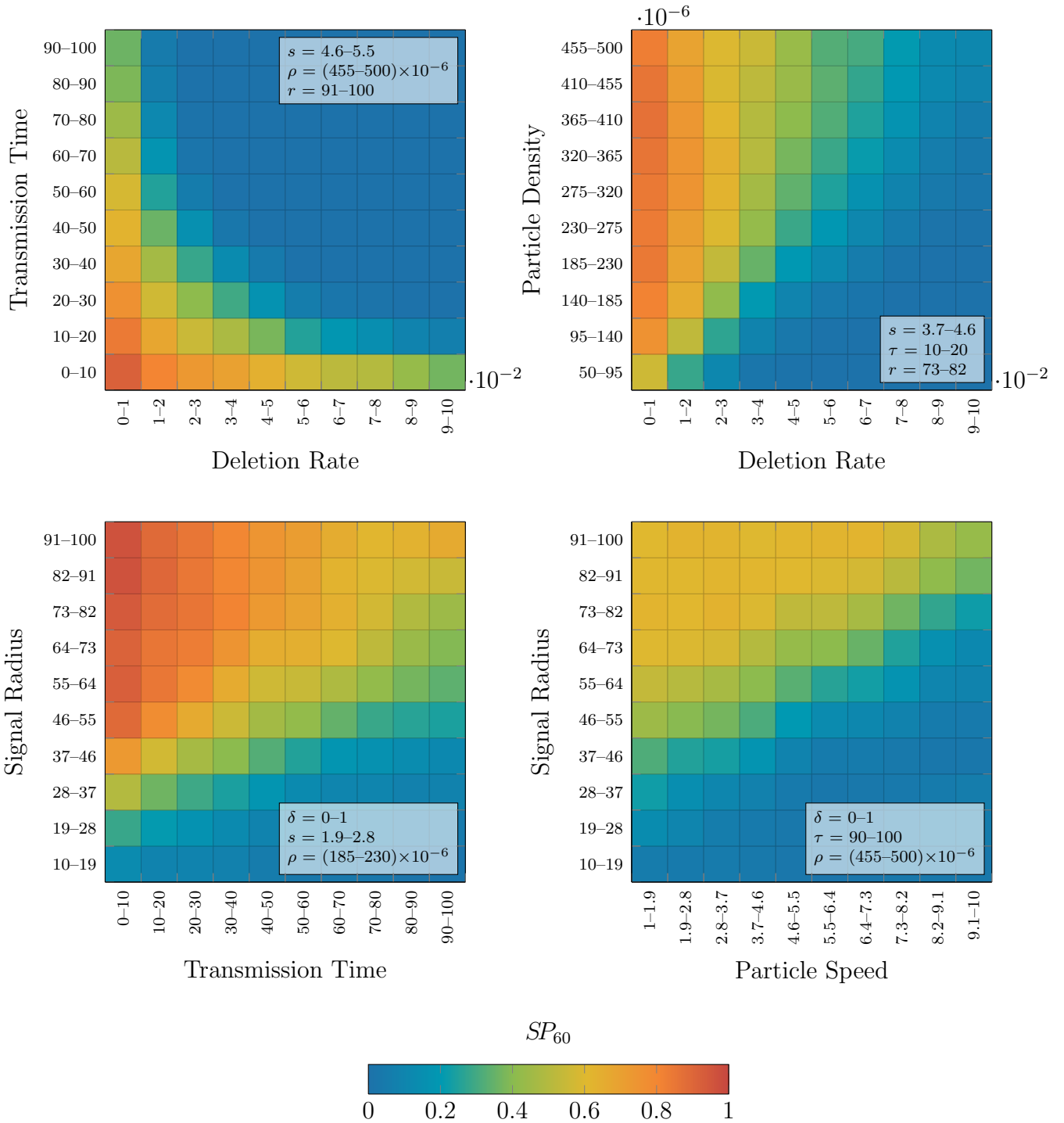
Figure 5.2: Four histogram plots, each displaying results from the lookup table for a comparison between two parameters. The colour of each cell represents the value of $SP_{60}$ for the corresponding parameter values, as indicated by the colour-bar below the plots. The value ranges of the remaining three parameters are displayed in a text-box within each axis.

shows the value of $SP_{60}$, as indicated by the colour-bar at the bottom of the figure. The results of each plot are now discussed.

**Transmission Time vs. Deletion Rate:** Figure 5.2 top-left. From this comparison, an engineer may learn that the deletion rate should be decreased to allow larger messages to persist. This makes sense as a longer transmission time reduces propagation (as seen in Section 4.2) and a higher deletion rate leads to fewer copies of the message in the network (as seen in Section 2.2.5).

**Particle Density vs. Deletion Rate:** Figure 5.2 top-right. This plot shows how the deletion rate should be adjusted depending on particle density. If the region is particularly dense, messages can be deleted more readily and still persist substantially. This makes sense as a higher particle density increases propagation (as seen in Section 4.2) and a higher deletion rate leads to fewer copies of the message in the network (as seen in Section 2.2.5).

**Signal Radius vs. Transmission Time:** Figure 5.2 bottom-left. An engineer may choose the signal radius of each particle based on the required transmission time. From this plot, it is clear that a larger signal radius should be used for messages that take a long time to transmit. This makes sense as a longer contact duration is required for longer transmissions.

**Signal Radius vs. Particle Speed:** Figure 5.2 bottom-right. Similarly, it is clear that a larger signal radius should be chosen in regions where particles move quickly. Again, this makes sense as it increases contact duration.

In Fig. 5.3, the results of two more comparisons are displayed, this time as surface plots. In the upper plot, signal radius is compared to particle density. It is clear that a larger signal radius should be used in regions of low particle density to ensure that the message persists in the network with high probability. The lower plot compares the effects of particle speed and transmission time on $SP_{60}$. This shows an interesting result, which shall be discussed in the following subsection.

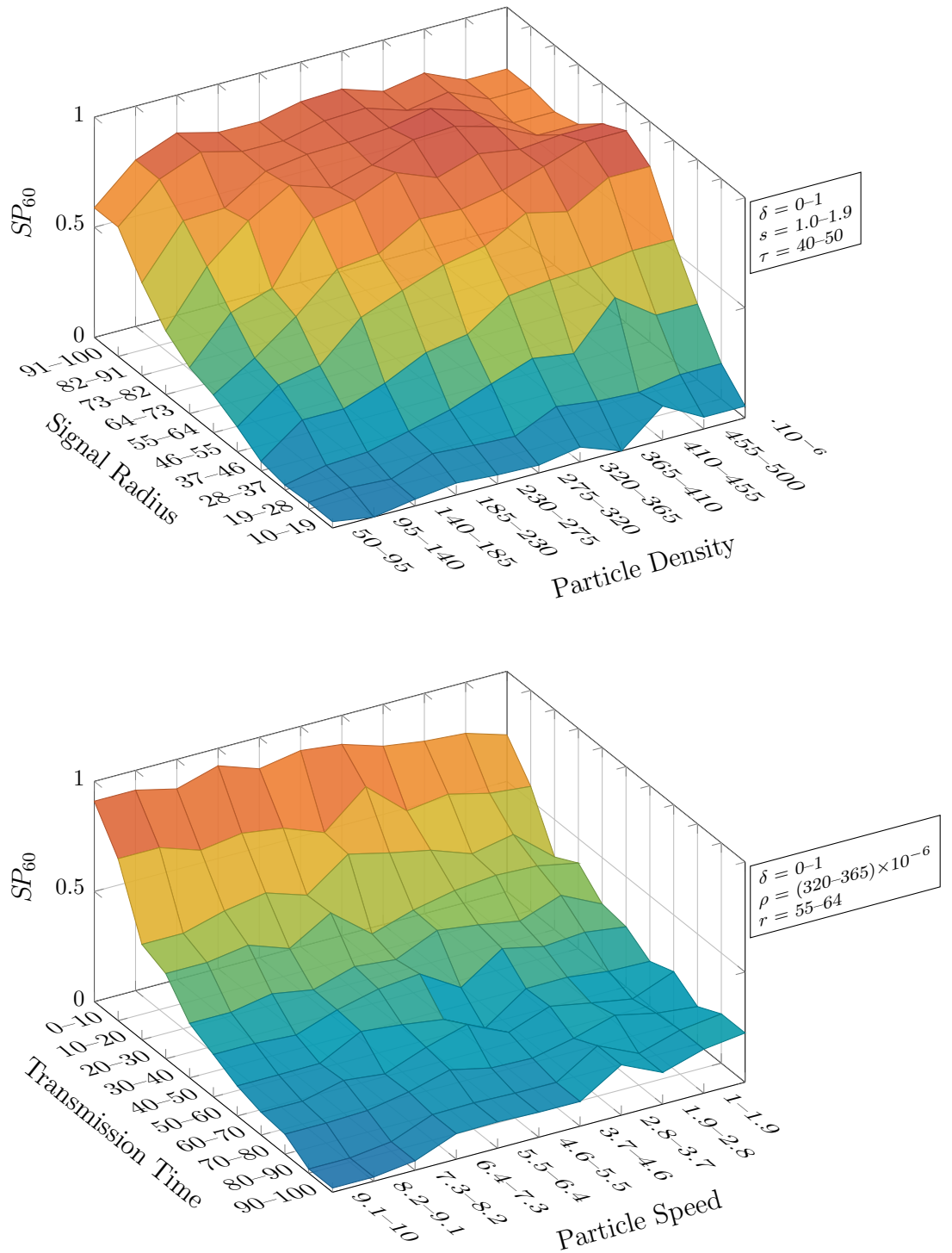**Example Results from Lookup Table**

Figure 5.3: Two surface plots, each displaying results from the lookup table for a comparison between two parameters. The height/colour of each cell represents the value of $SP_{60}$ for the corresponding parameter values. The value ranges of the remaining three parameters are displayed in a text-box beside each axis. All results are generated according to Section 5.2.1.

### 5.2.3   Transmission Time vs. Particle Speed

The focus of this section is on the relationship between transmission time and particle speed. Although it is usually not possible to control particle speed in real life, it is possible to observe the average speed and potentially use this information to make an informed choice about the amount of data to attempt to send.

The lower plot in Fig. 5.3 shows the relevant comparison from the lookup table. Interestingly, there appears to be a transition in how message propagation is affected by the parameters. It is clear that faster movement is beneficial when transmission time is short, but the opposite is true when transmission time is long. This finding shall be further probed by extending the study to include results for the other metrics described in Section 4.2.3: $T_{50}^{Q}$ (time until 50% of particles receive the message) and $T_{50}^{D}$ (time until the message travels 50 meters from its origin). These results are shown in Fig. 5.4.

Looking at Fig. 5.4, it is clear that faster particle movement is usually beneficial to data propagation. However, if the transmission time is sufficiently long, a threshold is reached beyond which any further increase in speed inhibits data propagation. The reason for this is that contact duration decreases as the speed of movement increases, as seen in Sections 3.3 and 4.6. A shorter contact duration leads to less successful transmissions if the transmission time is long. This is why detrimental effects are eventually seen on data propagation for larger messages. However, if the speed of movement is slow and/or the transmission time is short, this detrimental effect is not significant. Instead, an increase in speed is actually beneficial to data propagation as it increases the contact rate, as seen in Section 3.1. Later in this chapter (Section 5.5) an expression for the contact duration distribution in continuous-space models is obtained, confirming this theory.

## 5.3   Critical Deletion Rate

### 5.3.1   Definition

Recall that the deletion rate, $\delta$, is the probability per second that an infectious particle deletes the message from its buffer. The critical deletion rate, $\delta_c$, shall be defined as the smallest value of $\delta$ for which an epidemic no longer persists for a
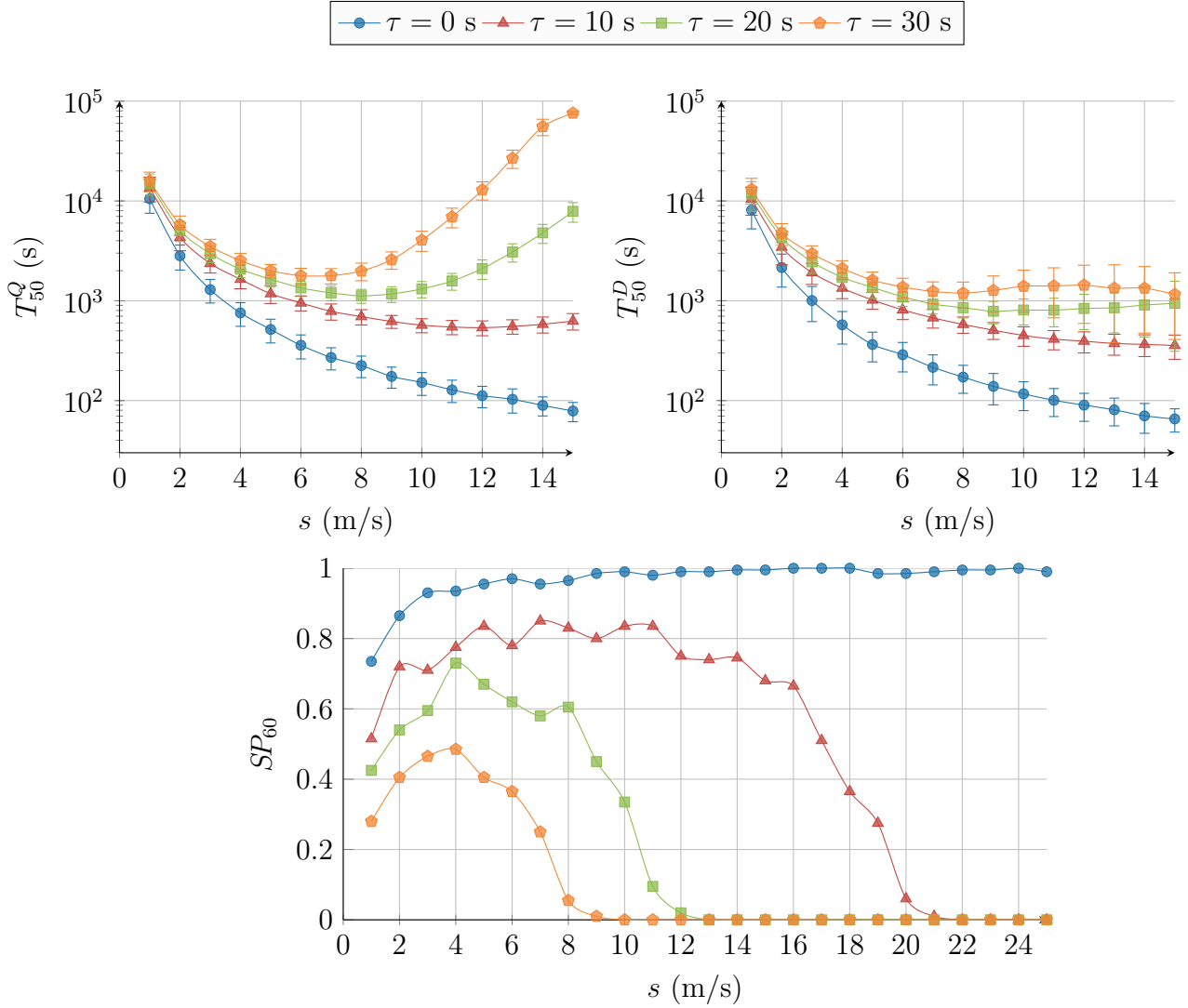
Figure 5.4: Study on particle speed for various transmission times. Each plot shows the results of 200 simulations. All particles move in 2D space according to the Random Direction model with absolute speed and an absolute turning rate of $1\ s^{-1}$. The following parameter values are used for all simulations: $\rho = 2 \times 10^{-4}$, $r = 40$ and $\delta = 0.0035$.

significant amount of time. This amount of time is chosen to be 60 minutes and the metric for measuring such persistence shall be denoted $SP_{60}$ (see Section 4.2.3).

**Study on Critical Deletion Rate**
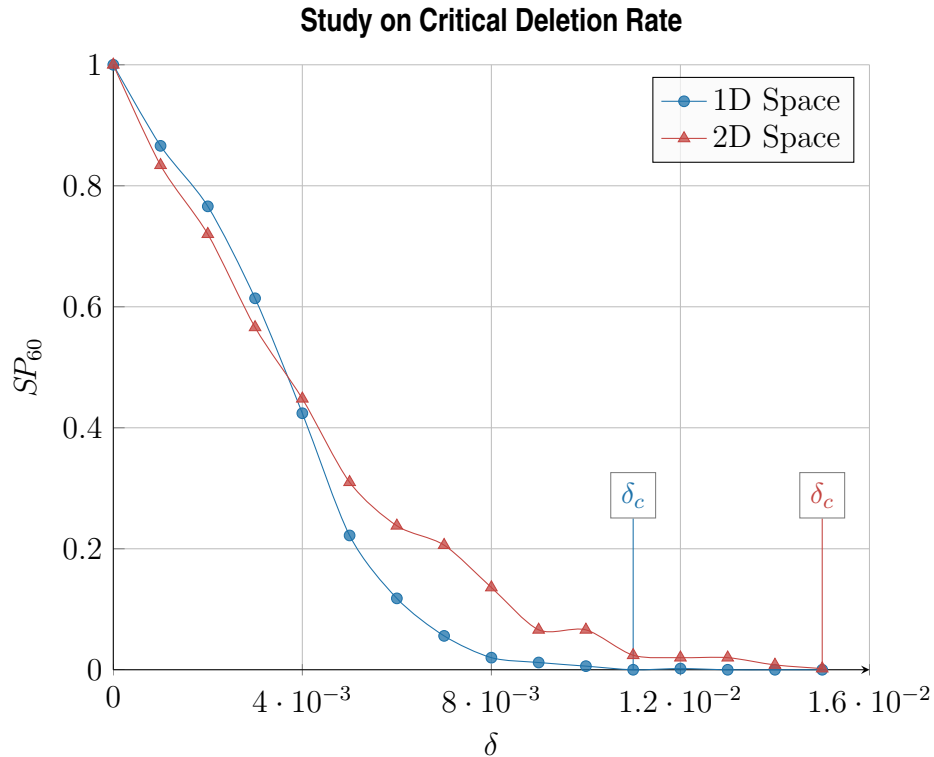


Figure 5.5: Study on $SP_{60}$ for various deletion rates in 1D and 2D space. An SIS interaction scheme is used for all simulations (see Section 2.1). The critical deletion rate ($\delta_c$) has been labelled for each plot.

Examples of $\delta_c$ are shown in Fig. 5.5 for 1D and 2D space. It is clear that an epidemic is less likely to persist as $\delta$ increases. This is expected as a a large value of $\delta$ means the message is being deleted more often. The smallest value of $\delta$ for which $SP_{60} = 0$ is $\delta_c$, as labelled in the plot.

## 5.3.2   Experimental Description

This experiment shows how $\delta_c$ scales as each fundamental parameter is adjusted. All simulations are performed using the 2D space mobility model described in Section 5.1, with a region size of 1 km × 1 km. A single broadcast message is disseminated using an SIS interaction scheme. Following this, $\delta_c$ is estimated by searching through the results of the various simulations (each with 200 trials).

### 5.3.3 Experimental Results

The results of the study on $\delta_c$ are shown in Fig. 5.6. Results have been transformed along the $x$-axis to show the linear relations to $\delta_c$; for example, $r^2$ is used on the $x$-axis of the third plot instead of $r$. By doing this, it is clear how $\delta_c$ is affected by the fundamental parameters. Taking all results into account, the following relation for $\delta_c$ is derived:

$$\delta_c \propto \frac{\rho r^2}{s \tau}. \tag{5.1}$$

As seen in Section 5.2.3, particle speed can affect data propagation in different ways depending on the transmission time. For this reason, the study is repeated on $\delta_c$ for various values of $s$ but this time instantaneous transmissions are used ($\tau = 0$). All other parameter values are left unchanged. The results are shown in Fig. 5.7. It is clear that as the average speed increases, particles can delete the message more quickly while still ensuring persistence. This is due to a higher contact rate caused by the faster particle movement.
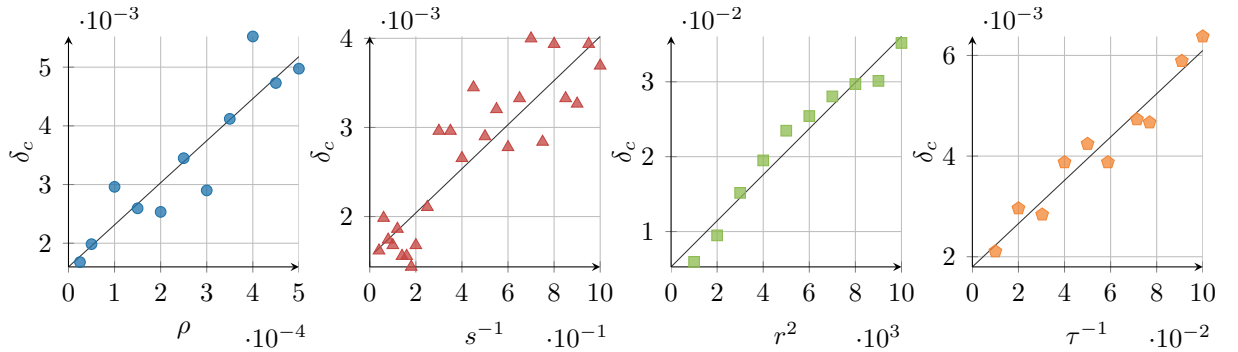


Figure 5.6: Plots to show how $\delta_c$ scales with each fundamental parameter. All simulated results are presented as scatter plots with lines of best fit. Plots are transformed along the $x$-axis to show their linear relations to $\delta_c$. All results are taken from the average of 200 simulations. The following default parameter values are used: $\rho = 2 \times 10^{-4}$, $s = 2$, $r = 20$, $\tau = 40$.

Comparing x-axis labels for Figs. 5.6 and 5.7 it is clear that particle speed affects data propagation in different ways depending on the transmission time. For instantaneous transmissions, faster particle speed is beneficial. For long transmission times, the opposite is true. The reasoning for this has been explained in Section 5.2.3. It is therefore concluded that for instantaneous transmissions, the $s$ in Eq. (5.1) moves to the numerator:

$$\delta_c \propto \frac{s \rho r^2}{\tau}.$$
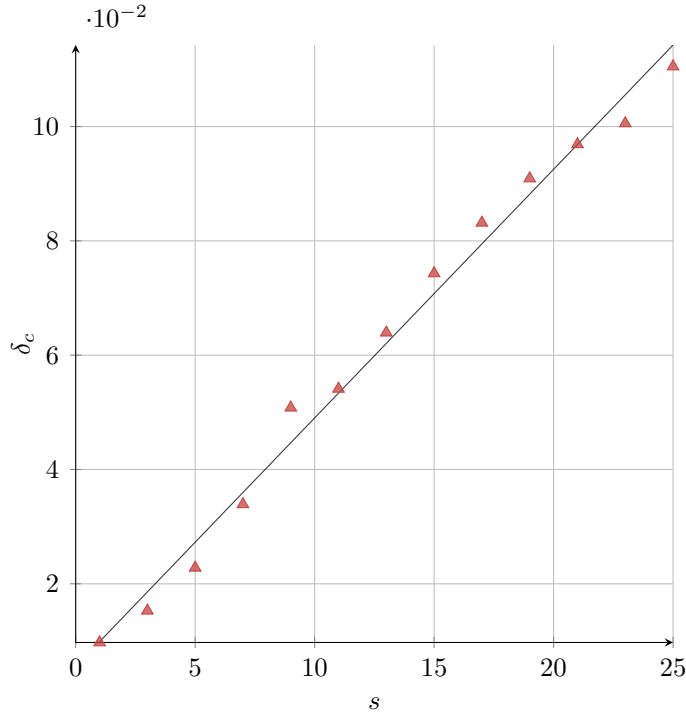
Figure 5.7: Plot to show how $\delta_c$ scales with particle speed for instantaneous transmissions. All results are taken from the average of 200 simulations with the following parameter values: $\rho = 2 \times 10^{-4}$, $r = 20$, $\tau = 0$. All particles move according to the Random Direction model with absolute speed and an absolute path length of 1.

## 5.4   Contact Rate

In this section, a theoretical model is presented for particle contact rate, $\nu_c$. The 2D continuous space mobility model described in Section 5.1 is considered. Note that the same model for $\nu_c$ is briefly presented in Klein *et al.* (2010), however, the full derivation is explained in this section. Furthermore, this model is extended for this thesis by simplifying it for use with the Normal speed distribution considered in this chapter.

**Theorem 5.4.1**

$$E(\nu_c) = \sqrt{8} \cdot \rho r E(s) \tag{5.2}$$

**Proof** Let $x$ be an arbitrary position that is stationary in our frame-of-reference so that all other particles are travelling at speed $\tilde{s}$ relative to $x$. The expected contact rate $E(\nu_c)$ at $x$ is the rate at which particles move to cover $x$ with their wireless

signal. This is equal to the expected number of particles per second that enter the disk of radius $r$, centred at $x$.
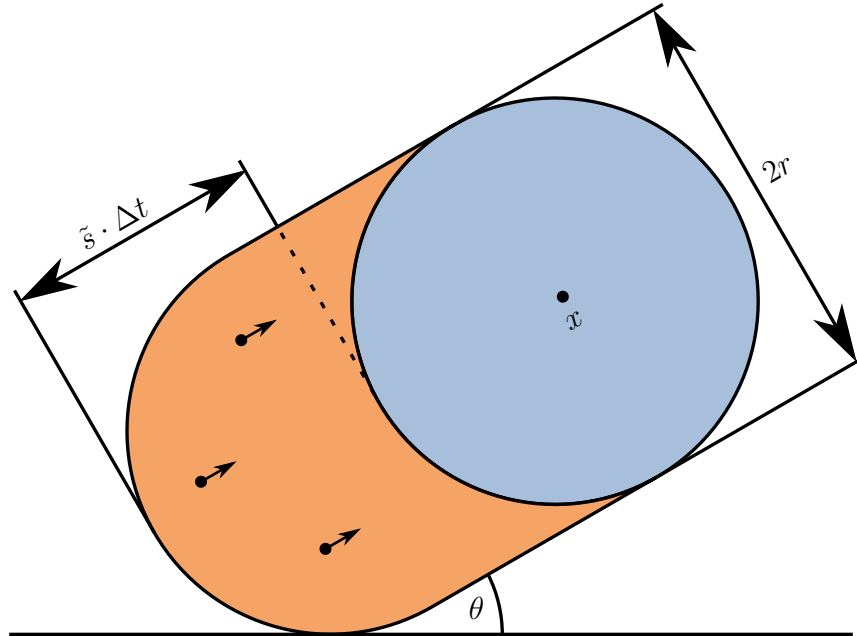


Figure 5.8: Diagram to show how the contact rate is calculated. The circular region depicts the signal coverage area of a particle positioned at $x$. All particles in the orange shaded strip will move into the blue circle in the next second; therefore, forming a contact with the particle at $x$.

Given particles travelling at angle $\theta$ and speed $\tilde{s}$, the contact rate is equal to the number of such particles that are at an appropriate position relative to $x$, so that they will move within distance $r$ of $x$ in $\Delta t$ seconds. Appropriate positions can be anywhere within a specific region, $A$, as depicted by the orange shaded strip in Fig. 5.8.

The area of $A$ is $2r\tilde{s}\Delta t$; therefore, the expected number of particles in $A$ (travelling at $\theta$ and $\tilde{s}$) is $2r\rho\tilde{s}\Delta t$. Integrating the expected number of particles in $A$ for all $\theta$ and all $\tilde{s}$ gives the contact rate, $\nu_c$. As $\theta$ does not appear in the equation, integrating for all $\theta$ has no effect. Integrating for all $\tilde{s}$ has the effect of replacing $\tilde{s}$ in the equation with its expected value from the Rayleigh distribution, $E(\tilde{s}) = \sqrt{2}E(s)$ (see Section 5.1). The full derivation of $E(\nu_c)$ is shown as follows. It is assumed that $\Delta t = 1$ so that

the rate, $\nu_c$, is per second.

$$E(\nu_c) = \int_0^{2\pi} \left[ \int_0^\infty 2\rho r \tilde{s} h(\tilde{s}) \, \mathrm{d}\tilde{s} \right] \frac{\mathrm{d}\theta}{2\pi}$$
$$= \int_0^\infty 2\rho r \tilde{s} h(\tilde{s}) \, \mathrm{d}\tilde{s}$$
$$= 2\rho r \cdot E(\tilde{s})$$
$$= \sqrt{8} \cdot \rho r E(s)$$

which agrees with a result of Klein *et al.* (2010). ∎

### 5.4.1 Experimental Results

In Fig. 5.9, the contact rate $E(\nu_c)$ is studied for a range of parameter values for signal radius, mean particle speed and particle density. Simulated results are produced for 1D space, and the developed theoretical model is compared with simulated results for 2D space. Table 5.2 shows the default parameter values used for each plot.

| Parameter | 1D Default | 2D Default |
|---|---|---|
| $\rho$ | 0.025 (particles/m) | $2 \times 10^{-4}$ (particles/m$^2$) |
| $E(s)$ | 1 (m/s) | 1 (m/s) |
| $r$ | 20 (m) | 40 (m) |

Table 5.2: Table of default parameter values used in the contact rate study. Note that $\tau$ is not listed as it does not affect contact rate.

Firstly, the results for 2D space are looked at in the lower plots. It is clear that the theoretical model fits perfectly for the entire range of parameter values studied. It is clear that $E(\nu_c)$ is affected by all three parameters, linearly increasing with signal radius, particle speed and particle density. This correlation appears to be the same for 1D space (upper plots) with one exception: signal radius does not appear to affect contact rate for 1D space. This is the same result that was seen in the previous chapter for the discrete-space models and is discussed in Section 4.4.

## 5.5 Contact Duration

In this section, an original contribution is provided for a theoretical model of contact duration $T_c$ in 2D continuous space. The 2D mobility model described in Section 5.1
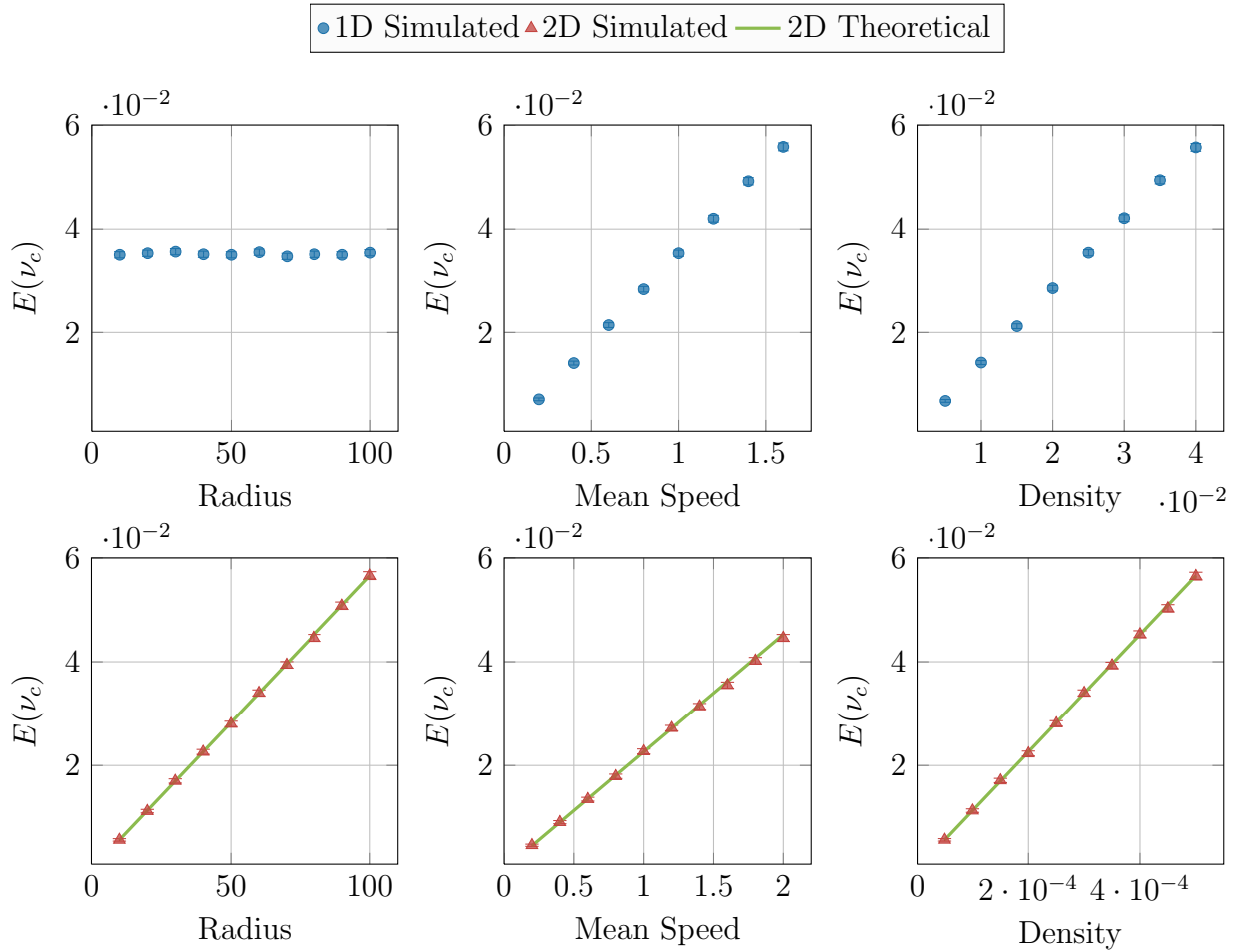
Figure 5.9: Plots to show how contact rate is affected by signal radius, mean particle speed and particle density for 1D and 2D space. All simulated results are the average of 20 simulations (each 500 seconds in duration) with standard error error bars (some are too small to see). Table 5.2 shows the default values used for each parameter. In all cases, the expected contact rate scales linearly with each parameter, except for signal radius in 1D space.

is considered.

**Theorem 5.5.1**

$$P(T_c \geq t) = \frac{\pi k}{\sqrt{2}} \cdot \exp\left(-\frac{\pi k^2}{4}\right) \cdot I_1\left(\frac{\pi k^2}{4}\right),$$

where $I_1$ is the modified Bessel function of the first kind and $k = \frac{r}{E(s)t}$.

**Proof** Consider an arbitrary particle that is stationary in our frame-of-reference so that all other particles are travelling at speed $\tilde{s}$, relative to our particle. Let $x$ denote the position of our particle and $B(x, r)$ denote a circle of radius $r$ centred at $x$, as illustrated in Fig. 5.10.
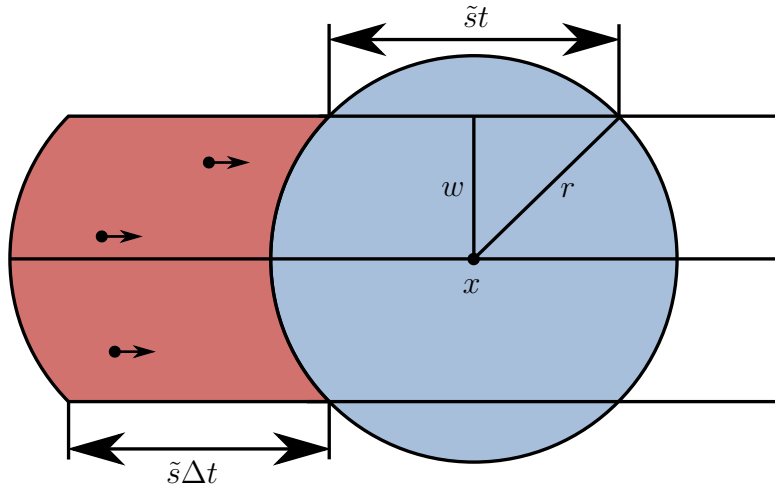


Figure 5.10: Diagram to show how contact duration is calculated. The circular region depicts the signal coverage area of a particle positioned at $x$. All particles positioned within the red shaded strip will enter the circle within one second (assuming a relative speed of $\tilde{s}$), and remain in the circle for at least $t$ seconds.

Any particle that enters $B(x, r)$ will remain within communication range of our particle for at least $t$ seconds if and only if the distance travelled within $B(x, r)$ is at least $\tilde{s}t$. This occurs if a particle passes within distance $w$ of $x$. Pythagoras' theorem is applied to the triangle in Fig. 5.10 to find the distance to the point of closest approach, $w$, as follows:

$$w = \sqrt{r^2 - \frac{\tilde{s}^2 t^2}{4}}.$$

Given the relative speed $\tilde{s}$, all particles in the red strip shown in Fig. 5.10 will enter $B(x, r)$ in the interval $[t, t + \Delta t]$. The area of the shaded strip is $2w\tilde{s}$ (assuming

130

$\Delta t = 1$). Multiplying this by $\rho$ gives the expected number of particles in the red strip at any time: $\rho \cdot (2w) \cdot \tilde{s}$.

If $\tilde{s} \leq 2r/t$, all particles in the red strip will be resident in $B(x,r)$ for at least $t$ seconds. Conversely, particles with $\tilde{s} > 2r/t$ will be resident in $B(x,r)$ for less than $t$ seconds, even if they pass through the centre of $B(x,r)$.

Integration is used to find the number of particles in the red strip for all values of $\tilde{s} \leq 2r/t$, where $\tilde{s}$ occurs with probability $h(\tilde{s})$. Dividing by the expected contact rate $E(\nu_c)$ (see Section 5.4) gives the proportion of contacts with a duration of at least $t$:

$$P(T_c \geq t) = \frac{1}{E(\nu_c)} \cdot \int_0^{\frac{2r}{t}} 2\rho w \tilde{s} \cdot h(\tilde{s}) \, d\tilde{s}. \tag{5.3}$$

Recall that

$$w = r\sqrt{1-y}, \text{ where } y = \frac{\tilde{s}^2 t^2}{4r^2} \tag{5.4}$$

and

$$h(\tilde{s}) = \frac{\pi \tilde{s}}{4E(s)^2} \cdot \exp\left(\frac{-\pi \tilde{s}^2}{8E(s)^2}\right). \tag{5.5}$$

Substituting Eqs. (5.4) and (5.5) into Eq. (5.3) gives:

$$P(T_c \geq t) = \frac{1}{E(\nu_c)} \cdot \int_0^{\frac{2r}{t}} 2\rho \cdot r\sqrt{1-y} \cdot \frac{\pi \tilde{s}^2}{4E(s)^2} \cdot \exp\left(\frac{-\pi \tilde{s}^2}{8E(s)^2}\right) \, d\tilde{s}. \tag{5.6}$$

Rearranging $y$ gives $\tilde{s}^2 = \frac{4yr^2}{t^2} = 4yk^2 E(s)^2$ which is substituted into Eq. (5.6):

$$P(T_c \geq t) = \frac{1}{E(\nu_c)} \cdot \int_0^{\frac{2r}{t}} 2\rho \cdot r\sqrt{1-y} \cdot \pi y k^2 \cdot \exp\left(\frac{-\pi y k^2}{2}\right) \, d\tilde{s}. \tag{5.7}$$

Taking the square root of $\tilde{s}^2 = \frac{4yr^2}{t^2}$ gives $\tilde{s} = \frac{2r}{t} y^{\frac{1}{2}}$ which is differentiated to get $d\tilde{s} = \frac{r}{t} y^{-\frac{1}{2}} \, dy$. Substituting this into Eq. (5.7) gives:

$$P(T_c \geq t) = \frac{1}{E(\nu_c)} \cdot \int_0^1 2\rho \cdot r\sqrt{1-y} \cdot \pi y k^2 \cdot \exp\left(\frac{-\pi y k^2}{2}\right) \cdot \frac{r}{t} y^{-\frac{1}{2}} \, dy. \tag{5.8}$$

Note the new integral limits, calculated from $y = \frac{\tilde{s}^2 t^2}{4r^2}$ for $\tilde{s} = \frac{2r}{t}$ and $\tilde{s} = 0$.

We now rearrange and simplify to get:

$$
\begin{aligned}
P(T_c \geq t) &= \frac{1}{E(\nu_c)} \cdot \frac{2\pi \rho r^2 k^2}{t} \cdot \int_0^1 \sqrt{y(1-y)} \cdot \exp\left(\frac{-\pi y k^2}{2}\right) dy, \\
&= \frac{2\pi \rho r^2 k^2}{\sqrt{8}\rho r E(s) \cdot t} \cdot \int_0^1 \sqrt{y(1-y)} \cdot \exp\left(\frac{-\pi y k^2}{2}\right) dy, \\
&= \frac{\pi k^3}{\sqrt{2}} \cdot \int_0^1 \sqrt{y(1-y)} \cdot \exp\left(\frac{-\pi y k^2}{2}\right) dy.
\end{aligned}
\tag{5.9}
$$

## Kummer's Function

We now attempt to simplify Eq. (5.9) with the use of Kummer's Function (Abramowitz and Stegun 1964). Firstly, Eq. (5.9) is written as follows:

$$
P(T_c \geq t) = \frac{\pi k^3}{\sqrt{2}} \cdot J, \text{ where } J = \int_0^1 \sqrt{y(1-y)} \cdot \exp\left(\frac{-\pi y k^2}{2}\right) dy.
\tag{5.10}
$$

$J$ is related to the confluent hypergeometric function (Abramowitz and Stegun 1964), also known as Kummer's function, represented as an integral below.

$$
M(a,b,z) = \frac{\Gamma(b)}{\Gamma(b-a)\Gamma(a)} \cdot \int_0^1 \exp(zt) \cdot t^{a-1}(1-t)^{b-a-1} dt,
$$

where $\Gamma$ is the Gamma Function (Weisstein 2014a), or alternatively

$$
M(a,b,z) = \sum_{n=0}^{\infty} \frac{a^{(n)} z^n}{b^{(n)} n!}
$$

and $a^{(n)} = a(a+1)\cdots(a+n-1)$ is the rising factorial.

In our case, $a = \frac{3}{2}, b = 3, z = -\frac{\pi}{2}k^2$. So,

$$
J = \frac{\Gamma\left(\frac{3}{2}\right)\Gamma\left(\frac{3}{2}\right)}{\Gamma(3)} \cdot M\left(\frac{3}{2}, 3, -\frac{\pi}{2}k^2\right) = \frac{\pi}{8} \cdot M\left(\frac{3}{2}, 3, -\frac{\pi}{2}k^2\right),
\tag{5.11}
$$

where we have used the fact that $\Gamma\left(\frac{3}{2}\right) = \frac{\sqrt{\pi}}{2}$ and $\Gamma(3) = 2$. Substituting Eq. (5.11) into Eq. (5.10) gives:

$$
P(T_c \geq t) = \frac{\pi^2 k^3}{8\sqrt{2}} \cdot M\left(\frac{3}{2}, 3, -\frac{\pi}{2}k^2\right).
\tag{5.12}
$$

## Properties of Kummer's function

The following properties of Kummer's function are used:

1. $M(a, b, z) = \exp(z) \cdot M(b - a, b, -z)$ (Kummer's transformation).

2. $M(a, 2a, z) = \exp\left(\dfrac{z}{2}\right) \cdot \left(\dfrac{z}{4}\right)^{\frac{1}{2}-a} \cdot \Gamma\left(a + \dfrac{1}{2}\right) \cdot I_{a-\frac{1}{2}}\left(\dfrac{z}{2}\right),$

   where $I_{a-\frac{1}{2}}(\cdot)$ is the modified Bessel function of the first kind.

Applying property 1 to Eq. (5.11) gives

$$J = \frac{\pi}{8} \cdot \exp\left(-\frac{\pi}{2}k^2\right) \cdot M\left(\frac{3}{2}, 3, \frac{\pi}{2}k^2\right). \tag{5.13}$$

Applying property 2 to Eq. (5.13) gives

$$J = \frac{\pi}{8} \cdot \exp\left(-\frac{\pi}{2}k^2\right) \left[\exp\left(\frac{\pi}{4}k^2\right) \cdot \left(\frac{\pi k^2}{8}\right)^{-1} \cdot \Gamma(2) \cdot I_1\left(\frac{\pi k^2}{4}\right)\right]$$

$$= \frac{1}{k^2} \cdot \exp\left(-\frac{\pi}{4}k^2\right) \cdot I_1\left(\frac{\pi k^2}{4}\right), \tag{5.14}$$

where we have used the fact that $\Gamma(2) = 1$. Substituting Eq. (5.14) into Eq. (5.10) gives:

$$P(T_c \geq t) = \frac{\pi k}{\sqrt{2}} \cdot \exp\left(-\frac{\pi k^2}{4}\right) \cdot I_1\left(\frac{\pi k^2}{4}\right). \quad \blacksquare \tag{5.15}$$

**Remark** Note that

$$k \to 0 \text{ as } \begin{cases} r \to 0 \\ E(s) \to \infty \\ t \to \infty \end{cases} \quad \text{and} \quad k \to \infty \text{ as } \begin{cases} r \to \infty \\ E(s) \to 0 \\ t \to 0 \end{cases},$$

in particular; this reduces the expression for instantaneous transmissions.

## Approximation for Small Values of $k$

A key contribution of this thesis is in the analysis of models for which it has been assumed that data transmissions may not occur instantaneously. A long transmission time leads to a small value of $k$; therefore, it is useful to create a simpler model to approximate contact duration for small values of $k$. To do this, the following

property of Kummer's Function is used:

$$M(a, b, z) \to 1 \text{ as } |z| \to 0.$$

Applying this to Eq. (5.12) give the following approximation for small values of $k$:

$$P(T_c \geq t) \simeq \frac{\pi^2 k^3}{8\sqrt{2}}.$$

### 5.5.1 Experimental Results

Figure 5.11 shows simulated results for 1D and 2D space (upper/lower plots, respectively). The parameter values used are shown in a box next to each plot. The speed of each particle is taken from the Normal distribution with mean $E(s)$. Each particle maintains its speed and direction for the entire simulation.

It is clear that, for both 1D and 2D space, the distribution of contact duration has a long tail and mimics the shape of a Rayleigh distribution. It is clear that the theoretical model perfectly matches the results for 2D space.

## 5.6 Message Spread

The theoretical model for contact rate and contact duration distribution are now discussed with regard to how they can be used to model the spatial spread of a message in 2D space. Furthermore, the model from Klein *et al.* (2010) is extended to work with non-instantaneous transmissions.

### 5.6.1 Reaction-Diffusion Equation

Klein *et al.* (2010) show that the spatial spread of a message in an OPNET can be modelled with a reaction-diffusion equation, such as the following:

$$\frac{\partial u}{\partial t} = -\alpha \frac{\partial u}{\partial x} + D \frac{\partial^2 u}{\partial x^2} + f(u),$$

where the terms on the right-hand side of the equation are respectively the *advection* term (the drift of particles due to a flow of movement in a particular direction), the
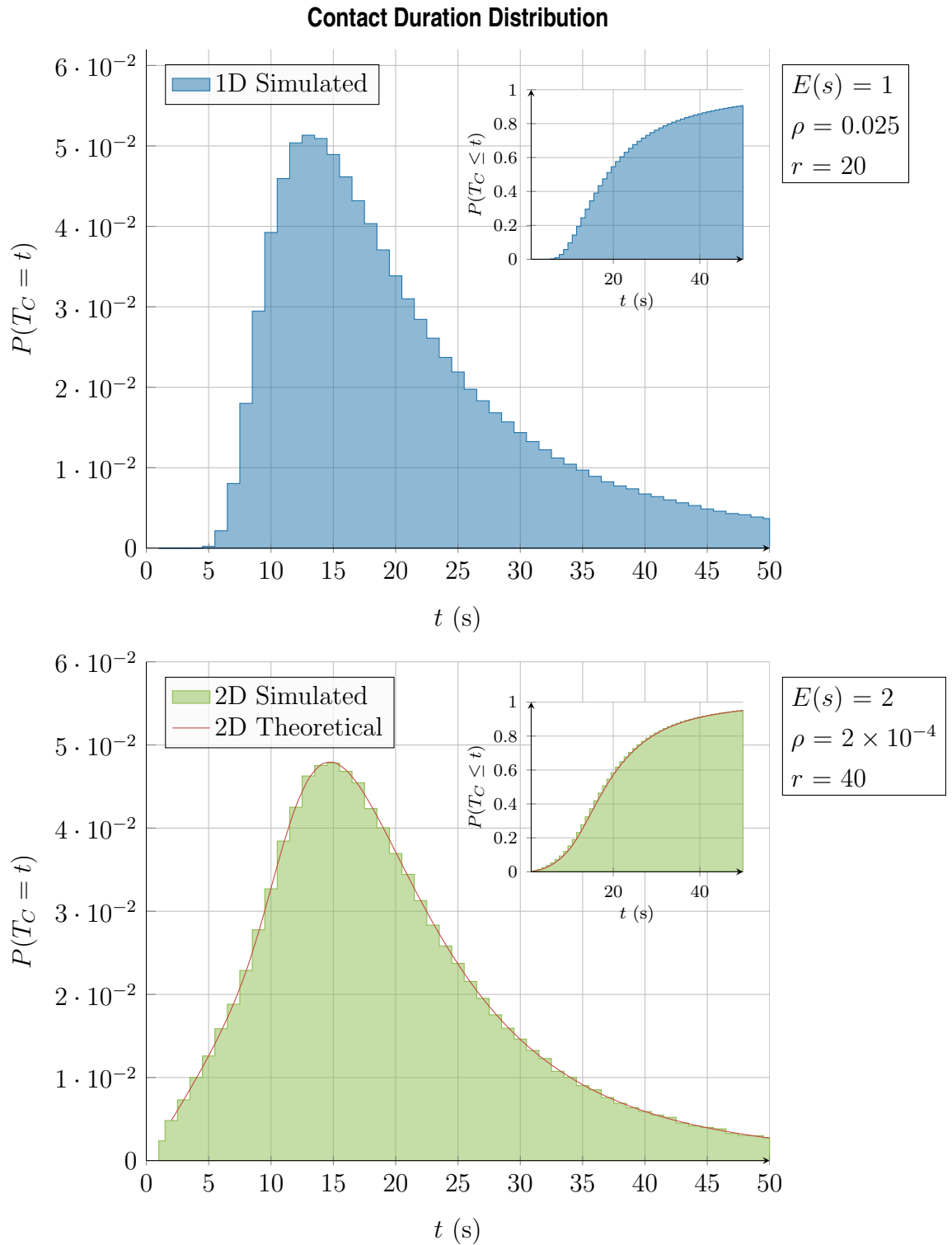
Figure 5.11: Experimental results for contact duration distribution in continuous space. The upper plot shows simulated results for 1D space. The lower plot compares simulated and theoretical results for 2D space. The probability density function can be seen in the main plots. The inset sub-plots show the cumulative distribution function. The parameter values used were decided based on trial and error of preliminary simulations and are displayed next to each plot.

*diffusion* term (movement due to concentration gradients) and the *reaction* term (representing the copying of messages among particles). In this chapter, isotropic movement is assumed so the advection term is zero. In this case, the classical KPP/Fisher equation is obtained, first studied by Kolmogorov *et al.* (1937) and Fisher (1937) to describe the spread of an advantageous gene through a population:

$$\frac{\partial u}{\partial t} = D\frac{\partial^2 u}{\partial x^2} + f(u). \tag{5.16}$$

It is well known that such reaction-diffusion systems have *travelling wave solutions* of the form $u(x, t) = w(x - ct)$, where c is the propagation speed of the wave. Using phase-plane analysis, it can be shown that travelling wave solutions of Eq. (5.16) exist for all $c \geq c_{min}$, where the minimum propagation speed is given by $c_{min} = 2\sqrt{D \cdot f'(0)}$. In this equation, $D$ is the *effective diffusion coefficient* which can be used to model particle movement in the system, while the reaction term, $f'(0)$, can be used to model the message passing aspect. The terms $D$ and $f'(0)$ will now be discussed.

## 5.6.2 Diffusion Properties

Diffusion theory is used to model the movement of infectious particles in the system. Typically, diffusion concerns particles whose mean squared displacement (MSD) is a linear function of time, $t$. Therefore, the displacement from the origin of the simulated particles must scale with $\sqrt{t}$. This can be achieved using the Random Direction mobility model, as explained below.

In the Random Direction mobility model, the turning rate, $\lambda$, can be increased until velocity jumps are sufficiently frequent to behave like diffusion. This makes it possible to model the movement of particles with diffusion theory. However, a higher turning rate creates difficulties in modelling message passing between particles, which is greatly simplified by the assumption that communicating particles move with constant velocity for the entire transmission. Fortunately, it is possible to enforce this assumption while maintaining the diffusion-like movement. Indeed, diffusive movement is only necessary on the macroscopic scale, while ballistic movement is only required on the microscopic scale to ensure particles do not change direction during communication.

The Random Direction mobility model is well-suited to achieving the described
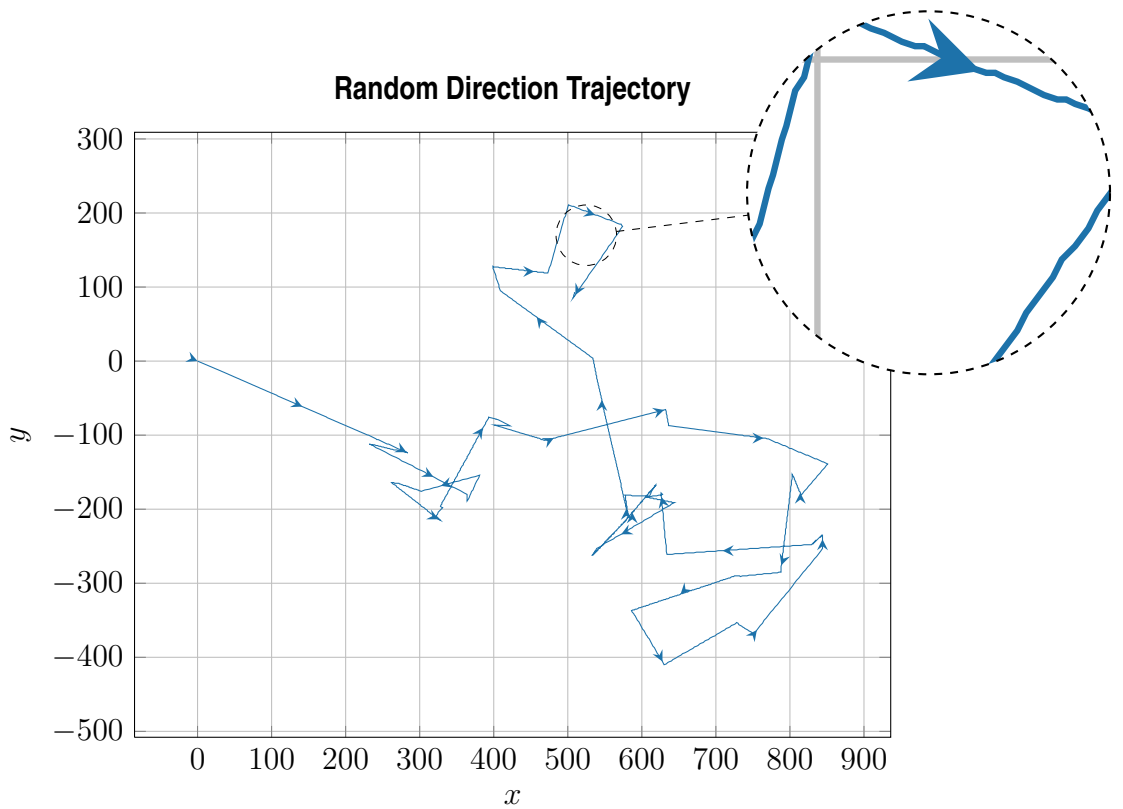
Figure 5.12: Example Random Direction trajectory with a zoomed-in section. It is clear that the trajectory consists of many direction changes on the macroscopic scale, but not on the microscopic scale. Arrows show direction of travel.

combination of ballistic and diffusive movement. Looking at the example trajectory in Fig. 5.12, is is clear that particles move in straight lines for small periods of time. Therefore, on the microscopic scale, trajectories appear ballistic. However, on the macroscopic scale, many velocity jumps are observed, yielding diffusive behaviour.

Figure 5.13 shows the combination of diffusive and ballistic behaviour for the Random Direction mobility model by looking at the MSD. Used parameter values match those of Klein *et al.* (2010). Lines of best fit are fitted to the simulated data on either side of the transition point that can be seen at around 22 seconds. The exponent of the green line (larger time-scale) is $1.01 \approx 1$, showing that the MSD scales approximately with time squared, meaning movement is diffusive on the macroscopic scale. Conversely, the exponent of the equation for the red line (smaller time-scale) is $1.91 \approx 2$, which means movement is ballistic on the microscopic scale.

### 5.6.2.1 Effective Diffusion Coefficient

It has been made clear that the Random Direction mobility model is compatible with the reaction-diffusion model described earlier. A value for the effective diffusion
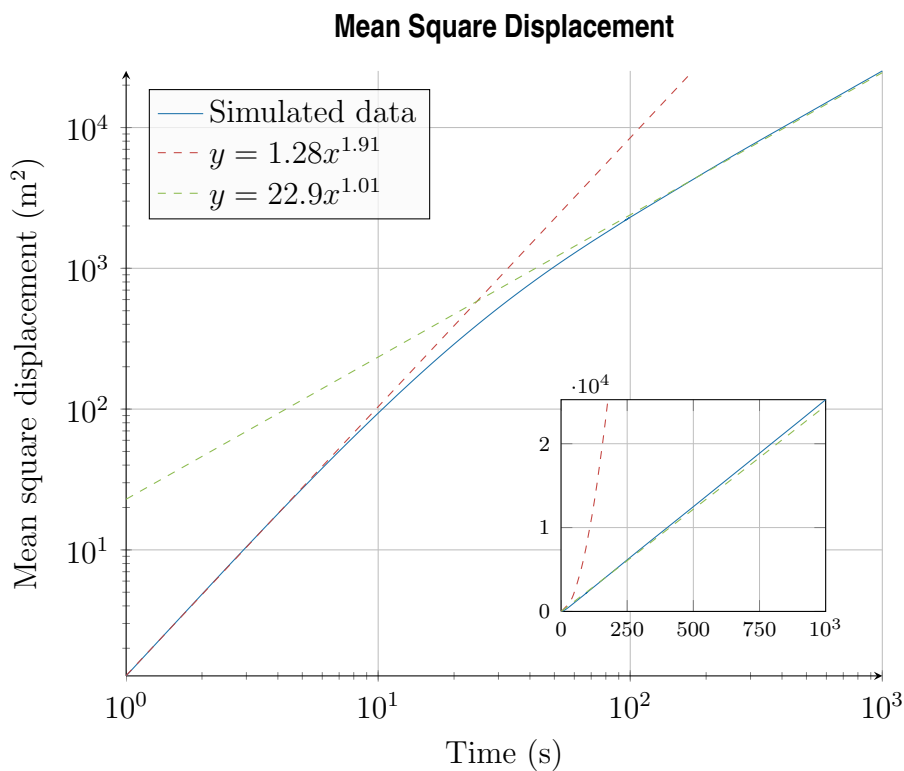
Figure 5.13: Plot to show how the Random Direction mobility model can simultaneously behave as ballistic on the microscopic scale and diffusive on the macroscopic scale. Dashed lines have been fitted and their equations show that MSD scales approximately linearly for large time-scales and with time squared for small time-scales. Used parameter values match those of Klein *et al.* (2010).

coefficient $D$, which describes the diffusive behaviour of the mobility model, is now needed. Unfortunately, it remains unclear how $D$ is calculated in Klein *et al.* (2010), and so this is left to future work. This means that, for the rest of this experiment, we are restricted to using the mobility model parameter values from Klein *et al.* (2010) as shown in Table 5.3.

| Parameter | Value |
|---|---|
| $\rho$ (particles/m$^2$) | $1.56 \times 10^{-5}$ |
| $s$ (m/s) | 1 (constant speed) |
| $E(\tilde{s})$ (m/s) | 1.27 |
| $r$ (m) | 100 |
| $\lambda$ (s$^{-1}$) | $900^{-1}$ |
| $D$ (m$^2$/s) | 28 |

Table 5.3: Table of parameter values used in Klein *et al.* (2010).

### 5.6.3 Extending Klein *et al.* (2010) for Non-Instantaneous Transmissions

Klein *et al.* (2010) show that the speed of the travelling wave for the dissemination of a message in an OPNET implemented on particles following the Random Direction mobility model is:

$$c = 2\sqrt{2\rho r E(\tilde{s})D}. \tag{5.17}$$

Klein *et al.* (2010) use the same 2D mobility model that is used throughout this chapter. Therefore, the contact rate model from Section 5.4 can be used to simplify Eq. (5.17) as:

$$c = 2\sqrt{D \cdot E(\nu_c)}.$$

To extend this model for non-instantaneous transmissions, the expected contact rate $E(\nu_c)$ is multiplied by the proportion of contacts that are long enough for a successful transmission, $P(T_c \geq \tau)$:

$$c = 2\sqrt{D \cdot E(\nu_c) \cdot P(T_c \geq \tau)}.$$

Note that the speed of particles in Klein *et al.* (2010) is constant, but the models assume Normally distributed speed. This is not a problem for the developed contact rate model as the expected relative speed is used, as provided by Klein *et al.* (2010).

However, the developed contact duration model must be adapted for constant speed and this is left to future work. For now, the average speed from the Normal distribution (used in the developed model for contact duration) shall match the constant speed from Klein *et al.* (2010).

### 5.6.4 Experimental Results

Fig. 5.14 shows the spread of a message in 2D continuous space for two different values of $\tau$. Looking down the rows, it is clear how the message spreads over time. The results in the left-hand column are from an exact replica of the experiment used by Klein *et al.* (2010), with instantaneous transmissions ($\tau = 0$). The results in the right-hand column are from an identical experiment only with $\tau = 60$. It is clear that the message spreads slower when $\tau = 60$, as expected. The black, dashed circle in each plot marks the theoretical model for message spread. It is clear that the theoretical model is accurate for both instantaneous and non-instantaneous message transmissions.

Figure 5.15 shows how a message spreads in 1D continuous space. The message spread profile is displayed after two time intervals. The theoretical modelling for this experiment is left to future work.

## 5.7   Real World Comparison

As mentioned in Section 1.5.1, all empirical studies in this thesis are performed with computer simulations. It is important to understand to what degree the simulated models represent the real-world. In this section, the results of the simulated models are further analysed using real-world data to find how accurately they match real-world OPNET behaviour.

As discussed in Section 1.5.1, time and cost constraints prevent the analysis of OPNETs operating in the real world. However, it is possible to gather real-world movement trajectories and simulate an OPNET on these trajectories. Although this is not the same as a fully implemented OPNET, it is a step closer to understanding how OPNETs behave in real life.
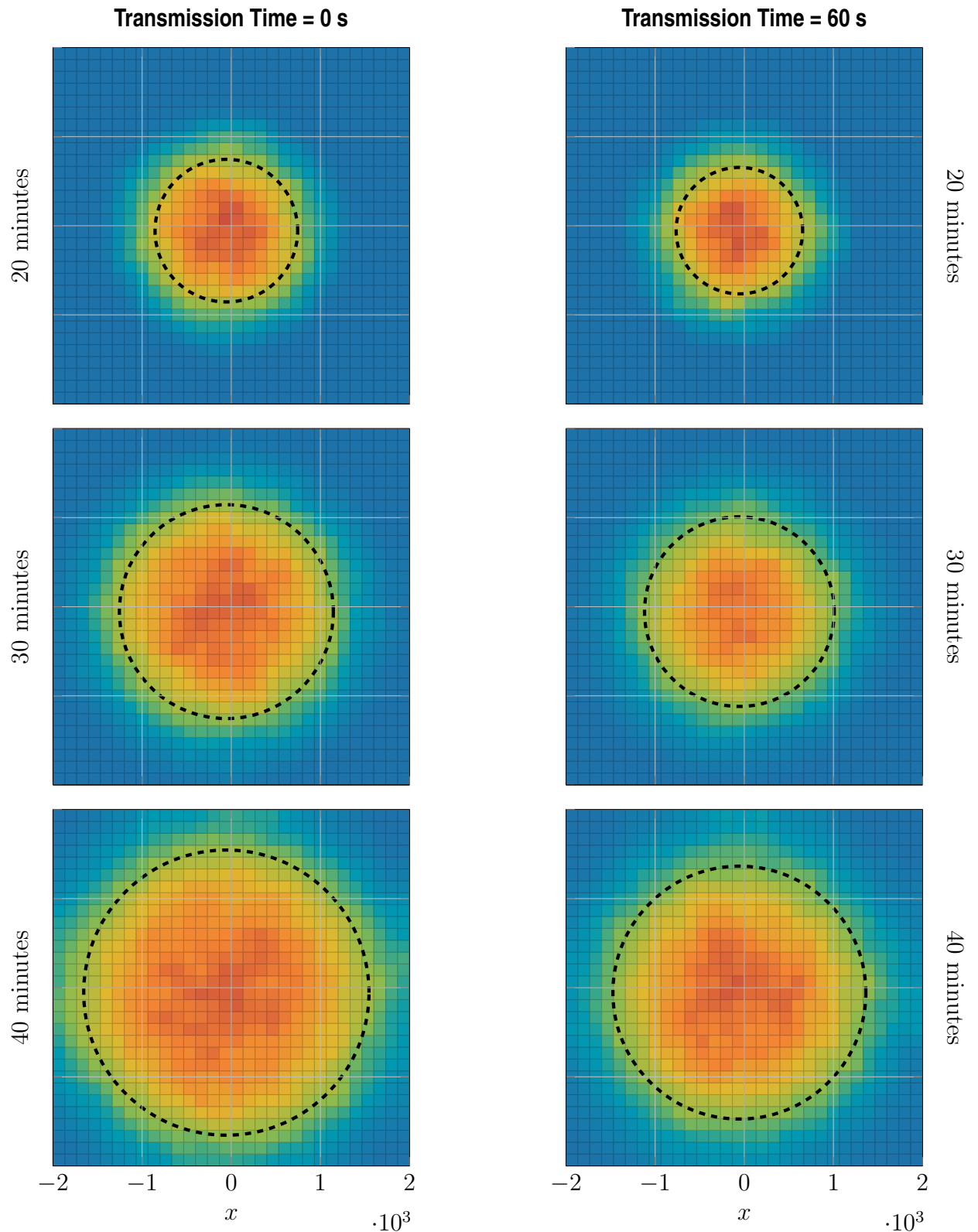
**Figure 5.14:** Plots to show the spread of a message in 2D continuous space. Time progresses down the rows of the plots. Each column is a separate experiment: the left-hand column is an exact replica from Klein *et al.* (2010) ($\tau = 0$). The right-hand column is identical except $\tau = 60$. The dashed circles are the theoretical model for message spread. It is clear that the message spreads slower when $\tau = 60$. Results generated from the average of 1000 simulations with parameters from Table 5.3.
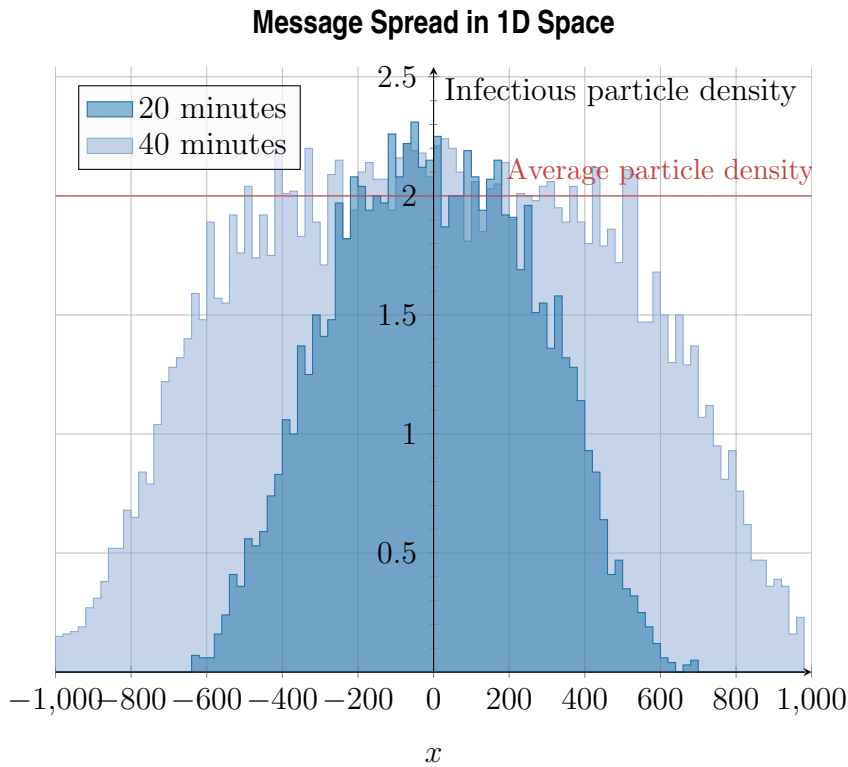
**Figure 5.15:** Plot to show message spread in 1D space. The average of 100 simulations is plotted. The Random Direction mobility model is used with Normal speed distribution and the following parameter values $r = 20$, $E(s) = 0.2$, $\tau = 20$, $\lambda = \frac{1}{60}$.

### 5.7.1 Trajectory Dataset

As many of the applications discussed in Section 1.2 relate to human movement, human trajectories shall be used for this study. Fortunately, several human trajectory datasets already exist and are available for use. Three of the most applicable datasets are described below:

**CRAWDAD Metadata: NCSU/Mobilitymodels (Rhee *et al.* 2009)**

> Gathered with hand-held GPS devices at five different locations, independently. The five locations include two university campuses, New York City, a theme park and a state fair. Each recorded trajectory is for a single person in a single day. The traces are presented as a list of X and Y coordinates at thirty second intervals. All coordinates are relative to a reference point and each trace starts at time = 0. The dataset is reasonably sparse, with fewer than 100 traces at any of the five locations.

**Infectious SocioPatterns Dynamic Contact Networks (Isella *et al.* 2011)**

> This dataset is gathered with RFID badges worn by visitors of a science gallery.

The dataset is presented as a list, stating who is in contact with whom at intervals of 20 seconds. Exact XY-coordinates are not available; however, it is possible to simulate an OPNET using only contact information. Unfortunately, the dataset only includes face-to-face contacts, rather than contacts within a certain proximity.

**Geolife Version 1.2 (Zheng *et al.* 2009, 2008, 2010)**

Gathered with hand-held GPS devices by 178 participants for over four years. This is the largest dataset with a total of 17,621 trajectories in and around the city of Beijing. The data are presented as a list of points (one for every 1–5 seconds), including longitude position, latitude position and absolute time.

The Geolife dataset is chosen for the study as it is the largest dataset and has the most information. Trajectories from a large region of the Geolife dataset can be seen in Fig. 5.16. In the figure, a geographic map is aligned adjacent to the trajectory plot to show the exact position of the relevant region in Beijing.
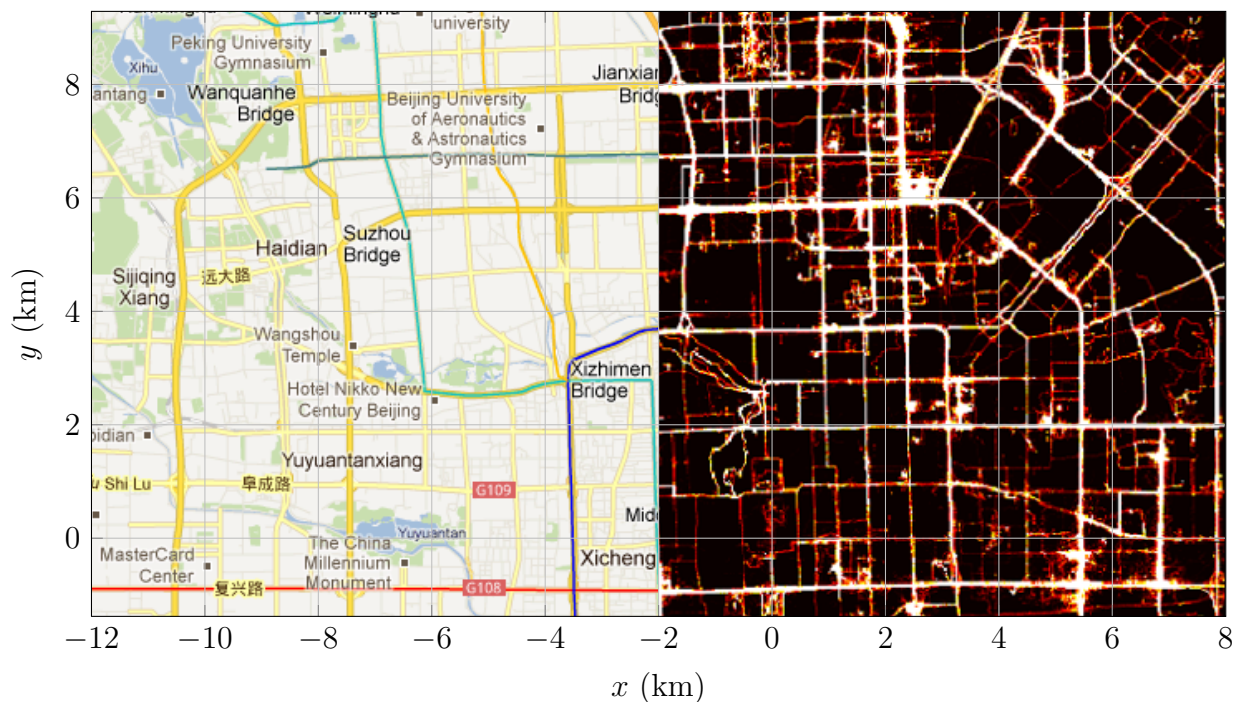


Figure 5.16: Figure to show trajectories from the Geolife dataset on a map of Beijing.

## 5.7.2 Overcoming Limitations

As a whole, the chosen dataset is large; however, it covers a vast area over a long period of time. The set of trajectories within any specific range of time and space

is actually too sparse to be useful in the simulations. It would not be an accurate representation of the number of people carrying mobile devices.

To overcome the problem of sparsity, the Geolife dataset is used as training data to create a statistically similar, synthetic mobility model. This is a novel technique and original contribution of this thesis, which has several benefits:

- it allows some control over the number of particles in the network, and
- it allows for Monte Carlo simulations (multiple trials).

### 5.7.3 Synthesising the Dataset

This section describes how the Geolife dataset is used as a training set to create a statistically similar, synthetic mobility model. Essentially, the Geolife trajectories are discretised to a grid and the rate of movement between each grid cell is matched by the synthetic mobility model. As far as the current author is aware, this is the first time this technique has been used, and is therefore an original contribution of this thesis. Below is a comprehensive algorithm:

1. Firstly, a densely populated 1km x 1km region is chosen from the dataset.
2. This region is divided into a uniformly distributed grid.
3. All Geolife data within the region are simulated on this grid and a log records the movement of particles between grid cells (including the time of day).
4. The entire log is flattened so that all movement happens on the same day. Only the time of day is important, not the date.
5. From the log, a cell transition rate matrix is created with three dimensions (current cell, destination cell, hour of day).
6. The rate at which particles move in/out of the region to/from each grid cell is also recorded.

A custom mobility model is created which uses this transition rate matrix to create statistically similar trajectories. The mobility model uses the same region and grid. Each particle selects a destination cell to move into (at random according to the matrix) and a specific, randomly chosen location within that cell. The particle then moves to its destination with a speed (chosen uniformly at random) that ensures an arrival within the next hour. On arrival, a new destination is chosen and the cycle is repeated.

A warm-up period is required to fill the region with synthetic particles as particles can only enter the region according to the transition rate matrix. Experimentation is used to decide on an appropriate warm-up duration to allow for the particle density to steady. The warm-up period is set to end at 9:00 am (simulation time), at which time the message is introduced to the network and the performance metrics begin to be recorded.



(a) Discretising Geolife trajectories      (b) Statistically similar, synthetic trajectory
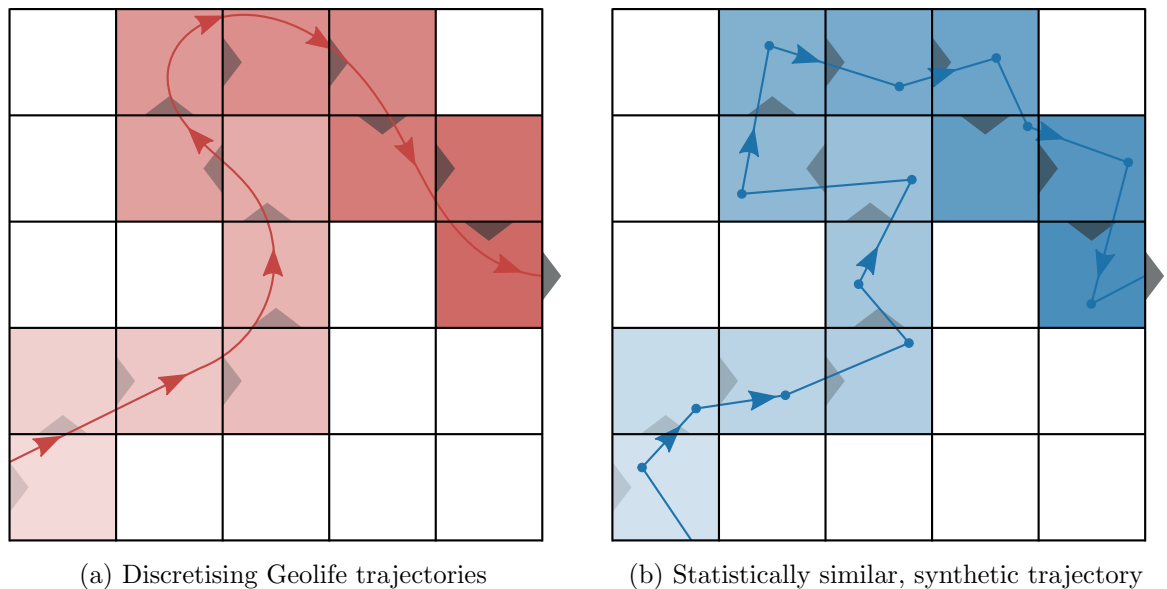
Figure 5.17: Diagrams to show how trajectories from the Geolife dataset are discretised to create grid cell transition rate data. Sub-figure (b) shows an example synthetic trajectory that uses the transition rate data from sub-figure (a).

Figure 5.17 shows an example of how a single Geolife trajectory is discretised into grid cells (left sub-figure). The right sub-figure shows an example synthetic trajectory that was generated using the transmission rate matrix from the left sub-figure. Note that exactly the same grid cells are passed through by both trajectories. This is because only one trajectory was used in the training data. A large set of training data yields a higher variance of the synthetic trajectories.

### 5.7.4 Geolife Data Preparation

The Geolife dataset contains the following fields (Zheng *et al.* 2009, 2008, 2010):

- Latitude in decimal degrees.
- Longitude in decimal degrees.
- Altitude in feet (-777 if not valid).
- Date—number of days (with fractional part) that have passed since 12/30/1899.

- Date as a string.

- Time as a string.

The following data must be extracted from the Geolife data in order to create the Synthetic Geolife mobility model:

- Time of day in seconds (regardless of date).

- X-coordinate in meters relative to a reference point in Beijing (greater value means further East).

- Y-coordinate in meters relative to a reference point in Beijing (greater value means further North).

Listing 5.1 shows the Bash/Awk script written by the current author which is used to extract the required data from the original Geolife dataset.

### 5.7.5 Speed and Velocity Distributions

In this section, speed and velocity distributions are compared for the Geolife real-world traces and the Synthetic Geolife mobility model developed in this chapter. This study will help to determine the similarity of the two models. Speed and velocity data are collected from the models by considering the distance moved (and the time taken) for all recorded adjacent positions of each particle. These data are grouped into appropriate bins for speed and velocity, and are presented as histograms. The histograms show the proportion of recorded speed and velocity values that are grouped within each bin.

Figure 5.18 shows the results of the speed and velocity study. The upper plots show the speed distributions of the Geolife traces (left-hand plot) and the Synthetic Geolife mobility model (right-hand plot). Although the shapes of the plots are similar, by looking at the scale of the x-axes it is clear that the distributions are dissimilar. The same outcome is seen in the velocity distributions, shown in the lower plots (with colour bars). Although there is a similar proportion of particles moving up, down, left and right, the scales used on the x and y-axes show that the results are dissimilar. Unfortunately, it is not possible to show the Geolife traces velocity distribution in more granularity due to low levels of detail in the dataset.

The study in this section has shown that speed and velocity distributions do not

Listing 5.1: Bash/Awk script to convert each line of each Geolife trajectory file to the following format: time of day in seconds, X-coordinate in meters from a reference point, Y-coordinate in meters from a reference point.

```bash
# Directory constants.
INPUT_DIR=`pwd`/OriginalData
OUTPUT_DIR=`pwd`/Data
cd $INPUT_DIR

# Loop through each file in every trajectory directory.
for dir in *; do
  cd $dir/Trajectory
  mkdir $OUTPUT_DIR/$dir

  for file in *; do
    for line in `tail -n +7 $file`; do # Use tail to skip headers.

      # EARTH_RADIUS, PI: Mathematical constants.
      # REF_LAT, REF_LON: Reference point in Beijing to be used as
         the origin for all coordinates.
      echo "$line" | awk -F, \
        -v EARTH_RADIUS=111000 -v PI=3.14159 \
        -v REF_LAT=39.913889   -v REF_LON=116.391667 '
      {
        # Print time of day in seconds.
        printf("%d ", ($5 - int($5)) * 86400);

        # Find longitudinal difference (within +-180 degrees).
        diff = $2 - REF_LON;
        if (diff > 180) diff -= 360;
        else if (diff < -180) diff += 360;

        # Convert lat/lon to x/y coordinates from origin in meters.
        printf("%d ", EARTH_RADIUS * diff * cos(PI*REF_LAT / 180));
        printf("%d\n", ($1 - REF_LAT) * EARTH_RADIUS);
      }' >> $OUTPUT_DIR/$dir/$file

    done
  done
  cd ../..
done
```
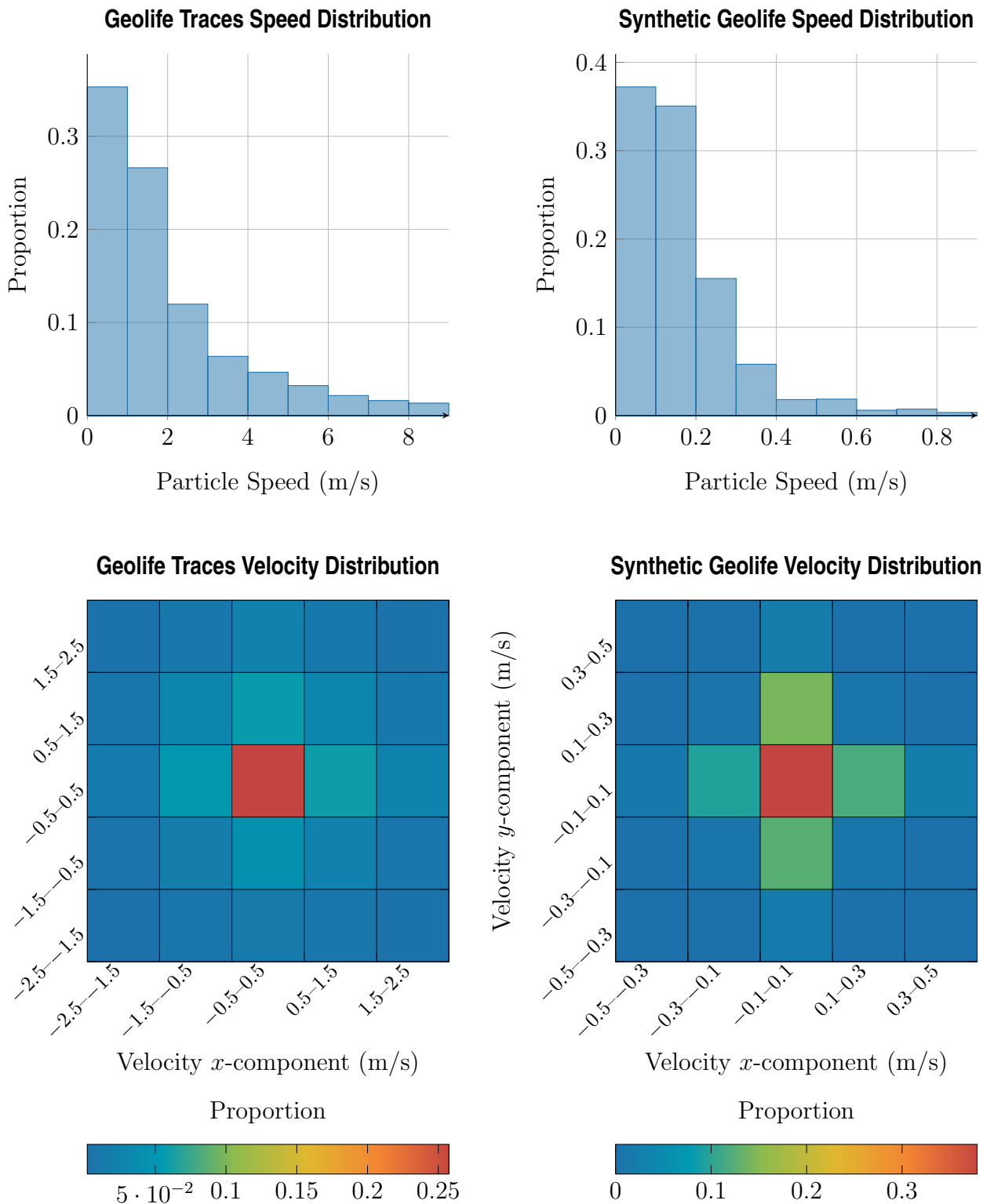
Figure 5.18: Plots to show speed distributions (upper plots) and velocity distributions (lower plots with colour bars) for the Geolife real-world traces (left-hand plots) and the Synthetic Geolife mobility model developed in this chapter (right-hand plots). Note the different scales used on the graph axes. It is clear that the distributions for the two models are dissimilar.

match for the Geolife traces and the Synthetic Geolife mobility model. This is an undesirable result as it shows that Synthetic Geolife does not model real-world movement as well as the current author had intended. The reason for this result is likely due to the difference in movement on the microscopic scale. Particles in the Synthetic Geolife model move directly between two locations with constant speed, once per hour. Conversely, the Geolife traces show much finer detail, with particles moving indirectly between destinations, with wiggly lines rather than straight lines. This explains why a higher average speed and velocity is observed in the Geolife traces, even though movement on the macroscopic scale may be similar to that of Synthetic Geolife.

### 5.7.6 Experimental Description

A methodical study is performed on the four fundamental parameters. Two mobility models will be compared: Synthetic Geolife, as described in this section and the 2D mobility model described in Section 5.1. It is not practical to study particle density $\rho$ or particle speed $s$ as these parameters are not configurable in the Synthetic Geolife mobility model; instead, they are set to match the real-word conditions. Therefore, only signal radius, $r$, and transmission time, $\tau$, will be studied.

Each parameter is studied individually, in much the same way as the individual parameter studies performed in Section 4.2. The parameter values used for the studies are shown in Table 5.4. These values have been chosen to match previously used values in Section 5.2.1 to allow comparison of results.

| Parameter | Default | Minimum | Maximum |
|---|---|---|---|
| $r$ (m) | 40 | 10 | 100 |
| $\tau$ (s) | 20 | 0 | 100 |

Table 5.4: Table of parameter values used in the individual parameter studies on real-life comparison.

All simulations use a region size of $1000 \times 1000$. For the Random Direction mobility model, $\rho = 2 \times 10^{-4}$ and $s = 2$.

As usual, a single message will be broadcast to all particles in the simulations. However, due to the nature of the Synthetic Geolife mobility model, the message will be introduced at a random position on the edge of the simulation region, as opposed

to the centre of the region. Because of this, the $T_{50}^D$ metric will not be recorded. Only $T_{50}^Q$ (time until 50% of particles receive the message) and $SP_{60}$ (probability that an information epidemic persists for at least one hour) will be recorded (using SI and SIS interaction schemes, respectively). For all SIS simulations, the deletion rate, $\delta = 0.0035$.

### 5.7.7 Experimental Results

The results of the studies on $r$ and $\tau$ are shown in Fig. 5.19. Looking at the results for $r$, it is clear that the behaviour is similar for both mobility models. For $T_{50}^Q$, a sharp drop is seen as $r$ increases, which levels off for larger values of $r$. For $SP_{60}$, a rise is seen as $r$ increases, giving the plots an S-shaped appearance. Looking at the results for $\tau$, similarities are seen again in the behaviour of the network for each mobility model. As $\tau$ increases, $T_{50}^Q$ steadily increases while $SP_{60}$ steadily decreases.

It is clear that the simulated networks behave similarly given Synthetic Geolife movement or Random Direction movement. This adds confidence that the OPNET simulation in this thesis, which use purely synthetic mobility models, adequately represent real-world behaviour.

## 5.8 Chapter Summary

In this chapter, the focus has been on OPNETs deployed in regions of continuous space. A lookup table of simulated results was created, that show how the behaviour of OPNETs scales with the fundamental parameters. This behaviour was further analysed with a study on the critical deletion rate. Following this, particle contact rate and contact duration were studied. Following this, it was shown how these models can be combined with a diffusion coefficient to model the spread of a message.

This is the final chapter in which an original contribution is provided. The next chapter concludes the thesis and discusses some of the future work that the current author would like to undertake.

## Parameter Study on Signal Radius
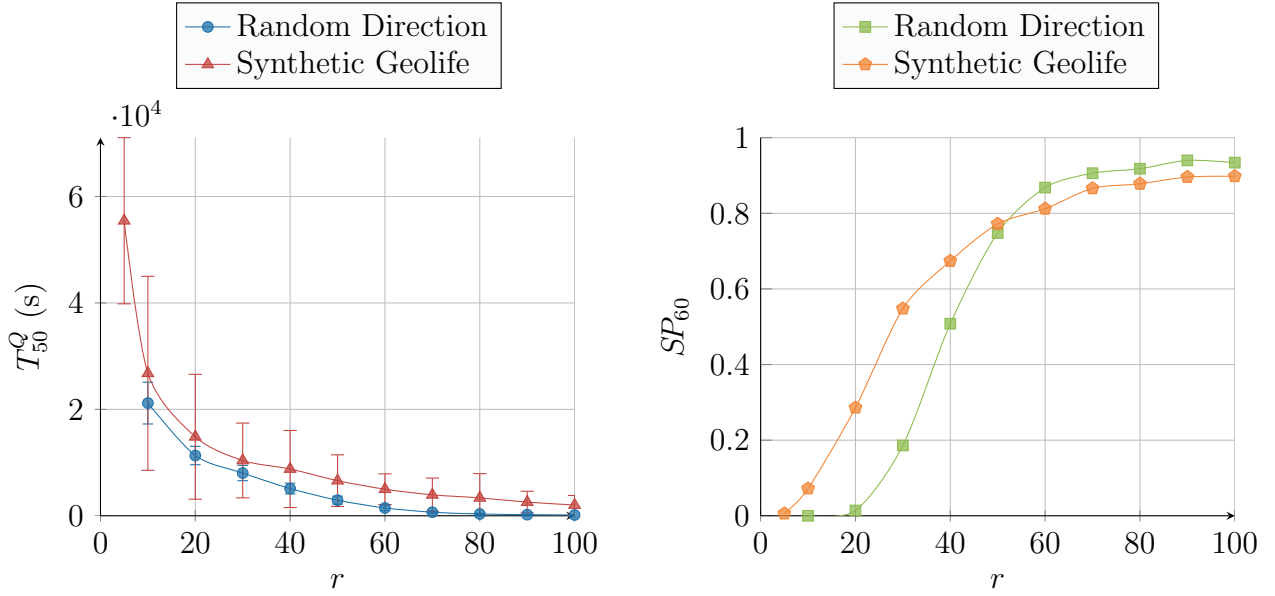


## Parameter Study on Transmission Time
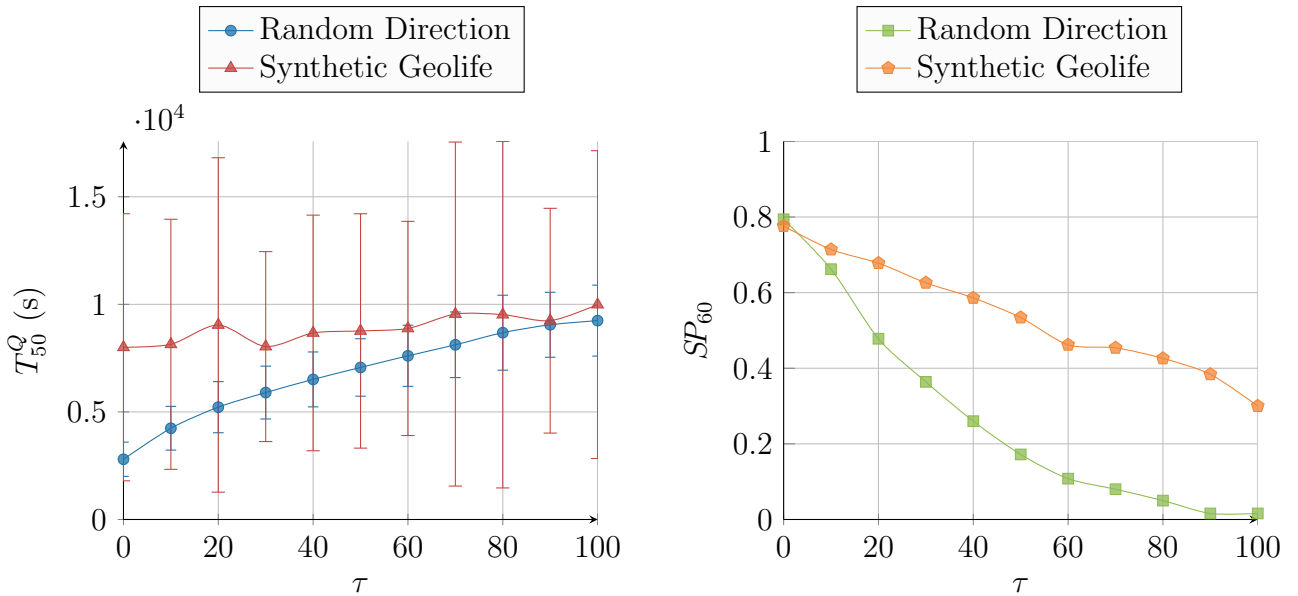


Figure 5.19: Parameter study on signal radius and transmission time using Geolife-based trajectories. Results are compared to those that use the Random Direction model. Results appear to be similar, regardless of mobility model. All results show the average of 200 simulations, with standard error error bars for $T_{50}^Q$. The term $\tau = 20$ for upper plot and $r = 40$ for lower plot.

# CHAPTER 6

# Conclusions

In this final chapter, the thesis is summarised and the key contributions are discussed. This thesis is assessed with regard to the initial proposal. Furthermore, this work is reflected upon with a critical evaluation. Finally, the direction of this research is assessed and areas of future work are suggested.

## 6.1  Summary of Thesis

This thesis proposes that information dissemination in an OPNET can be modelled in terms of the four fundamental parameters: the particle density ($\rho$), the wireless transmission range ($r$), the speed of the particles ($s$) and the message transmission time ($\tau$). It is also proposed that the behaviour of an OPNET could be optimised by selecting the values of these four parameters.

The area of research in this thesis was motivated by the fact that OPNETs are a young and potentially revolutionary technology with much to be learnt about their complex behaviour. By developing this understanding, it is hoped that the technology will become more appealing, more efficient and lower in cost.

It was found in the related literature that there is very little research in the area of OPNETs that take into account the time taken to transmit data between particles. It was found that this is an important factor, and furthering the understanding of this aspect of OPNET behaviour has been focused upon.

This thesis has focused on the theoretical modelling of OPNET message propagation through space and time. To make this complex idea easier to understand, the following types of spatial model have been progressed through:

- non-spatial (experiments where spatial aspects were not significant in the spread of the message),
- 1D discrete space,
- 2D continuous space.

Furthermore, the theoretical modelling of message propagation has been simplified by breaking the problem down into several smaller modules: message spread was modelled by defining it in terms of particle contact rate and contact duration distribution which, in turn, were modelled using the four fundamental parameters. As well as reducing complexity, this also has the benefit of making the developed theoretical models easier to generalise to other scenarios, such as a new mobility model, as the modules can easily be replaced with another theoretical or empirical model.

Throughout this thesis, the potential real-world applications for OPNETs have been kept in mind. This was done by choosing appropriate parameter values for the experiments. A study was also performed using the real-world movement traces from the Geolife dataset (Section 5.7). The work in this thesis has been kept fairly abstract to allow other areas of research and similar systems to benefit from findings in this thesis, such as the field of epidemiology.

## 6.2 Contributions

In this section, the key contributions of this thesis are discussed.

**Interaction Schemes:** The idea of SIR models were adopted from epidemiology and applied to OPNETs as interaction schemes (see Section 2.2). It was shown how certain parameters of the interaction schemes, such as the message deletion rate, can be adjusted to vary the concentration of the steady presence of a message in the network. This is useful for striking a balance between efficient message propagation and efficient use of resources. It was also shown how a logistic equation can be used to approximate the number of infectious devices in a network (see Section 2.2.3.1).

**Methodical Parameter Study:** In Section 4.2, a methodical study was performed on the five parameters that have the most significant impact on message propagation: particle density, particle speed, wireless signal radius, transmission time and message deletion rate. From these studies, valuable information was gained about how OPNETs behave and how their behaviour can be improved. It is shown that message propagation is less effective in 1D rather than 2D regions, in sparsely populated regions, for smaller wireless signal radii and for higher deletion rates. Furthermore, it is shown how particle speed and transmission time combine to affect network behaviour, and how they can be balanced appropriately for efficient message propagation (Section 5.2.3). Some interesting phenomena have also been discovered, such as the spread of a message in the opposite direction to the movement of particles (see Section 4.3).

**Parameter Study Lookup Table:** As part of the methodical parameter study, a large dataset of performance statistics was created, in the form of a lookup table (see Section 5.2). This table could be useful to an OPNET developer, or anybody that would like to deploy a message in an OPNET. It would be easy to create a user interface for the table, such as a smart phone app, which would make the information more accessible.

**Non-Spatial Theoretical Models:** Theoretical models of particle distribution (Section 3.1.1), particle contact rate (Section 3.2) and contact duration (Section 3.3) were created for graph-based transport networks. These models revealed that contact rate increases with particle speed and particle density, while contact duration decreases with particle speed. The transport networks were referred to as non-spatial as the spatial aspects did not impact the spread of a message by means of a susceptible/infectious boundary, as seen in 1D and 2D cases later in the thesis. This made it easier to create a theoretical model for message spread based on the developed contact rate and contact duration models. The theoretical model for message spread is developed in Section 3.4.

**Models for 1D Discrete Space:** Theoretical models of particle contact rate and contact duration were developed for 1D discrete space (Sections 4.4 and 4.6, respectively). Gambler's Ruin theory was adopted and extended for the developed contact duration

model. An empirical study was performed on message spread and it was discussed how the developed models of contact rate and contact duration could be used to model message spread (Section 4.7).

**Models for 2D Continuous Space:**   Theoretical models of particle contact rate and contact duration were created for 2D continuous space (Sections 5.4 and 5.5, respectively). It was discussed how these models could be used to model message spread theoretically using a reaction-diffusion equation (Section 5.6). It has been shown that the Random Direction mobility model is suitable for use with a reaction-diffusion equation as it has ballistic properties on the microscopic scale and diffusive properties on the macroscopic scale. The developed models were used to extend the work of Klein *et al.* (2010) to the case of non-instantaneous message transmissions.

**Real-World Study:**   In Section 5.7, a novel approach is used to create a synthetic mobility model based on real-world traces. Properties of the artificially generated traces are compared to the real-world traces and are shown to be statistically similar. The synthetic mobility model is then used for OPNET simulations. The behaviour of an OPNET is compared for the artificially generated trajectories and for the Random Direction mobility model. It is shown that an OPNET behaves similarly for both mobility models. This provides evidence to show that the findings in this thesis—where the Random Direction mobility model has been used—are applicable in real-world situations.

## 6.3   Critical Evaluation

Throughout this thesis, the focus has been on modelling message propagation with little more than the particle contact rate and contact duration distributions. However, in Chapter 4, a surprising result showed this methodology did not extend to 1D space. It was found that message spread in 1D space is dependent on the wireless signal radius ($r$), but neither the contact rate nor the contact duration were dependent on $r$. This was an unexpected result, which may hint that focusing exclusively on contact rate and contact duration may not be the best way to learn about message propagation.

It was never found where $r$ should appear in a theoretical model of message spread in 1D space. However, the current author speculates that the observed effects of $r$ are due to initial conditions of the model. A source device with a larger signal radius will be within range of more devices at the start of a simulation. These devices will become infectious soon after the simulation begins. This will have a knock-on effect on the rest of the simulation, as more devices are carrying and propagating the message, leading to accelerated message spread.

A more positive aspect of using contact rate and contact duration to model message spread is that they are modular. This means that any mobility model, or even movement traces can be "plugged in" to the message spread model. Theoretical models of contact rate/duration can be used or, if the movement is too complex, empirical measurements can be used instead. Therefore, this work can be easily extended to other particle movement models, which is useful as only the Random Direction model has been focused on in this thesis.

The work of Klein *et al.* (2010) has been a key inspiration for this thesis. Unfortunately, their value for the diffusion coefficient could not be reproduced, despite much research into diffusion theory. As a consequence, this thesis has been restricted to using their experimental parameters when evaluating the theoretical models against their results.

An OPNET engineer could learn a lot from this thesis about what can be achieved with OPNETs and the best approach to use. For example, smaller messages spread more effectively than larger messages. The lookup table from Section 5.2 can be used to find the optimal balance of parameter values for a message in an OPNET. Furthermore, the developed theoretical models can be used to provide accurate performance estimates, which can provide evidence to show whether a new project will be feasible.

## 6.4   Future Work

Based on the direction of research in this thesis and the critical evaluation, potential future work is discussed.

**Investigate 1D Message Spread Theory:**   As discussed in Chapter 4, message spread in 1D space is more difficult to model theoretically than expected. This was due to the dependency on signal radius, which was not accounted for in the contact rate model. This complication must be further investigated before a theoretical model for message spread in 1D space can be created.

**Investigate 2D Message Spread Theory:**   As previously discussed, the 2D message spread theoretical model could not be completed as the effective diffusion coefficient used by Klein *et al.* (2010) could not be derived. Further efforts should be made to understand the approach of Klein *et al.*, combined with further research into elementary diffusion theory (Einstein 1905).

**Real-World Experiments:**   The message spread models developed in this thesis are intended for use in real-world situations. Indeed, all of the theoretical models for message spread are designed to work with any type of particle movement. The focus has been on the Random Direction mobility model in this thesis and the testing of other movement models is left to future work. It would be particularly interesting to test the accuracy of the developed message spread models for human movement in a real-world situation. By doing this, the research in this thesis would become far more valuable to the development of OPNET technology.

**Message Frames:**   This thesis has shown how large messages propagate more slowly than small messages. This is due to an increased likelihood of communicating particles moving out of range before the transmission completes. When this happens, the data transmission is wasted as the partially received message is deleted. A key focus of this thesis is on larger messages that take longer to transmit, therefore, it is desirable to increase the efficiency of propagation for such messages. One way that large messages could be propagated more effectively is to divide them into a sequence of smaller frames. The frames could each be transmitted individually while the sender and receiver remain in contact. Should contact be lost, the partially received message is not wasted as transmission can continue when the receiver moves within range of the sender again, or with another particle that holds a copy of the same message. An interesting area to study would be the optimal size for message frames. If frames are too large then more data are lost when a connection is broken.

However, if frames are too small, the overhead of each transmission may decrease the speed of propagation.

## 6.5   Conclusion

This thesis has made much progress in the field of modelling and optimising OPNET behaviour. Although all of the questions posed at the outset of this research project could not be fully answered, a solid base has been created on which to build upon. The current author feels privileged to have contributed to this emerging technology at this early stage of its development. Lastly, the current author hopes to have demonstrated that OPNET technology is an exciting area of research, and he looks forward to being part of its development in the future.

# Table of Abbreviations

# Bibliography

Abramowitz, M. and Stegun, I. A. 1964. *Handbook of Mathematical Functions: With Formulas, Graphs, and Mathematical Tables*. Courier Dover Publications. Available at: `http://books.google.com/books?id=MtU8uP7XMvoC&pgis=1`.

Akyildiz, I. and Wang, X. 2005. A survey on wireless mesh networks. *Communications Magazine, IEEE* (September), pp. 23–30. Available at: `http://ieeexplore.ieee.org/xpls/abs_all.jsp?arnumber=1509968`.

Arndt, J. 1967. Role of product-related conversations in the diffusion of a new product. *Journal of marketing Research* 4(3), pp. 291–295. Available at: `http://www.jstor.org/stable/3149462`.

Atkinson, R. P. D., Rhodes, C. J., Macdonald, D. W. and Anderson, R. M. 2002. Scale-free dynamics in the movement patterns of jackals. *Oikos* 98(1), pp. 134–140. Available at: `http://www.blackwell-synergy.com/links/doi/10.1034/j.1600-0706.2002.980114.x`.

Austin, D., Keshet, L. and Sjerve, D. 1998. *The Logistic Equation and Integration by Partial Fractions*, [Online]. Available at: `http://www.ugrad.math.ubc.ca/coursedoc/math101/notes/moreApps/logistic.html`.

Baccelli, E., Jacquet, P., Mans, B. and Rodolakis, G. 2011. Information propagation speed in bidirectional vehicular delay tolerant networks. In: *2011 Proceedings IEEE INFOCOM*. IEEE, 6, pp. 436–440, Available at: `http://ieeexplore.ieee.org/lpdocs/epic03/wrapper.htm?arnumber=5935199`.

Bartumeus, F., Peters, F., Pueyo, S., Marrasé, C. and Catalan, J. 2003. Helical Lévy walks: adjusting searching statistics to resource availability in microzooplankton. *Proceedings of the National Academy of Sciences of the United States of America*

100(22), pp. 12771–5. Available at: `http://www.pnas.org/content/100/22/12771.short`.

Bass, F. M. 1969. A New Product Growth for Model Consumer Durables. *Management Science1* 15(5), pp. 215–227.

Basu, P. and Chau, C.-K. 2008. Opportunistic forwarding in wireless networks with duty cycling. In: *Proceedings of the third ACM workshop on Challenged networks - CHANTS '08*. New York, New York, USA: ACM Press, p. 19, Available at: `http://portal.acm.org/citation.cfm?doid=1409985.1409991`.

Becchetti, L., Clementi, A., Pasquale, F., Resta, G., Santi, P. and Silvestri, R. 2011. Information Spreading in Opportunistic Networks is Fast. Tech. rep., CERN, Available at: `http://arxiv.org/abs/1107.5241`.

Bertsekas, D. P. and Tsitsiklis, J. N. 2002. *Introduction to probability*. Cambridge, Massachusetts: Massachusetts Institute of Technology. Available at: `http://books.google.com/books?id=bcHaAAAAMAAJ&pgis=1`.

Bettstetter, C. 2001. Mobility modeling in wireless networks: categorization, smooth movement, and border effects. *ACM SIGMOBILE Mobile Computing and Communications Review* 5(3), pp. 55–66. Available at: `http://portal.acm.org/citation.cfm?id=584056`.

Blower, S. and Go, M.-H. 2011. The importance of including dynamic social networks when modeling epidemics of airborne infections: does increasing complexity increase accuracy? *BMC medicine* 9(1), p. 88. Available at: `http://www.biomedcentral.com/1741-7015/9/88`.

Boldrini, C., Conti, M. and Passarella, A. 2008. User-Centric Mobility Models for Opportunistic Networking. *Bio-Inspired Computing and Communication* 5151, pp. 255–267. Available at: `http://www.springerlink.com/index/yrgt130235860563.pdf`.

Boyer, D., Miramontes, O., Ramos-Fernández, G., Mateos, J. L. and Cocho, G. 2003. Modeling the Searching Behavior of Social Monkeys. *Physica A: Statistical Mechanics and its Applications* 342(1-2), p. 7. Available at: `http://www.sciencedirect.com/science/article/pii/S0378437104004960`.

Bratley, P., Fox, B. and Schrage, L. 1987. *A Guide to Simulation.* Springer, 1987. Available at: `http://books.google.com/books?hl=en&amp;lr=` `&amp;id=aHf4bPtGeyMC&amp;oi=fnd&amp;pg=PR19&amp;dq=A+guide+to+` `simulation&amp;ots=Twq_dpQhT6&amp;sig=2ylfFpCxREQsNXL6KHyK73zQg-k`.

Brauer, F., den Driessche, P. V. and Wu, J. 2008. *Mathematical Epidemiology,* vol. 1945 of *Lecture Notes in Mathematics.* Berlin, Heidelberg: Springer Berlin Heidelberg. Available at: `http://www.springerlink.com/index/10.1007/` `978-3-540-78911-6`.

Brockmann, D., Hufnagel, L. and Geisel, T. 2006. The scaling laws of human travel. *Nature* 439(7075), pp. 462–5. Available at: `http://www.ncbi.nlm.nih.` `gov/pubmed/16437114`.

Buscarino, A., Fortuna, L., Frasca, M. and Latora, V. 2008. Disease spreading in populations of moving agents. *EPL (Europhysics Letters)* 82(3), p. 38002. Available at: `http://stacks.iop.org/0295-5075/82/i=3/a=38002?key=crossref.` `8d21895228e599389a4806865e671ce5`.

Buttyan, L. and Hubaux, J.-P. 2000. Enforcing service availability in mobile ad-hoc WANs. In: *2000 First Annual Workshop on Mobile and Ad Hoc Networking and Computing. MobiHOC (Cat. No.00EX444).* IEEE, pp. 87–96, Available at: `http:` `//ieeexplore.ieee.org/lpdocs/epic03/wrapper.htm?arnumber=869216`.

Buttyán, L. and Hubaux, J.-P. 2003. Stimulating Cooperation in Self-Organizing Mobile Ad Hoc Networks. *Mobile Networks and Applications (MONET)* 8(5), pp. 579–592. Available at: `http://portal.acm.org/citation.cfm?id=942421`.

Camp, T., Boleng, J. and Davies, V. 2002. A survey of mobility models for ad hoc network research. *Wireless Communications and Mobile Computing* 2(5), pp. 483–502. Available at: `http://citeseerx.ist.psu.edu/viewdoc/download?doi=` `10.1.1.13.268&amp;rep=rep1&amp;type=pdf`.

Divecha, B., Abraham, A., Grosan, C. and Sanyal, S. 2007. Impact of node mobility on MANET routing protocols models. *Journal of Digital Information Management* 5(1), p. 19. Available at: `http://www.freepatentsonline.com/article/` `Journal-Digital-Information-Management/186470767.html`.

Eagle, N. and Pentland, A. S. 2005. Reality mining: sensing complex social systems. *Personal and Ubiquitous Computing* 10(4), pp. 255–268. Available at: `http://www.springerlink.com/index/10.1007/s00779-005-0046-3`.

Einstein, A. 1905. Über die von der molekularkinetischen Theorie der Wärme geforderte Bewegung von in ruhenden Flüssigkeiten suspendierten Teilchen. *Annalen der Physik* 322(8), pp. 549–560. Available at: `http://doi.wiley.com/10.1002/andp.19053220806`.

ElBatt, T. A., Krishnamurthy, S. V., Connors, D. and Dao, S. 2000. Power management for throughput enhancement in wireless ad-hoc networks. *Communications, 2000. ICC 2000. 2000 IEEE International Conference* 3, pp. 1506–1513. Available at: `http://ieeexplore.ieee.org/lpdocs/epic03/wrapper.htm?arnumber=853748`.

Feller, W. 1957. *An Introduction to Probability Theory and Its Applications, Volume I.* University of Michigan: Wiley. Available at: `http://scholar.google.com/scholar?hl=en&btnG=Search&q=intitle:An+Introduction+to+Probability+Theory+and+Its+Applications,+Volume+1#0`.

Fisher, R. A. 1937. The Wave of Advance of Advantageous Genes. *Annals of Eugenics* 7(4), pp. 355–369. Available at: `http://digital.library.adelaide.edu.au/dspace/bitstream/2440/15125/1/152.pdf`.

Frasca, M., Buscarino, A., Rizzo, A., Fortuna, L. and Boccaletti, S. 2006. Dynamical network model of infective mobile agents. *Physical Review E* 74(3), p. 036110. Available at: `http://link.aps.org/doi/10.1103/PhysRevE.74.036110`.

Gardner-Stephen, P. 2011. The Serval Project: Practical Wireless Ad-Hoc Mobile Telecommunications. Tech. Rep. June, servalproject.org, Available at: `http://developer.servalproject.org/files/CWN_Chapter_Serval.pdf`.

Gardner-Stephen, P. and Challans, R. 2012. *Serval Project*, [Online]. Available at: `http://www.servalproject.org/`.

Golmie, N. and Mouveaux, F. 2001. Interference in the 2.4 GHz ISM band: Impact on the Bluetooth access control performance. *Communications, 2001. ICC 2001* Available at: `http://ieeexplore.ieee.org/xpls/abs_all.jsp?arnumber=936608`.

Gonzalez, M., Hidalgo, C. and Barabasi, A. 2008. Understanding individual human mobility patterns. *Nature* 453(7196), pp. 779–82. Available at: `http://www.ncbi.nlm.nih.gov/pubmed/18528393`.

Groenevelt, R., Nain, P. and Koole, G. 2005. The message delay in mobile ad hoc networks. *Performance Evaluation* 62(1-4), pp. 210–228. Available at: `http://linkinghub.elsevier.com/retrieve/pii/S0166531605000970`.

Guo, S., Gu, Y., Jiang, B. and He, T. 2009. Opportunistic flooding in low-duty-cycle wireless sensor networks with unreliable links. In: *Proceedings of the 15th annual international conference on Mobile computing and networking.* ACM, pp. 133–144, Available at: `http://portal.acm.org/citation.cfm?id=1614336`.

Gustafson, J. L. 2012. *Little's Law*, [Online]. Available at: `http://www.springerreference.com/docs/html/chapterdbid/311359.html`.

Heinemann, A. 2007. *Collaboration in opportunistic networks*. Ph.D. thesis, Available at: `http://tuprints.ulb.tu-darmstadt.de/id/eprint/834`.

Heinemann, A., Kangasharju, J. and Muehlhaeuser, M. 2008. Opportunistic Data Dissemination Using Real-World User Mobility Traces. In: *22nd International Conference on Advanced Information Networking and Applications - Workshops (aina workshops 2008)*. IEEE, pp. 1715–1720, Available at: `http://ieeexplore.ieee.org/xpls/abs_all.jsp?arnumber=4483168`.

Heyman, D. P. and Sobel, M. J. 2003. *Stochastic Models in Operations Research: Stochastic Processes and Operating Characteristics*. Courier Dover Publications. Available at: `http://books.google.com/books?id=IcVlwPSOqCwC&pgis=1`.

Hildebrand, A. J. 2009. Asymptotic Analysis Lecture Notes , Math 595 , Fall 2009. Tech. rep.

Hsu, W.-j., Spyropoulos, T., Psounis, K. and Helmy, A. 2007. Modeling Time-Variant User Mobility in Wireless Mobile Networks. In: *IEEE INFOCOM 2007 - 26th IEEE International Conference on Computer Communications*. IEEE, pp. 758–766, Available at: `http://ieeexplore.ieee.org/lpdocs/epic03/wrapper.htm?arnumber=4215676`.

Hubaux, J.-P., Buttyán, L. and Capkun, S. 2001. The quest for security in mobile ad hoc networks. In: *Proceedings of the 2nd ACM international symposium on Mobile ad hoc networking & computing - MobiHoc '01*. New York, New York, USA: ACM Press, p. 146, Available at: `http://portal.acm.org/citation.cfm?id=501437>`.

Isella, L., Stehlé, J., Barrat, A., Cattuto, C., Pinton, J.-F. and den Broeck, W. V. 2011. What's in a crowd? Analysis of face-to-face behavioral networks. *Journal of Theoretical Biology* 271(1), pp. 166–180. Available at: `http://www.sciencedirect.com/science/article/B6WMD-51M60KS-2/2/cb31bee32b340b3044c724b88779a60e`.

Jacquet, P., Mans, B. and Rodolakis, G. 2007. Information Propagation Speed in Mobile and Delay Tolerant Networks. *IEEE Transactions on Information Theory* 56(10), pp. 5001–5015. Available at: `http://ieeexplore.ieee.org/lpdocs/epic03/wrapper.htm?arnumber=5571893`.

Jacquet, P., Mans, B. and Rodolakis, G. 2008. Information propagation speed in Delay Tolerant Networks: Analytic upper bounds. In: *2008 IEEE International Symposium on Information Theory*. IEEE, pp. 6–10, Available at: `http://ieeexplore.ieee.org/lpdocs/epic03/wrapper.htm?arnumber=4594937`.

Jacquet, P., Mans, B. and Rodolakis, G. 2009a. Broadcast delay of epidemic routing in intermittently connected networks. In: *2009 IEEE International Symposium on Information Theory*. IEEE, pp. 839–843, Available at: `http://ieeexplore.ieee.org/lpdocs/epic03/wrapper.htm?arnumber=5205611`.

Jacquet, P., Mans, B. and Rodolakis, G. 2009b. Information Propagation Speed in Mobile and Delay Tolerant Networks. In: *IEEE INFOCOM 2009 - The 28th Conference on Computer Communications*. IEEE, pp. 244–252, Available at: `http://ieeexplore.ieee.org/lpdocs/epic03/wrapper.htm?arnumber=5061927`.

Jacquet, P., Mans, B. and Rodolakis, G. 2010. On Space-Time Capacity Limits in Mobile and Delay Tolerant Networks. In: *2010 Proceedings IEEE INFOCOM*. IEEE, Theorem 1, pp. 1–9, Available at: `http://ieeexplore.ieee.org/lpdocs/epic03/wrapper.htm?arnumber=5462164`.

Janssen, C. 2014. *What is a Markov Chain? - Definition from Techopedia*, [Online]. Available at: `http://www.techopedia.com/definition/8249/markov-chain`.

Jardosh, A., Belding-Royer, E. M., Almeroth, K. C. and Suri, S. 2003. Towards realistic mobility models for mobile ad hoc networks. In: *Proceedings of the 9th annual international conference on Mobile computing and networking - MobiCom '03*. New York, New York, USA: ACM Press, p. 217, Available at: `http://portal.acm.org/citation.cfm?id=939008`.

Johnston, L. 1940. The Fibonacci sequence and allied trigonometric identities. *The American Mathematical Monthly* 47(2), pp. 85–89. Available at: `http://www.jstor.org/stable/10.2307/2303358`.

Kamal, A. and Al-Karaki, J. 2007. A new realistic mobility model for mobile ad hoc networks. In: *Proceedings of the IEEE International Conference on Communications (ICC 07)*. Citeseer, p. 33703375, Available at: `http://scholar.google.com/scholar?hl=en&btnG=Search&q=intitle:A+New+Realistic+Mobility+Model+for+Mobile+Ad+Hoc+Networks#0`.

Kermack, W. O. and McKendrick, a. G. 1927. A Contribution to the Mathematical Theory of Epidemics. *Proceedings of the Royal Society A: Mathematical, Physical and Engineering Sciences* 115(772), pp. 700–721. Available at: `http://rspa.royalsocietypublishing.org/cgi/doi/10.1098/rspa.1927.0118`.

Khelil, A., Becker, C., Tian, J. and Rothermel, K. 2002. An epidemic model for information diffusion in MANETs. In: *Proceedings of the 5th ACM international workshop on Modeling analysis and simulation of wireless and mobile systems - MSWiM '02*. New York, New York, USA: ACM Press, p. 54, Available at: `http://portal.acm.org/citation.cfm?doid=570758.570768`.

Kim, M., Kotz, D. and Kim, S. 2006. Extracting a Mobility Model from Real User Traces. In: *Proceedings IEEE INFOCOM 2006. 25TH IEEE International Conference on Computer Communications*. IEEE, pp. 1–13, Available at: `http://ieeexplore.ieee.org/lpdocs/epic03/wrapper.htm?arnumber=4146826`.

Kim, S., Lee, C.-H. and Eun, D. Y. 2010. Superdiffusive Behavior of Mobile Nodes and Its Impact on Routing Protocol Performance. *IEEE Transactions on Mobile*

*Computing* 9(2), pp. 288–304. Available at: `http://ieeexplore.ieee.org/lpdocs/epic03/wrapper.htm?arnumber=5161265`.

Klein, D. J., Hespanha, J. and Madhow, U. 2010. A Reaction-Diffusion Model for Epidemic Routing in Sparsely Connected MANETs. In: *2010 Proceedings IEEE INFOCOM*. IEEE, pp. 1–9, Available at: `http://ieeexplore.ieee.org/lpdocs/epic03/wrapper.htm?arnumber=5462133`.

Kolmogorov, A., Petrovsky, I. and Piscounoff, N. 1937. Etude de l'équation de la diffusion avec croissance de la quantité de matière et son application à un problème biologique. Tech. rep., Bull. Univ, Etat. Moscou Ser. Int. A.

Kotz, D., Henderson, T. and Abyzov, I. 2004. *CRAWDAD data set dartmouth/campus (v. 2004-12-18)*, [Online]. Downloaded from http://crawdad.org/dartmouth/campus.

La, R. J. 2010. Distributional Convergence of Intermeeting Times under the Generalized Hybrid Random Walk Mobility Model. *IEEE Transactions on Mobile Computing* 9(9), pp. 1201–1211. Available at: `http://ieeexplore.ieee.org/xpls/abs_all.jsp?arnumber=5453379`.

Lee, K., Hong, S., Kim, S. J., Rhee, I. and Chong, S. 2009. SLAW: A New Mobility Model for Human Walks. In: *IEEE INFOCOM 2009 - The 28th Conference on Computer Communications*. IEEE, pp. 855–863, Available at: `http://ieeexplore.ieee.org/lpdocs/epic03/wrapper.htm?arnumber=5061995`.

Lengyel, T. 2009. The conditional gamblers ruin problem with ties allowed. *Applied Mathematics Letters* 22(3), pp. 351–355. Available at: `http://linkinghub.elsevier.com/retrieve/pii/S0893965908001572`.

Li, Q., Zhu, S. and Cao, G. 2010. Routing in Socially Selfish Delay Tolerant Networks. In: *2010 Proceedings IEEE INFOCOM*. IEEE, pp. 1–9, Available at: `http://ieeexplore.ieee.org/xpls/abs_all.jsp?arnumber=5462138`.

LLC. 2012. *Grindr*, [Online]. Available at: `http://grindr.com/`.

Misra, S., Woungang, I. and Misra, S. C. 2009. *Guide to Wireless Ad Hoc Networks*. London: Springer. Available at: `http://www.springer.com/computer/communication+networks/book/978-1-84800-327-9`.

Moussaïd, M., Perozo, N., Garnier, S., Helbing, D. and Theraulaz, G. 2010. The walking behaviour of pedestrian social groups and its impact on crowd dynamics. *PloS one* 5(4), p. e10047. Available at: `http://www.pubmedcentral.nih.gov/articlerender.fcgi?artid=2850937&tool=pmcentrez&rendertype=abstract`.

Musolesi, M. and Mascolo, C. 2007. Designing mobility models based on social network theory. *ACM SIGMOBILE Mobile Computing and Communications Review* 11(3), p. 59. Available at: `http://portal.acm.org/citation.cfm?id=1317433`.

Navidi, W., Camp, T. and Bauer, N. 2004. Improving the accuracy of random waypoint simulations through steady-state initialization. In: *Compute.* Citeseer, June, pp. 319–326.

Nelson, K. E. and Williams, C. M. 2007. *Infectious Disease Epidemiology: Theory and Practice.* Jones & Bartlett Learning, illustrate ed. Available at: `http://books.google.com/books?id=o_j-G4zJ4cQC&pgis=1`.

Nelson, S. C., Bakht, M. and Kravets, R. 2009. Encounter-Based Routing in DTNs. In: *IEEE INFOCOM 2009 - The 28th Conference on Computer Communications.* IEEE, pp. 846–854, Available at: `http://ieeexplore.ieee.org/lpdocs/epic03/wrapper.htm?arnumber=5061994`.

Nordström, E., Gunningberg, P. and Rohner, C. 2012. Haggle: Relevance-aware content sharing for mobile, devices using search. *URL http://haggle. googlecode. com* Available at: `http://user.it.uu.se/~erikn/papers/haggle-arch.pdf`.

Panisson, A., Barrat, A., Cattuto, C., Van den Broeck, W., Ruffo, G. and Schifanella, R. 2012. On the dynamics of human proximity for data diffusion in ad-hoc networks. *Ad Hoc Networks* 10(8), pp. 1532–1543. Available at: `http://linkinghub.elsevier.com/retrieve/pii/S1570870511001272`.

Pelusi, L., Passarella, A. and Conti, M. 2006. Opportunistic networking: data forwarding in disconnected mobile ad hoc networks. *IEEE Communications Magazine* 44(11), pp. 134–141. Available at: `http://ieeexplore.ieee.org/lpdocs/epic03/wrapper.htm?arnumber=4014485`.

Pietiläinen, A.-K. and Diot, C. 2009. Experimenting with Opportunistic Networking. In: *Proc. of the ACM MobiArch Workshop*. Available at: `http://thlab.net/~apietila/pubs/mobiarch09pietilainen.pdf`.

Princeton University. 2003. *The ZebraNet Wildlife Tracker*, [Online]. Available at: `http://www.princeton.edu/~mrm/zebranet.html`.

Rhee, I., Shin, M., Hong, S., Lee, K., Kim, S. and Chong, S. 2009. {*CRAWDAD*} *data set ncsu/mobilitymodels (v. 2009-07-23)*, [Online]. Downloaded from http://crawdad.cs.dartmouth.edu/ncsu/mobilitymodels.

Rhee, I., Shin, M., Hong, S., Lee, K., Kim, S. J. and Chong, S. 2011. On the Levy-Walk Nature of Human Mobility. *IEEE/ACM Transactions on Networking* 19(3), pp. 630–643. Available at: `http://ieeexplore.ieee.org/lpdocs/epic03/wrapper.htm?arnumber=5750071`.

Saad, M. and Zukarnain, Z. 2009. Performance Analysis of Random-Based Mobility Models in MANET Routing Protocol. *European Journal of Scientific Research* 32(4), pp. 444–454. Available at: `http://www.eurojournals.com/ejsr_32_4_01.pdf`.

Scellato, S., Mascolo, C., Musolesi, M. and Latora, V. 2007. Epcast: Controlled Dissemination in Human-based Wireless Networks by means of Epidemic Spreading Models. *Arxiv preprint arXiv:0711.2780* Available at: `http://arxiv.org/abs/0711.2780`.

Second Life. 2011. *Second Life*, [Online]. Available at: `http://www.secondlife.com`.

Siegrist, K. 2014. *The Rayleigh Distribution*, [Online]. Available at: `http://www.math.uah.edu/stat/special/Rayleigh.html`.

SocioPatterns. 2011. *SocioPatterns*, [Online]. Available at: `http://www.sociopatterns.org/`.

Song, C., Qu, Z., Blumm, N. and Barabási, A.-L. 2010. Limits of predictability in human mobility. *Science (New York, N.Y.)* 327(5968), pp. 1018–21. Available at: `http://www.ncbi.nlm.nih.gov/pubmed/20167789`.

Stehlé, J., Voirin, N., Barrat, A., Cattuto, C., Colizza, V., Isella, L., Régis, C., Pinton, J.-F., Khanafer, N., Van den Broeck, W. and Vanhems, P.

2011. Simulation of an SEIR infectious disease model on the dynamic contact network of conference attendees. *BMC medicine* 9(1), p. 87. Available at: `http://www.pubmedcentral.nih.gov/articlerender.fcgi?artid=3162551&tool=pmcentrez&rendertype=abstract`.

Tuduce, C. and Gross, T. 2005. A mobility model based on WLAN traces and its validation. In: *Proceedings IEEE 24th Annual Joint Conference of the IEEE Computer and Communications Societies.* IEEE, pp. 664–674, Available at: `http://ieeexplore.ieee.org/lpdocs/epic03/wrapper.htm?arnumber=1497932`.

Vahdat, A. and Becker, D. 2000. Epidemic routing for partially connected ad hoc networks. Tech. rep., Citeseer, Available at: `http://citeseerx.ist.psu.edu/viewdoc/download?doi=10.1.1.34.6151&rep=rep1&type=pdf`.

Viswanathan, G. M., Afanasyev, V., Buldyrev, S. V., Murphy, E. J., Prince, P. A. and Stanley, H. E. 1996. Lévy flight search patterns of wandering albatrosses. *Nature* 381(6581), pp. 413–415. Available at: `http://www.nature.com/doifinder/10.1038/381413a0`.

Vodafone Group. 2014. *Base stations*, [Online]. Available at: `http://www.vodafone.com/content/index/about/sustainability/mpmh/how_mobiles_work/base_stations.html`.

Warthman, F. 2003. Delay Tolerant Networks (DTN): A Tutorial. Tech. Rep. March, warthman.com, Available at: `http://prius.ist.osaka-u.ac.jp/en/pdf/20080528-PRIUSlecture-Chai.pdf`.

Weisstein, E. W. 2010. *Random Walk–1-Dimensional*, [Online]. Available at: `http://mathworld.wolfram.com/RandomWalk1-Dimensional.html`.

Weisstein, E. W. 2014a. *Gamma Function – from Wolfram MathWorld*, [Online]. Available at: `http://mathworld.wolfram.com/GammaFunction.html`.

Weisstein, E. W. 2014b. *Generating Function*, [Online]. Available at: `http://mathworld.wolfram.com/GeneratingFunction.html`.

Weisstein, E. W. 2014c. *Vieta's Formulas*, [Online]. Available at: `http://mathworld.wolfram.com/VietasFormulas.html`.

Wi-Fi Alliance. 2012. *Wi-Fi Direct*, [Online]. Available at: `http://www.wi-fi.org/discover-and-learn/wi-fi-direct`.

Yang, H., Luo, H., Ye, F. and Lu, S. 2004. Security in mobile ad hoc networks: challenges and solutions. *IEEE Wireless Communications* 11(1), pp. 38–47. Available at: `http://ieeexplore.ieee.org/lpdocs/epic03/wrapper.htm?arnumber=1269716`.

Zhang, X., Neglia, G., Kurose, J. and Towsley, D. 2007. Performance modeling of epidemic routing. *Computer Networks* 51(10), pp. 2867–2891. Available at: `http://linkinghub.elsevier.com/retrieve/pii/S1389128606003720`.

Zheng, Y., Li, Q., Chen, Y., Xie, X. and Ma, W.-Y. 2008. Understanding mobility based on GPS data. In: *Proceedings of the 10th international conference on Ubiquitous computing - UbiComp '08*. New York, New York, USA: ACM Press, UbiComp '08, p. 312, Available at: `http://portal.acm.org/citation.cfm?doid=1409635.1409677`.

Zheng, Y., Xie, X. and Ma, W.-Y. 2010. GeoLife: A Collaborative Social Networking Service among User, Location and Trajectory. *IEEE Data Eng. Bull.* 33(2), pp. 32–39.

Zheng, Y., Zhang, L., Xie, X. and Ma, W.-Y. 2009. Mining interesting locations and travel sequences from GPS trajectories. In: *Proceedings of the 18th international conference on World wide web - WWW '09*. New York, New York, USA: ACM Press, WWW '09, p. 791, Available at: `http://portal.acm.org/citation.cfm?doid=1526709.1526816`.

Zyba, G., Voelker, G. M., Ioannidis, S. and Diot, C. 2011. Dissemination in opportunistic mobile ad-hoc networks: The power of the crowd. In: *2011 Proceedings IEEE INFOCOM*. IEEE, pp. 1179–1187, Available at: `http://ieeexplore.ieee.org/lpdocs/epic03/wrapper.htm?arnumber=5934896`.